CUKUROVA UNIVERSITY

INSTITUTE OF NATURAL AND APPLIED SCIENCES

MSc THESIS

Two Dimensional Numerical Analysis of PVDs Under an Embankment with Different Matching Methods

Abrasse Théodore SOAVINJANAHARY

Civil Engineering Department

November, 2024

CUKUROVA UNIVERSITY

INSTITUTE OF NATURAL AND APPLIED SCIENCES

MSc THESIS APPROVAL

Two Dimensional Numerical Analysis of PVDs Under an Embankment with Different Matching Methods

---

Abrasse Théodore SOAVINJANAHARY

Civil Engineering Department

This Master's Thesis was evaluated by the following Jury Members on …/.../…… and was approved by unanimity / majority of votes.

Jury : Prof. Dr. Abdulazim YILDIZ (Advisor) ……

: Assoc. Prof. Dr. Ahmet DEMİR (Member) ……

: Assoc. Prof. Dr. Bahadır OK (Member) ……

This Thesis was written in the Department of Civil Engineering, Institute of Natural and Applied Sciences.

Thesis Number:

Prof. Dr. Sadık DİNÇER
Director
Institute of Natural and Applied Sciences

CONTENTS

CUKUROVA UNIVERSITY
INSTITUTE OF NATURAL AND APPLIED SCIENCES

MSc THESIS

Two Dimensional Numerical Analysis of PVDs Under an Embankment with Different Matching Methods

Abrasse Théodore SOAVINJANAHARY

Advisor: Prof. Dr. Abdulazim YILDIZ

Department of Civil Engineering

ABSTRACT

Because of the significant amount of vertical drains beneath a real embankment in soft soil, it is must be examined in three dimensions (3D). Nevertheless, 3D modeling is extremely difficult, taking time, as well as requires an efficient machine. As a result, axisymmetric vertical drains require being transformed to identical plane-strain settings before being evaluated in 2D. Various matching methods using the unit cell concept were established throught the published work, and these methods are implemented by modifying the drainage spacing and/or permeability of the soil in accordance with the fundamental requirements. The present study examines the performance and accuracy of different matching methods to use in the numerical assessment of large-scale consolidometer along with two different case study full embankments. The computational study was performed using the numerical program PLAXIS 2D. The settlement and Excess Pore Pressure (EPP) findings have been compared to the experimental and field measurement. The numerical analysis findings show that the matching approaches give extraordinarily well with field measurement when the smear zone is included. This is evident that these approaches provide both valuable answers and advantages to geotechnical researchers and engineers.

Keywords: PVD, Embankment, Numerical modelling, Consolidation, Matching approaches

ÇUKUROVA ÜNİVERSİTESİ
FEN BİLİMLERİ ENSTİTÜSÜ

YÜKSEK LİSANS TEZİ

Dolgu Altındaki Prefabrik Düşey Drenlerin Farklı Eşleme Yöntemleri ile İki Boyutlu Sayısal Analizi

Abrasse Théodore SOAVINJANAHARY

Danışman: Prof. Dr. Abdulazim YILDIZ

İnşaat Mühendisliği Anabilim Dalı

ÖZ

Prefabrik düşey drenlerle (PDD) güçlendirilmiş yumuşak zeminlerdeki ölçekli dolgu, bir dolgunun altındaki çok sayıda düşey dren nedeniyle 3 boyutlu (3B) olarak incelenmelidir. Bununla birlikte, 3B analiz son derece zordur, zaman alıcıdır ve verimli bir bilgisayar gerektirir. Sonuç olarak, eksenel simetrik düşey drenajlar 2 boyutlu (2B) olarak analiz edilmeden önce aynı düzlem şekil değiştirme koşullarına dönüştürülmelidir. Literatürde birim hücre konseptini kullanan çeşitli eşleme yöntemleri oluşturulmuştur ve bu yöntemler basit talimatlara göre dren mesafesi ve/veya zemin geçirgenliği değiştirilerek elde edilebilir. Bu çalışma, büyük ölçekli konsolidometre ve farklı ölçekli dolguların sayısal analizinde kullanılacak farklı eşleme yöntemlerinin performansını ve doğruluğunu incelemektedir. Sayısal çalışma, PLAXIS 2D yazılım programı kullanılarak gerçekleştirilmiş ve oturma ve Boşluk Suyu Basıncı (BSB) sonuçları laboratuvar ve arazi ölçümleriyle karşılaştırılmıştır. Sayısal analiz bulguları, örselenmiş bölgesi dahil edildiğinde eşleme yaklaşımlarının arazi ölçümleriyle olağanüstü iyi sonuçlar verdiğini göstermektedir. Bu yöntemlerin geoteknik mühendislerine faydalı çözümler ve önemli faydalar sunduğu açıktır.

Anahtar Kelimeler: Prefabrik Düşey Drenaj, Sayısal analiz, Konsolidasyon, Dolgu, Eşleme yöntemler

GENİŞLETİLMİŞ ÖZET

Bu tezde, PDD ile iyileştirilmiş yumuşak zeminlerin konsolidasyonunun 2B sayısal analizinde eşleme yöntemlerinin performansı ve etkinliği araştırılmıştır. Yumuşak zemin modellemesi, düşey yükler altında büyük konsolidasyon oturmalarına neden olan önemli sıkıştırılabilirlikleri ve yetersiz hidrolik iletkenlikleri nedeniyle geoteknik mühendisliğinde ciddi bir sorun olmaya devam etmektedir. Yumuşak killer sınırlı kayma mukavemetine ve hidrolik iletkenliğe sahiptir, bu nedenle yumuşak zemin üzerinde temel tasarımı yapmak önemli zorluklar ortaya çıkarmaktadır. Bu durum, vakumlu ön yükleme, taş kolonlar, düşey drenajlı veya drenajsız ön yükleme gibi çeşitli yaklaşımlar kullanılarak dengesizliği en aza indirecek şekilde geliştirilebilir. PDD'ler, daha kısa drenaj mesafeleri ve konsolidasyon sürelerinin yanı sıra gelişmiş yumuşak zemin mukavemeti de dahil olmak üzere birçok fayda sağlar. Uygulamada, sahada inşa edilen birçok PDD'nin kantitatif olarak 3B olarak incelenmesi gerekir. Ancak, zorlukları ve karmaşıklıkları nedeniyle, 3B çalışmalar pratikte yaygın olarak kullanılmamaktadır. Sonuç olarak, silindirik şekle sahip çok sayıda PDD'den oluşan bir sistemin 2B koşullarına çevrilmesi gerekir. Bir dizi çalışma, birim hücre fikrini kullanarak 3B'yi 2B PDD analizine dönüştürmek için eşleme yöntemleri geliştirmiştir. Eşleme yöntemleri, sistemin geometrisini veya zemin permeabiliteyini değiştirerek elde edilebilir. Bu tezde, literatürde yürütülen büyük ölçekli konsolidometre deneyi, Çin'in doğusundaki ölçekli dolgu ve Dover, New Hampshire'daki (NH) 3 farklı segment ölçekli dolgu farklı eşleme yöntemleri kullanılarak incelenmiştir.

Bu çalışmanın analizi üç bölümde gerçekleştirilmiştir. İlk olarak, bu eşleme yöntemleri doğruluğunu belirlemek için laboratuvar konsolidometresi Sonlu Elemanlar Analizi (SEA) kullanılarak değerlendirilmiştir. Bu bölümde ilk olarak literatürde yer alan laboratuvar konsolidometre deneyi eksenel simetrik olarak modellenmiş ve ardından analizlerde kullanılan parametreler doğrulanmıştır. Daha sonra deneysel düzenek üç farklı eşleme yöntemi kullanılarak düzlem deformasyon koşullarına dönüştürülmüş ve sayısal sonuçlar deneysel verilerle karşılaştırılmıştır. Bu çalışmanın ikinci bölümünde, Çin'in doğusunda PDD ile iyileştirilmiş çok katmanlı zemine ve çoklu düşey drenler sahip ölçekli dolgu, bu eşleme yöntemleri verimliliğini değerlendirmek için düzlem deformasyon koşullarına dönüştürülmüştür. Büyük ölçekli konsolidometre kullanılanlara benzer üç farklı eşleme yöntemi kullanılmış ve tüm SEA sonuçları arazi ölçümleriyle karşılaştırılmıştır. Son olarak, Dover, NH'de PDD ve çok düşey drenajlarla iyileştirilen ölçekli dolgusunun 3 segmenti, bu eşleme yöntemleri verimliliğini değerlendirmek için düzlem deformasyon koşullarına dönüştürülmüştür. Bu bölümde, diğer üç eşleme yöntemi SEA'da incelenmiştir. Sayısal analiz, arazi ölçümleriyle karşılaştırılarak doğrulanmıştır.

ACKNOWLEDGEMENTS

Before getting into the thesis's specifics, I would like to express my sincere thanks to everyone who have contributed in any way to the realization of this modest work through their invaluable advice and contributions.

In particular, I would like start by thanking my advisor, Prof. Dr. Abdulazim YILDIZ, for his guidance and encouragement during my graduate studies, for offering me with numerous professional chances and educational experiences, and for becoming an exceptional supervisor and friendship. This thesis would not be considered feasible without his advice and continuous support.

I would also like to express my deep gratitude to Dr. Ahmet Demir for his contribution, continuous support and his advice.

I would like to recognize NHDOT for providing me with entry to so extensive information and for enabling me to work on such an exceptional endeavor. I would like to acknowledge Amy Getchell for performing a substantial piece of the investigation as a component of her study and for her expert support with this research.

My next appreciation goes to all teachers and professors who taught me at all academic levels. I am convinced my thesis probably would not have been finished without their efforts.

Furthermore, I would like to thank my parents for providing me with unchanging, compassionate assistance during the course of my education.

LIST OF TABLES

LIST OF FIGURES

SYMBOLS AND ABBREVIATIONS

AI : Artificial İntelligence

AOS : Apparent opening size

a_v : Coefficient of compressibility

c : Cohesion

C_c : Compression Index

C_h : Horizontal coefficient of consolidation

C_r : Recompression index

CSL : Critical state line

C_v : Coefficient of consolidation in the vertical direction

C_α : Secondary compression index

$C_\alpha{}'$: Modified secondary compression index

D_e : Equivalent unit cell diameter

D_s : Diameter of the smear zone

DTE : Dover test embankment

D_w : Equivalent diameter of a band-shaped drain

E : Young's modulus

e : Void ratio

E_{50}^{ref} : Secant stiffness in standard drained triaxial test

E_{50} : Triaxial secant stiffness

E_i : Initial tangent modulus

E_{oed}^{ref} : Tangent stiffness for primary oedometer loading

e_p : Void ratio at end of primary consolidation

EPP : Excess Pore Pressure

E_{ur}^{ref} : Unloading / reloading stiffness

$\bar{f}$: Stress state

F_{fc} : Reduction factors due to filtration and clogging

f : Yield function

F_c : Reduction factors due folding or drain condition

FEA : Finite element analysis

F_t : Reduction factors due to time

H_c : Thickness of clay layer

HN : Hangzhou-Ningbo

HSM : Hardening soil model

k_{filter} : Permeability of geotextile filters

k_{soil} : Soil permeability

K : Cam-Clay swelling index

K* : Modified swelling index

K_0^{nc} : Coefficient of lateral stress in normal consolidation

k_h : Permeability in the undisturbed zone

k_s : Permeability of the smear zone

k_v : Vertical permeability of the soil

k_w : Permeability of the drain

l_m : Maximum discharge length

m : Power for stress-level dependency of stiffness

MCCM : Modified Cam-Clay Model

MCM : Mohr-Coulomb Model

m_v : Coefficient of volume compressibility

n : Drain spacing ratio

NH : New Hampshire

OCR : Overconsolidation ratio

P^0 : Initial mean effective stress

P^{ref} : Reference confining pressure

P_P : Pre-consolidation stress

PVDs : Prefabricated vertical drains

$\tilde{q}$: Similar deviatoric stress quantity

q_{req} : Theoretical discharge capacity

q : Deviatoric stress

q_{wmin} : Minimum discharge capacity

q_w : Discharge capacity

r : Radial coordinate

R : Well resistance factor

r_s : Radius of smear zone

r_w : Radius of equivalent drain

SBIA : Second Bangkok International Airport

S_c : Consolidation primary settlement

S_s : Secondary compression settlement

SSCM : Soft Soil Creep Model

SSM : Soft Soil Model

t : Time

t_1 : Time duration to complete primary consolidation

t_2 : Total desired time duration

T_h : Time factor for horizontal consolidation

$\bar{U}$: Average degree of consolidation of the soft soil

$\bar{U}_r$: Average degree of consolidation for radial flow

$\bar{U}_z$: Average degree of consolidation vertical flow

U_{10} : 10% degree of consolidation

u_0 : Initial pore water pressure

UNH : University of New Hampshire

V : Changes in total volume

γ_w : Unit weight of water

Δe : Change in void ratio

ε_1 : Hyperbolic relation among vertical strain

ε_v : Logarithmic relationship between volumetric strain

Λ : Cam-Clay compression index

λ* : Modified compression index

μ* : Modified creep index

ν : Poisson's ratio

φ : Friction angle

ψ : Dilatancy angle

1. INTRODUCTION

Because of significant population expansion, development projects all around the world are increasingly focusing on low-lying regions like peat and organic soil. However, these soil type have a considerable influence on important infrastructures which include roads, buildings, and trains because of their somewhat limited load-bearing capacity (Holtz, 1991; Indraratna et al., 2000). To avoid significant settlement, it is critical to consolidate the soft soil before to beginning the construction process. The soil can be consolidated through the use of loads to provide support construction building. Nevertheless, due to its limited vertical permeability, achieving the desired settlement takes significantly longer than the available construction timeframe (Holtz, 1987; Indraratna et al., 1994). To enhance soft soil, a variety of vertical drainage techniques have been utilized, including sand settling piles and PVDs. As a result, Kjellman (1948) devised PVD-based methods for soil enhancement that made use of cardboard wick drains. The technique for developing PVDs underneath embankment constitutes one of the more extensively used methods for decreasing the time of consolidation, as it provides horizontal drainage in apart from vertical drainage and quickly dissipates excess pore pressure Hansbo (1987). Employing PVDs, the channel for water drainage decreased via the depth of the ground surface to the diameter of the drain's contact area, that speeds up consolidation (Hansbo, 1981).

Nevertheless, although advances regarding comprehending embankment behavior on soft soil over the last decade (Jardine, 1987; Jemal, 2020; Leroueil, 1985; Mamat, 2022), estimating the settlement and EPP of improved subsoils with PVDs continues a challenge in geotechnical engineering. In addition, conducting field tests is typically a costly and time-consuming operation (Quang, 2022). As a result, modern algorithms such as FEA are quite advantageous. In the development phase, engineers favor computational approaches over analytical ones because they can minimize project expenses and length (Rufaizal, 2019). Furthermore, this technique can assist engineers in solving greatly complicated soil problems and increasing their overall capacity to simulate deformations and detect collapse (Hird et al., 1995; Rufaizal, 2019). In addition to numerical models, geotechnical experts invented and employed computational intelligence technologies throughout past thirty years. These techniques were chosen for their ability to predict complex nonlinear interactions (Reiner, 2022). Throughout soil consolidation with PVDs, water flows vertically as well horizontally, demanding 3D computational modeling for estimating PVD consequences (Yildiz, 2009). Nevertheless, 3D modeling takes an extensive period of time and requires a powerful computer. In actuality, numerous drains are placed beneath an embankment in a major project. Consolidation of PVDs in FEA typically tackles size issues in proportion to the total dimensions of the challenge (Sloan, 2019). PVDs typically have a square section that is less than the dimension of a road embankment, resulting in a distance of 1-2m. In addition, utilizing a 3D examination, precise contours of each drain portion must be represented in many different layers of

soil (Sloan, 2019). Thus, the mesh of finite elements must be extremely tiny in order to precisely capture the contours of PVDs, resulting in significant operational and simulation setup costs.

Hence, **t**o simplify the computation length, most released computational study on PVD-reinforced embankments is carried out for 2D plane strain conditions (Jemal, 2020; Perera, 2017; Rujikiatkamjorn et al., 2008). Barron (Barron, 1948) and Hansbo (Hansbo, 1981) proposed the early consolidation theory of soils with fine particles using individual drain wells.

However, some drawbacks have been revealed in this study, including the failure to address the influence of length on the well and the variation in elasticity between soil around and materials in the sandy well (Nguyen, 2020). Afterwards that, multiple methods were established for determining the identical value of the axisymmetric calculation into plane strain conditions (Chai, 2001; Hird et al., 1995). Shinsha et al. (1982), Hird et al. (1992), Bergado et al. (1994), Lee et al. (1997), Indraratna et al. (1997), Lin et al. (2000), Chai et al. (2001), Tran et al. (2008) and Ba-Phu (2019) were presented various methods to analyze soft ground reinforced by PVD under plane-strain circumstances. Such methods mainly served to implement a unit cell idea utilizing only one PVD, as well FEA transitions in axial symmetry to plane strain settings by modifying the spacing among vertical drainage and/or the permeability of the ground surrounding it.

A numerical study for the present research was divided into three components. These matching approaches have been designed using the simple cell paradigm using only one vertical drain. Rujikiatkamjorn (2005) and Saowapakpiboon et al. (2011) conducted laboratory-based large-scale consolidometer experiments with this reason. As a result, in the present investigation, the experimental experimental consolidometer was analyzed using FEA to determine the accurateness of these matching approaches. For this section, the laboratory consolidometer experiment from the literature (Saowapakpiboon, 2011) is initially simulated for axisymmetric, then the settings utilized in the analysis are verified.

The test setup is then transformed into plane-strain settings utilizing three distinct matching approaches, and the computational findings are evaluated in relation to the experimental data. For the second phase of this research, a real embankment using numerous PVD with multiple soil layers in eastern China was subjected to plane-strain settings to examine the performance as well as effectiveness of these matching techniques.

Three different matching methods, similar to those utilized in the large-scale consolidometer, are utilized, and all FEA results are compared to field measurements. Finally, 3 segments of test embankment improved by PVD and multiple vertical drains in Dover, NH were changed to plane-strain settings to evaluate the efficacy of matching approaches. In this part, another three matching methods were investigated in FEA. The numerical analysis was verified by comparing to field measurements.

2. PRELIMINARY WORK

2.1. History and Evolution of Vertical Drains

Vertical drains aim to shorten consolidation time by providing quicker horizontal drainage pathways. Vertical drains are most commonly used for finely ground, inorganic soils having significant water content and weak cohesiveness (Holtz et al., 1991).

This notion was initially conceived around the 1920s then presented in 1926 by American engineer Daniel Moran. As reported by Johnson (1970), Moran proposed using sand drains for the first time to improve the wet soil beneath the highway entrance to the San Francisco Oakland Bay Bridge. Nonetheless, Aboshi (1992) indicated that vertically sand drain efficiency had been overlooked since the structure's bearing strength was assumed to be adequate to hold the entire load right away following execution, which led to common structure failure.

Thus, Kjellman (1948), a Swedish engineer, was first introduced to ground improvement methods utilizing PVDs in 1937. In a field test, Kjellman installed the prefabricated drains using wood/fiber tubes. Kjellman devised and developed a shaped cardboard drainage and technique for inserting it in the ground in 1939 since these tubes were insufficient and costly. To make this cardboard wick, two different types of cardboard were attached together.

Around 1971, Wager improved Kjellman's prefabricated design by including a drain tube made entirely of ribbed polyethylene material, minimizing risk of rapid disintegration. The plastic core was then replaced with paper and woven textile filters. PVD initially found use mainly for projects for transportation, but it has since been employed in a variety of construction categories, including residential construction, department stores, etc. PVD have become extensively available and used in soft soil treatment methods in the past few years. Currently, over fifty distinct varieties of PVDs have been employed globally (Indraratna et al., 2010).

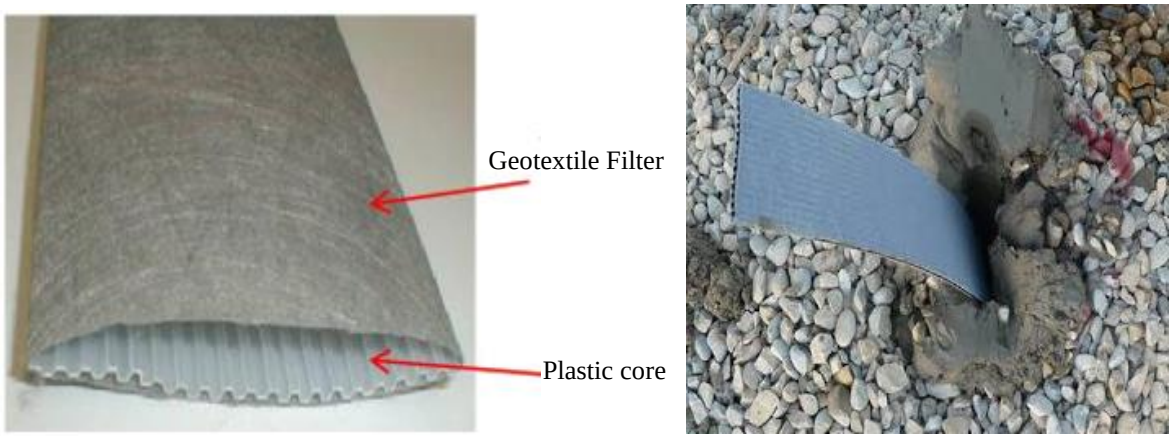

(a) (b)

Figure 2.1. (a) Internal tubes and outside geotextile fibers components of a PVD; (b) Image of a PVD constructed in the ground. (http://www.layfieldgeosynthetics.com)

2.2. Categories of Vertical Drainage

Various kinds of vertical drainage employed to treat soft ground. Both of the most prevalent kinks are sand drains and prefabricated drains, which will be slightly detailed throughout the next sections, but the present study focuses on the second type.

2.2.1. Sands drainage

A sand drain is a hole constructed into solid soil and filled with sand. Sand contains larger particles, which enhances its permeability and allows water to flow through. These holes are backfilled with the appropriate grade of sand. A Sand Blanket, or blanket of sand, connects all of the holes above. In addition, a surcharge load is applied to improve the consolidation rate or speed drainage. Surcharges are often in the form of deposited sand. Surcharge loads increase pore pressures of water in the embankment, resulting in drainage in a vertical as well as horizontal orientation. Surcharge-induced dissipation EPP causes horizontally drainage.

Vertical sand drains are often employed in the fabrication of road and airport foundations over compressible or soft soils, dams on soft ground, and building foundations, among other applications. Sand drains typically have a diameter of 25 to 40 cm and can go as deep as 40 to 45 meters. The goal is to guarantee that all settlement takes place before/during construction, not after. Sand drains offer several disadvantages as well, and these are outlined following (Sathananthan, 2005) :

- Finding suitable sandy materials close to the location can be challenging;
- Sand drains might get inconsistent because of the side soil movements and create gap instability;
- The big diameter of sand drains can lead to structure issues;
- Sand discharge support can lead to inefficient preliminary loading for consolidation on soil.

2.2.2. Prefabricated Vertical Drain

PVD is a vertical drainage constructed by a geotextile material covering a polyethylene inner. It was designed to prevent obstruction and promote consolidation by shortening water circulation way. Construction of a PVD permits water to flow faster by moving axially through the drain and upward under stress down the drainage up to it is released at the bottom layer of drainage (Fox, 2014). Vertical drainage's influence on a certain subsurface state is determined by a number of factors, including drain distance and corresponding drain size, discharge capacity, disturbance area, as well as drainage border state (Miura, 2000). The efficiency of a PVD is determined by the state of the ground, drain type and characteristics, and the efficiency of employment performed throughout framework or installation. Since Kjellman's initial deployment of a prefabricated drain, the amount

of marketplace-ready PVD expanded dramatically. Market offers many commercial versions of PVD, which are commonly made out of a plastic inner covered in a geotextile material. According to Holtz (1987), drains are normally 100 mm x 4 mm in size, and several instances are shown in Figure 2.2.

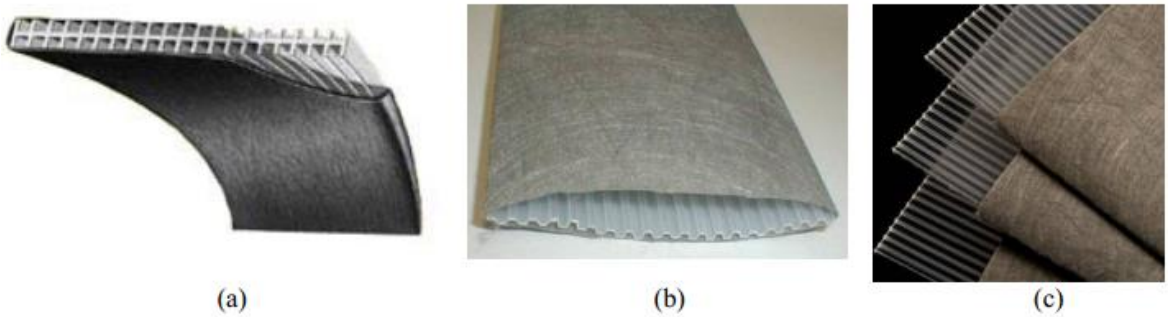

Figure 2.2. Typical PVD's (Ali Parsa, 2014). (a) Membra drain, (b) Layfield, (c) Ce Teau

Installation Procedure

PVD is inserted in the ground using the open mandrel until it is withdrawn, but anchor keeps PVD in position. When the mandrel reaches the ground's bottom, PVD cuts off and anchor of the following drain is installed. A mechanical digger or cranes provides the device that supports and powers the mandrel. The installation equipment is depicted in Figure 2.3. Although it is a vibrating power, static alternatives exist for regions around subterranean infrastructure. To keep the drain in place, thread the wick around the metal anchor at the mandrel's base. When the required level is attained, attach the drain and remove the mandrel. To cut the wick drain, remove the mandrel from 15 to 20 cm above the surface.

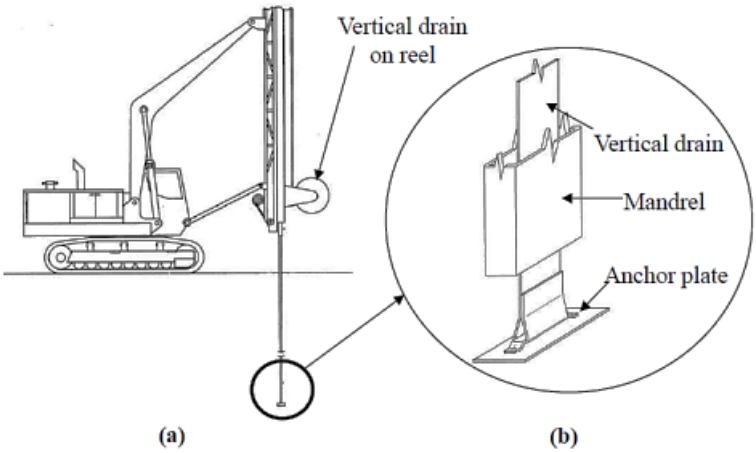

Figure 2.3. Construction machinery of PVD, (a) drain distribution structure, (b) vertical drain enclosed with an empty mandrel and connected to the anchorage sheet (Ali, 2014).

Figure 2.4. Mandrel-installed Prefabricated Vertical Drains at a site
https://gssb.com.my/sand-drain-vs-wick-drain-what-difference

Advantages of using PVDs

The following are some of the advantages of installing PVD:

- Reduce the duration necessary of consolidation;
- Reduce the quantity of overload needed;
- Improve the rate of strength achievement for soft ground with instability issues.

Compared with sandy drainage systems:

- Economically profitable;
- Reduced damage to ground area than movement sand drains;
- Quick and easy construction.

2.3. Properties of Vertical Drains

2.3.1. Equivalent Diameter of PVD

The diameter of PVD may be simply calculated using the dimension of the mandrel, that is typically cylindrical in sectional area. Nevertheless, while the majority of PVD having rectangular cross-sections as shown in Figure 2.5, standard radial consolidation theory is designed and analyzed with the cylindrical drain section area in mind. As a result, the square section must be translated into the corresponding circular of the same size.

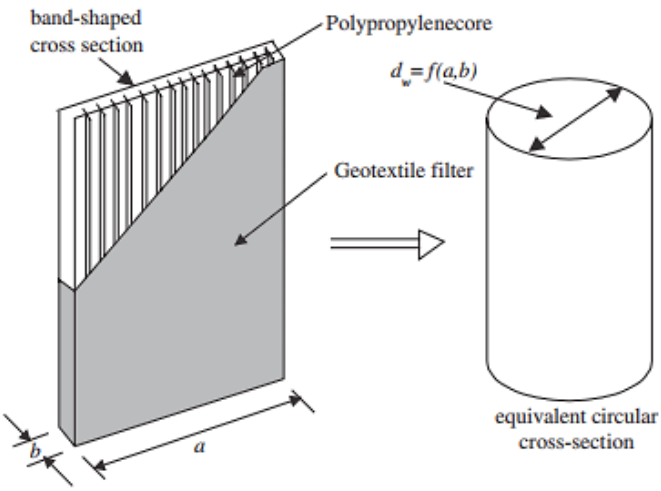

Figure 2.5. Theoretical design of PVD and comparable size (Sathananthan, 2005)

A drain's draining impact is mostly determined by the diameter of its section, with minimal influence from the sectional area (Kjellman, 1948). As stated by Hansbo (1979), computation shows that cylindrical and shape of drains consolidate similarly when their dimensions are identical. Similarly to the preceding approach, by comparing the perimeters of both forms, the corresponding diameter d_w of a shape of the drain having width a and thick b may be determined:

$$d_w = \frac{2(a+b)}{\pi} \tag{2.1}$$

To give consideration for the corner impact, when the movement of patterns quickly converge, Eldred (1981) suggested using a reduction factor of $\pi/4$ in Equation 2.1. Rixner et al. (1986) and Hansbo (1987) used computational modeling to validate this. Which results in:

$$d_w = \frac{(a+b)}{\pi} \tag{2.2}$$

According to Fellenius et al., (1985), the drain's equivalent size may be estimated using its cross-sectional area:

$$d_w = \left[\frac{4(ab)}{\pi}\right]^{0.5} \tag{2.3}$$

Long et al. (1994) proposed the following method for determining d_w as follows with an electrically analog area the graphing tool:

$$d_w = 0.5a + 0.7b \quad (2.4)$$

Rixner et al. (1986) proposed that d_w be calculated using the typical width and thickness of the drain, considering seriously the geometry of the drains and the area of drainage.

$$d_w = \frac{(a+b)}{2} \quad (2.5)$$

To determine the identical size of band-shaped drains, Pradhan et al. proposed using the water would completely surrounding the ground would have a cylindrical of size d_e should be taken into account Figure 2.6. There is no research that can conclusively prove that any of these approaches is better than the others Figure 2.6. Each of them has its own independent support from various studies on this subject. The Hansbo (1979) recommendation for an identical drain size is utilized in the present investigation since it is the most frequently employed method amongst the formulas shown previously.

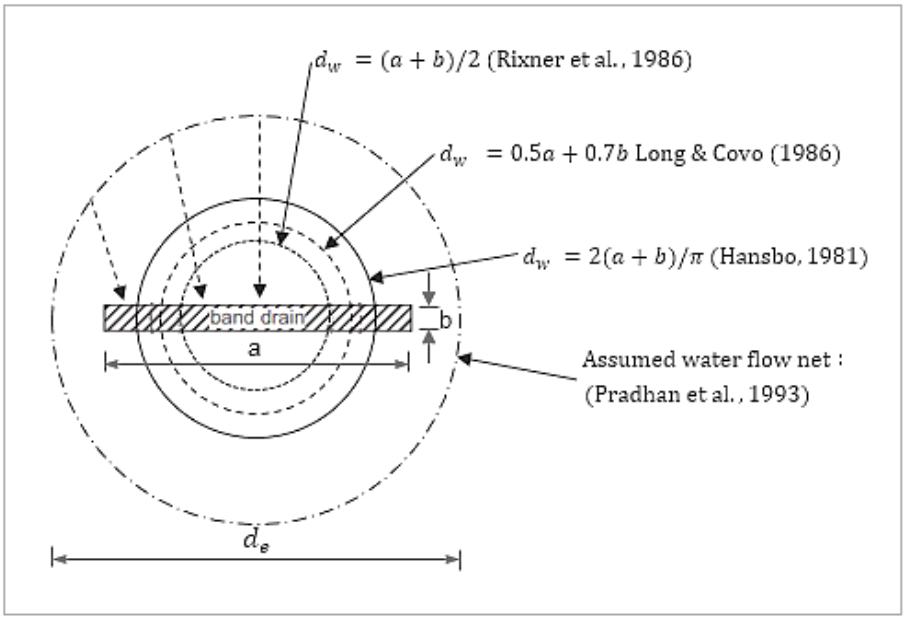

Figure 2.6. Alternative approaches for the corresponding size of drain, based on Indraratna et al. (2003)

2.3.2. Dimension of the impact area

PVD is typically set up in a rectangular or triangle configuration, which is apparent in Figure 2.7. The vast majority of vertical drain consolidation assessments assume that both the drain and its effect area are circular. A cylindrical shape with a similar sectional size is frequently used to describe the influence area. Hansbo (1981) suggested calculating the effect area size using the distance *S* in the following way:

$$D_e = 1.13\ S \tag{2.6}$$

$$D_e = 1.05\ S \tag{2.7}$$

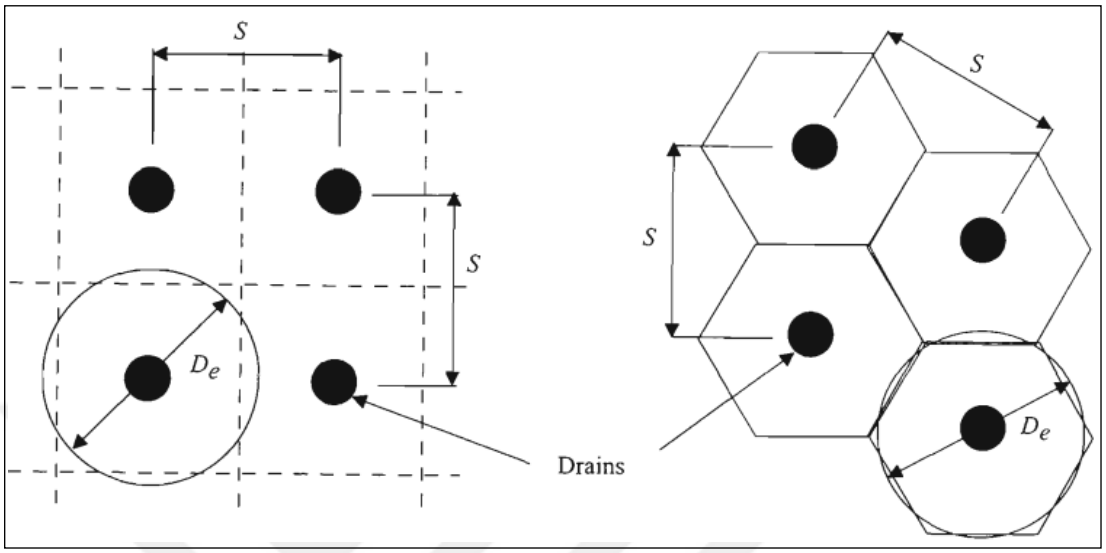

$D_e = 1.13\ S$

Square pattern

$D_e = 1.05\ S$

Triangular pattern

Figure 2.7. Impact area of PVD based on various construction schemes (Sathananthan, 2005)

2.3.3. Filter and Pore Size

A successful PVD performs two primary filtering roles: initially, it holds particles of soil, and secondly, it allows water to move through the ground towards the PVD inner. The filter's permeability or appearance open size (AOS) must satisfy the concept specifications. Hansbo (1979) suggested that the perforations in a geotextile material filter jacket be sufficient in size to avoid particles of soil from going inside. Nevertheless, it should not be extremely small since it needs to have enough permeability. AOS of a geotextile material is determined using beads of glass filtered over it in accordance with ASTM D 4751 specification. AOS is the estimated greatest dimension of particles which may move across a geotextile material. Such small soil fragments can produce sedimentation, reducing PVD discharge capacity (Hansbo, 1981).

To be deemed an efficient filter, geotextile material must not clog or blind, as illustrated in Figure 2.8. Clogging can happen when elements of soil migrate and accumulate inside the textile's framework, lowering permeability due to small fragments entering the geotextile filter. Blinding happens while elements of soil are stopped in accessing or moving into the geotextile and cover its outermost layer, generating a filter layer that greatly decreases the geotextile's permeability.

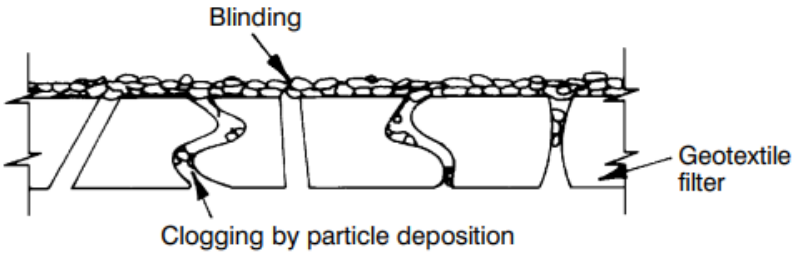

Figure 2.8. Explanation of clogged drainage and blinding procedure (Bell and Hicks, 1980)

Giroud (1982) research implies that the permeability of geotextile material filters, accounting for clogging, should be just 10 times more than the permeability of the ground. This geotextile filter hydraulic characteristic is often specified throughout the choosing process.

$$k_{filter} \geq 10\, k_{soil} \tag{2.8}$$

The geotextile filtration jacket's ability to function as a reliable and efficient ground filtration is determined by a number of variables (McGown, 1976):

- The geotextile filtering bodily and structural properties, such as pore dimensions and circulation, permeability, size, and flexibility;
- The soil's properties, such as particles dimensions, pore size, permeability, and cohesion;
- Externally pressures and strains on the ground structure, such as traffic and fundamental load.

2.3.4. Discharge capacity of PVD

The discharge capacity is a particularly essential factor that influences the efficiency of PVD. Just PVD with appropriate discharge capacity is capable of operating properly. There are two major questions about the discharge capacity of a vertical drain. The initial step is to determine the needed discharge capacity for engineering (Holtz et al.,1991), and the following step is to determine the drain's discharge capacity in the experimental setting and in natural environments. To accurately evaluate discharge capacity, locations must be reproduced as nearly as practical.

Holtz (1991) found that discharge capacity is principally determined by the drain core's free volume, horizontal soil pressure, and potential bending, kinking and folding as shown in Figure 2.9.

When the ground settles down the substance of clay shrinks causing the drain to bend and/or kink. Certain of the potential bending/kinking processes are depicted in the Figure 2.9 (Ali, 1991).

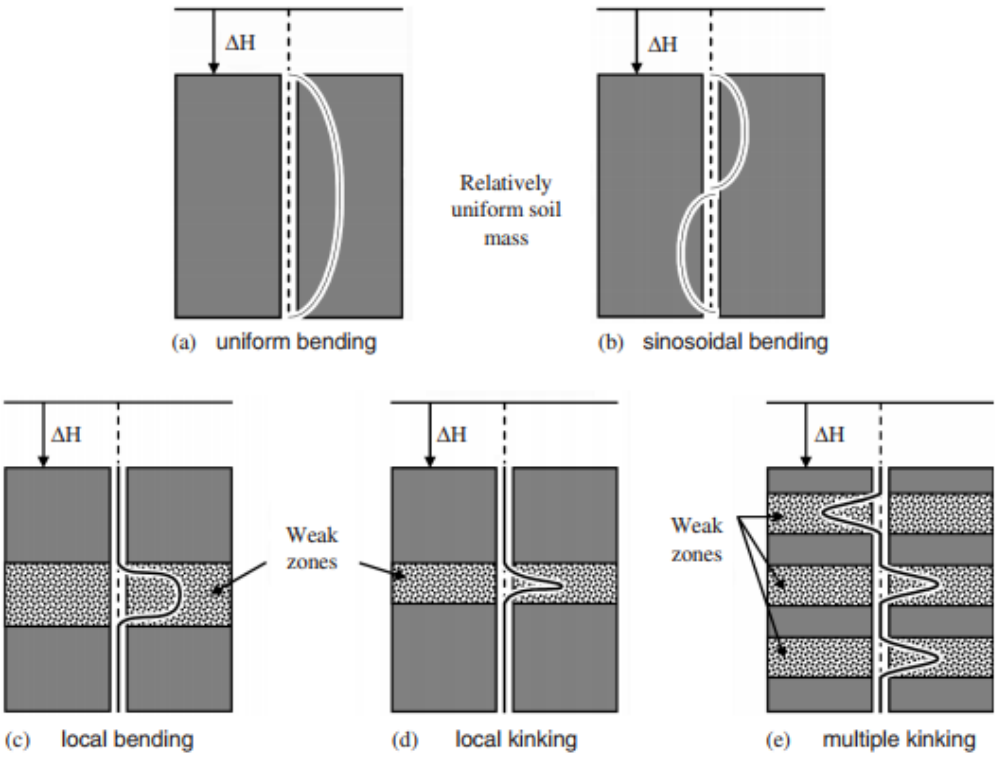

Figure 2.9. PVD deformation patterns (Holtz et al.,1991)

After integrating the aforementioned parameters, the real discharge capacity (q_w), can be calculated by:

$$q_w = (F_t)(F_c)(F_{fc})q_{req} \tag{2.9}$$

Where, F_t, F_c and F_{fc} represent decreased effects caused by time, folding, or drain situation, as well as filtering and clogging. q_{req} is the hypothetical discharge capacity determined using Barron's consolidation concept, that is provided through the following:

$$q_{req} = \frac{\varepsilon_f U_{10} l \pi c_h}{4T_h} \tag{2.10}$$

Where, ε_f is the ultimate settlement of soft ground that is equal to 25% of the total length of the drain set up into soft soil; U_{10} is the 10% degree of consolidation, l is the length of the vertical drain , c_h is horizontal coefficient of consolidation and T_h is the time factor for horizontal consolidation.

The decreased value caused by time F_t, was determined through experiments in the laboratory to be among 1.03 to 1.48, having a typical value of 1.25 (Bergado et al.,1996), while the decrease in the value of the damaged folding or drain state, F_c is around 2. Filtration studies

demonstrate that captured small particles of soil reduce the PVD's permeability as well as discharging capability. This damage is exacerbated by microbiological and biochemical development within the geotextile filtration. Filtration experiments reveal that the amount of F_{fc} ranges among 2.8 and 4.2, and a median of around 3.5. Following evaluating all the most catastrophic events that can happen in the site, the discharge capacity q_w might be 500-800 $m^3/year$ however fall to 100-300 $m^3/year$ when the gradient of water is constant under increasing pressure from the sides (Rixner et al.,1986).

According to Kremer et al. (1982), the smallest vertical discharging capability is 160 $m^3/year$ with a gradient of water of 0.625 over a 40 cm drain height and a restricting pressure of 100 kPa. According to Jamiolkowski et al. (1983), a satisfactory drain performance requires q_w to reach no less than 10-15 $m^3/year$ in a lateral strain between 300-500 kPa for drains up to 20 m in length. According to Hansbo (1987), lengthy drains with capacities smaller than 50-100 $m^3/year$ need an important characteristic of q_w. According to Holtz (1991), the q_w of PVD varies between 100-800 $m^3/year$. PVD with strong vertical deformation along with elevated lateral stress can lower q_w numbers to 25-100 $m^3/year$ (Holtz et al.,1991). Table 2.1 shows the present suggested settings.

Table 2.1. Present suggested discharging capability specifications.

Reference	Measure	Horizontal pressure (kPa)
Den Hoedit (1981)	95	50-300
Kremer et al. (1982)	256	100
Kremer et al. (1983)	790	15
Jamiolkowski et al. (1983)	10-15	300-500
Koda et al. (1989)	100	50
Rixner et al. (1986)	100	Not given
Van Zanten (1986)	790-1580	150-350
Hansbo (1987)	50-100	Not given
Lawrence and Koerner (1988)	150	Not given
Holtz et al. (1989)	100-150	300-500
De Jager and Oostveen (1990)	315-1580	150-300

2.4. Variables factor impacting consolidation using PVD

2.4.1. Disturbed area

PVDs are set up in the site by pushing a metallic mandrel in the soil static or dynamic followed by withdrawing it, establishing the drain in the ground underneath. This procedure induces reconstructing of the ground around the mandrel, resulting in considerable disturbances to the permeability properties of the ground next the drain. The "smear zone" is the ground nearby area

which has been perturbed remolded, and has a lower horizontal permeability magnitude, which has a negative impact on the procedure for consolidation.

To understand the smear impact, two factors are required: the size of the smear area (d_s) and the permeability proportional (k_h/k_s), which is measured in the undamaged area (k_h) within the smear region (k_s). The smear zone's size and permeability are challenging to measure and evaluate using experiments, and there is currently no complete or accepted approach for measuring them. Site and experimental studies (Bergado et al., 1996; Indraratna et al., 1998; Madhav, 1993) demonstrated a constant fluctuation in the permeability of the ground with a radial separation along the drain axis. The smear area size (d_s) has recently been extensively discussed in PVD studies.

Barron (1948) and Hansbo (1981) examined the impact of perturbation and considered a smear area of soil with size, (d_s), adjacent to the corresponding drain size, (d_w) as shown in Figure 2.10.

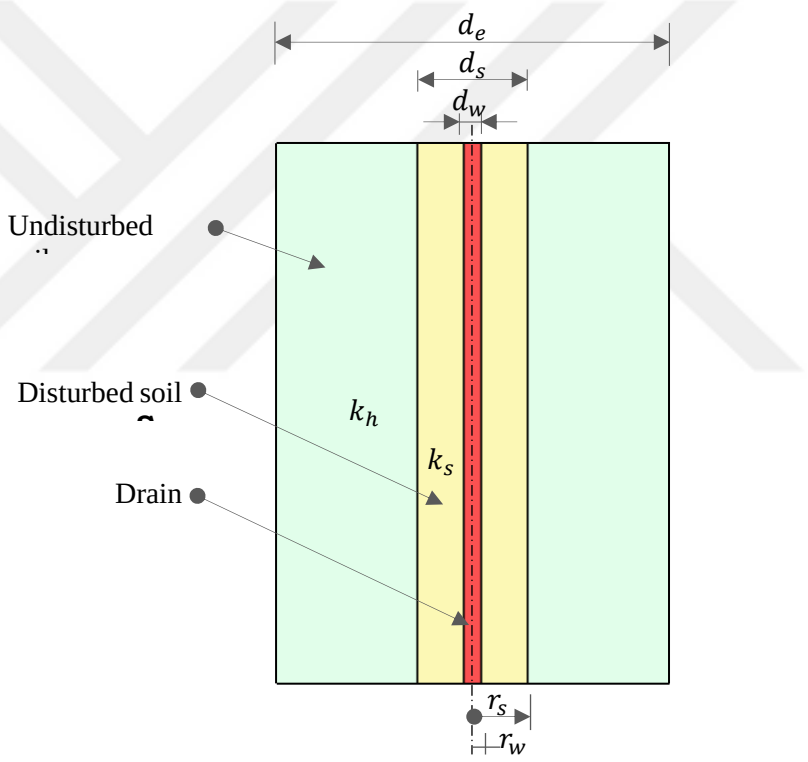

Figure 2.10. Identical ground cylindrical including smear impact.

Because the mandrels utilized to construct drains in the ground are not always cylindrical in form, estimating the corresponding smear size becomes more difficult. According to Indraratna et al. (Indraratna et al., 1998; Sharma, 2000), the smear region size should be 2-3 times the size of the mandrel.

Investigations by Holtz (1973) and Akagi (1977) propose the following:

$$d_s = 2d_m \tag{2.11}$$

Where, d_m is the dimension of the circular that's dimension equals the circumference of the mandrel. Jamiolkowski et al. (1981) suggested this :

$$d_s = \frac{(5\ to\ 6)}{2} d_m \tag{2.12}$$

Hansbo (1997; 1981) presented an alternative connection that goes like this:

$$d_s = (1.5 - 3.0) d_w \tag{2.13}$$

Where, d_w is the identical drain size. According to experimental research and statistical assessment, Bergado et al. (1991) hypothesized that the following connection may be considered:

$$d_s = 2 d_w \tag{2.14}$$

2.4.2. Macro Fabric of Soil

The efficiency of PVDs is thus dependent on the macro fabric of the the ground, which is the proportion of horizontal permeability (k_h) with vertical permeability (k_v) of the ground. The degree and permeability of the smear region change alongside the method of setup, the dimensions and form of the mandrel, and the kind and vulnerability of the ground surface. A further significant variable influencing PVD effectiveness is the presence of longitudinal sedimentary glasses in the ground layer. Since these types of glasses offer a smaller draining channel for pore water adjacent to PVDs, these could impact the consolidated characteristic of the PVD-improved soil. Nevertheless, if the sand or silt lenses are constant in the plane of horizontal displacement and the amount of such glasses is large, there is a quick draining of pore water regardless of whether PVDs are put or not, implying that the efficiency of PVDs is reduced in this situation.

Many academics have presented alternative formulae to estimate smear area permeability. A few studies proposed that the lateral permeability of the smear region is equivalent to the vertical permeability (Bergado, 1991; Hansbo, 1981; Indraratna et al., 1998). Laboratory experiments on samples obtained at various levels from the drain revealed that the smear area permeability close the ground is reduced to one-fifth of the untouched permeability of the ground (Madhav et al., 1993). According to Indraratna et al. (2000), the proportion of untouched ground permeability to smear area permeability varies between 1 and 8. Table 2.2 highlights the smear area value recommendations made by multiple investigators.

Table 2.2. Suggested Smear Area Characteristics (Xiao, 2001)

Reference	Dimension	Permeability	Notes

Barron (1948)	r_s = 1.6r_w	k_h/k_s = 3	Expected
Hansbo (1979)	r_s = 1.5-3r_w	Open	According to the available information at that moment
Hansbo (1981)	r_s = 1.5r_w	k_h/k_s = 3	Based on in studies of cases
Bergado et al. (1991)	r_s = 2r_w	k_h/k_v = 1	Experimental examination and reverse investigation for the Bangkok soils
Onoue (1991)	r_s = 1.6r_w	k_h/k_s = 3	Through testing analysis
Almeida et al. (1993)	r_s = 1.5-2r_w	k_h/k_s = 3-6	In accordance with observations
Indraratna et al. (1998)	r_s = 4-5r_w	k_h/k_v1.15	Experimental study (Sydney Clay)
Chai & Miura (1999)	r_s = 2-3r_w	$k_h/k_s = C_f$ (k_h/k_s)	C_f is the proportion among laboratory and field readings
Hird et al. (2000)	r_s = 1.6r_w	k_h/k_s = 3	Suggested conception
Xiao (2000)	r_s = 4r_w	k_h/k_s = 1.3	Experimental study (kaolin clay)

r_s: radius of disturbed area, k_s: disturbed area permeability, r_w: radius of identical drain, k_h: horizontal permeability, and k_v : vertical permeability.

2.4.3. Mandrel's diameter and form

The dimension and form of the mandrel are proportional to the degree of ground disturbed. Disturbance often rises depending on the mandrel's overall sectional size; hence it is recommended to position as near to the drain as feasible to reduce movement. Although researching the impact of mandrel drains in soils, Akagi (1977, 1981) discovered the moment a closed-end mandrel is pushed in saturating soil, there is a significant amount of EPP caused by raise and lateral movement, that results in a reduction in the durability and value of consolidation of the ground around it.

Nevertheless, the surplus EPP quickly decreased, resulting in consolidation when the mandrel was installed or before the material was put. Bergado (1991) found that in an investigation analysis of a Bangkok soil embankment reinforced by PVDs, settling occurred quicker when the drains were constructed using a mandrel with a lower sectional area than that of a bigger one. That confirms the development of a less smear area in the first case. According to the minimal information available, it is reasonable to expect considerable disruption, calculating d_s as 2.5-3 times the identical size of the mandrel utilized during implantation (Holtz et al., 1991).

2.4.4. Well Resistance

To analyze the resistance issue in the drainage effectively, PVDs' discharge capacity must be taken into account. PVDs are designed to take in entire horizontal movement from surrounding consolidated ground and express it upward. Well resistance is characterized as the resistance to the

passage of water via a borehole. As the drain's height rises, so does the well's resistance, prolonging the consolidation procedure. It slows considerably the disappearance of pore pressure and settling. Well resistance increases because of a variety of factors, including longer of drain, filters degradation, lower drain section, clay penetration in the filters, decreased pore size, and greater resistance to drain bending. Many vertical drains have a restricted discharging capability, that indicates that the system has a maximum outflow.

$$q_w = \pi \, . r_w^2 \, . k_w \tag{2.15}$$

Where, k_w represents the drain's permeability. The drainage capability of PVDs is significantly affected by the type of drain utilized.

Furthermore, when there is an upward trajectory in pressure on the lateral side on the soil, the discharging capability decreases. The reduction of the sectional dimension of the drain can be caused by either the filter being squeezed into the channels or the channels themselves being squeezed together for drains without a filter sleeve. Sengul et al. (2013) discovered that lateral stress increases from 25 kPa to 200 kPa, resulting in a 40% decrease in discharging capability. Based on Sengul et al. (2013), the discharging capability of PVDs is influenced by soil type through clogging of the core area, deformation shapes, PVD structure, and resistance against buckling.

Bo (2004) discovered that drain discharging capabilities tested in the site reach their highest in the first few months following construction. For many distances, the highest discharging capability obtained at the first phase is double that of the discharging capabilities recorded in the site.

Well resistance is determined by criteria including drain discharging capability q_w, permeability of the ground k_h, highest discharging distance l_m, and any geometric inadequacies in the drains. Mesri (1991) proposed a formula for vertical flow through a vertical drain which incorporates into consideration high EPP at the soil-drain boundary. Mesri's theory defines, $\pi \frac{k_w}{k_h} \left(\frac{r_w}{l_m}\right)^2$ as the well resistance aspect, indicating EPP. The well's resistance ratio (R) may be stated as follows:

$$R = \frac{q_w}{k_h l_m^2} \tag{2.16}$$

Mesri (1991) suggested that the well resistance of vertical drains in clay layers is negligible if (*R)* is above 5, implying that the minimum discharging capability $q_{w(\min)}$ of the vertical is necessary to achieve negligible well resistance.

$$q_{w(\min)} = 5k_h l_m^2 \tag{2.17}$$

Lin et al. (2000) found that the minimal q_w amount for insignificant well resistance is 2 to 80 m^3/year, according to average k_h and l_m measurements for clays and vertical drain systems. At the beginning of consolidation, q_w numbers are only required since as k_h drops over time, less water enters the drain and a lower q_w is sufficient. Table 2.3 highlights the well resistance component recommendations made by several studies investigating the influence of limited drain discharging on horizontal consolidation. It must be mentioned that the suggested indicators are also used to calculate Mesri's (1991) well resistance ratio *(R)*. Aside beyond the definition suggested by Aboshi and Yoshikuni (1967) and Kotzias (1985), that includes the drain distance, (R) is the main variable determining all of the above indicators.

Table 2.3. Summary of proposed well resistance indexes (Sathananthan, 2005)

Reference	Well Resistance Impact
Aboshi and Yoshikuni (1967)	$R_i = \frac{(n^2-1)}{4F(n)n^2}\frac{k_h}{k_w}\left(\frac{l_m}{r_w}\right)^2 = \frac{\pi(n^2-1)}{4F(n)n^2}\frac{1}{R}$
Yoshikuni and Nakanodo (1974) and Onoue (1988)	$L = \frac{8}{\pi^2}\frac{k_h}{k_w}\left(\frac{l_m}{r_w}\right)^2 = \frac{8}{\pi}\frac{1}{R}$
Hansbo (1981)	$W = 2\frac{k_h}{k_w}\left(\frac{l_m}{r_w}\right)^2 = 2\pi\frac{1}{R}$
Stamatopoulos and Kotzias (1985)	$R_i = \frac{1}{F(n)}\frac{k_h}{k_w}\left(\frac{l_m}{r_w}\right)^2 = \frac{\pi}{F(n)}\frac{1}{R}$
Zeng and Xie (1989)	$G = \frac{1}{4}\frac{k_h}{k_w}\left(\frac{l_m}{r_w}\right)^2 = \frac{\pi}{4}\frac{1}{R}$
Mesri and Lo (1991)	$R = \pi\frac{k_h}{k_w}\left(\frac{l_m}{r_w}\right)^2 = \frac{q_w}{k_h l_m^2}$

Radial consolidation's rate is influenced by both k_h and D_e, as well as the q_w/k_h ratio when well resistance is factored in.

Based on site and experimental investigations, the discharging capacity of the majority of modern PVDs have little effect on clay consolidation rates, especially in drains that are not excessively lengthy (Indraratna et al., 1994). Consolidation period may substantially rise if the q_w quantity crosses 100-150 m^3/year and the drains are shorter than 30 m. In most practical cases, well resistance for commercial PVDs is minor, depending on the drains' excessive length and geometric flaws during installation. Well resistance can be ignored in soft clays shorter than 15 meters in length.

2.5. Consolidation Theory

Materials can deform or strain when they are loaded or stressed. The layer's consolidation (compression) is the result of external load over time. This is done by using the oedometer test to determine the effective pressure and void ratio. Discharge of water from the void space of saturated soils leads to volumetric deformation during consolidation, which is a time-dependent process (Taylor, 1948; Terzaghi, 1925). Consolidation decreases the overall size of a stratum, which causes the load to settle downwards. Its strength, however, increases. Clay soils responding gradually as time passes, but certain materials bend rapidly and instantly when loaded. In linearly elastic materials, the connection among strain and stress is linear, and removing the load causes the substance to revert to its initial state (Holtz et al., 2011). Modifications in the overall volume *(V)* are also caused by variations in the ratio of voids *(e)* and water content. Predicting the magnitude of consolidation in terms of the void ratio is convenient. When ground becomes bent, it is unable to recover to its former shape once unloaded; rather, it keeps a certain strain or persistent bending, which is called plasticity. Soils are difficult to simulate because of their complicated stress-strain connection, time-varying load reaction, stress history, and part elastic, partly plastic characteristics (Holtz et al., 2011).

2.5.1. Vertical displacement

To understand the behavior of soils, it would be beneficial to provide information about certain terms and definitions. Settlement is the term used to describe the overall vertical displacement at the soil surface caused by the load. The rate at which volume decreases due to unit load is known as compressibility. Consolidation occurs once saturating ground is loaded outwardly, and the water is then pushed out, resulting in a long period of shrinkage depending on the soil's permeability. To understand the relationship between water and soil, which involves swelling and shrinkage, it's important to provide additional statements. The volume of soil expands when there is a rise in water content, and shrinkage occurs when there is a decline in water content. Load distribution settlements include instantaneous, initial, secondary, and tertiary consolidation.

2.5.2. One-Dimensional Consolidation

Civil engineers have been dealing with deformation problems for decades, but Terzaghi (1925) one-dimensional theory was the first to introduce a rational and quantitative approach, that many believe this to be the origin of contemporary ground mechanics. Throughout that period, a substantial number of improvements were put forward to improve prediction precision. The use of an oedometer test allows for the determination of soil's behavior during one-dimensional consolidation or swelling. The procedure is performed by putting a metal ring over a specimen of soil with a size of 75 mm and a thickness of 20 mm. The consolidation test equipment is shown in Figure 2.11. The goal of adding permeable discs at the top and bottom of the soil samples

is to remove water. Water is utilized preceding the loading procedures to avoid pore pressure. Following that, compression is performed out repeatedly utilizing a load increase, that is typically 0.25 kg/cm^2, 0.5 kg/cm^2, 1.0 kg/cm^2, 2.0 kg/cm^2, and 4.0 kg/cm^2 (depending on project stresses) and using a transducer, soil samples are periodically measured to determine their vertical settlement.

After settlement has occurred, the additional load enhancement is finished (Figure 2.11b). The consolidation test proceeds till the task's stress limits are met and all consolidation is accomplished. The sample's void ratio may be determined for each increasing stage, and the test results can be used to create a graph showing the void ratio versus effective pressure, as shown in Figure 2.12a (Smith, 2014). To determine the deformation properties of the ground the specimen, the unloading process can be done by releasing the load every 24 hours. Figure 2.12b shows the expanding and recompression contours.

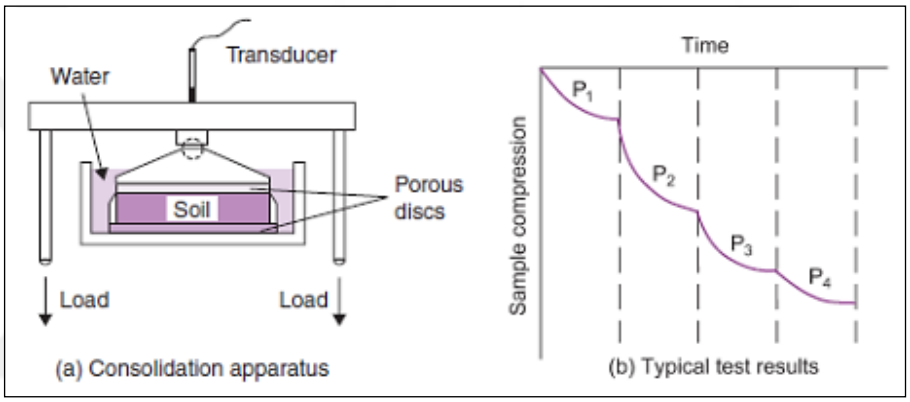

Figure 2.11. Consolidation examination equipment and findings (Smith, 2014)

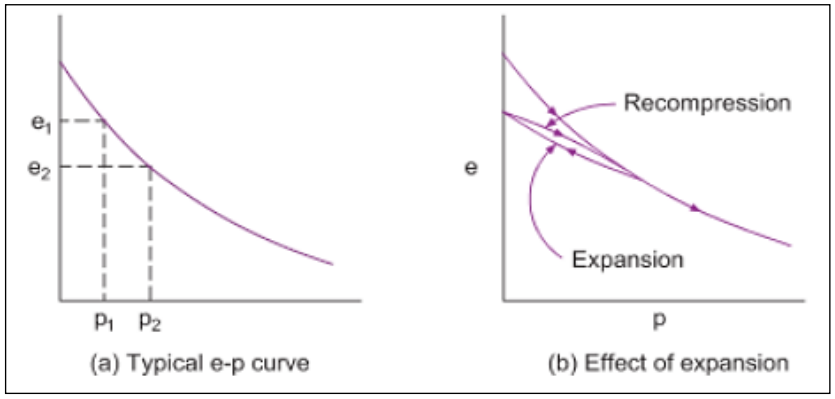

Figure 2.12. Void ratio and effective stress plot (Smith, 2014)

Terzaghi proposed this equation for 1-D dissipation of EPP, taking into account these assumptions:

$$\frac{\partial u}{\partial t} = c_v \frac{\partial^2 u}{\partial z^2} \tag{2.18}$$

Where, *u* is EPP, *t* is time, *z* is the depth, that is the spacing determined vertically below the highest point of a consolidating ground level, and c_v is the value of the coefficient of consolidation in the upward direction, that could be represented as,

$$c_v = \frac{k_v}{\gamma_w m_v} = \frac{k_v(1+e)}{a_v \gamma_w} \tag{2.19}$$

Where, k_v is the value of vertical permeability, γ_w is the water unit weight, m_v is the value of volume compressibility, a_v is the value of compressibility, and *e* is the void ratio of the ground.

Volumetric Change

While the ground layer undergoes to a consolidation stress, the drainage situation alters the quantity of soil. The volumetric variation is caused by the distinction among the starting volume ($V_1 = e_1 + 1$) and the end volume ($V_2 = e_2 + 1$) relative to the original volume.

$$\Delta V = \frac{V_1 - V_2}{V_1} = \frac{e_1 - e_2}{1 + e_1} \tag{2.20}$$

Coefficient of compressibility

The compressibility of soil changes during consolidation and the rise in efficient pressure decreases its compressibility. The coefficient of compressibility (a_v). is determined by the rate of the void ratio- efficient pressure relation.

$$a_v = -\frac{\Delta e}{\Delta \sigma} \tag{2.21}$$

Ratio of compression of volume

The value of the coefficient of compressible volume represents how much pressure enhances a soil's compression per unit height. The coefficient of compressible volume is calculated by multiplying the compression ratio by the soil's original volume.

$$m_v = -\frac{a_v}{1 + e_1} \tag{2.22}$$

2.5.3. Primary Consolidation

Settlement in saturating ground particles with inadequate permeability happens in a period-dependent procedure known as primary consolidation, which has an immediate relationship to load growth. The rate of pore water drainage is what governs it (Holtz et al., 2011). When saturated cohesive soils experience a volume change because of the removal of water that inhabits void spaces, it is called primary consolidation (Das, 2013). The assumption is that this will happen after practically all of EPP is dissipated. In the theory, the completion of 100% primary consolidation occurs at this point.

Pre-consolidation stress

Ground possesses memories and recalls the events of previous loads. When pressure is increased in the recompression area, the soil will remember past loading and experience fewer settlements. However, in virgin compression, the soil is first exposed to the highest stress value, which results in greater settlement than in the recompression zone. Pre-consolidation pressure ($\sigma_c{}'$) is identical with the maximum effective stress from past loading. Furthermore, it is the intersection of the recompression slope and the compression slope. The method of Casagrande (1936) provide 4 steps, that gives a method for estimating pre consolidation pressure:

- Produce a straight line starting the viewpoint P;
- Construct TS straight to represent the angle's bisector;
- The connection of the bisector alignment and the extended line (Slope = C_c) yields T, whose log stress element corresponds with the pre-consolidation stress.
- Expanding the PR axis at position P, to the location of highest curve;

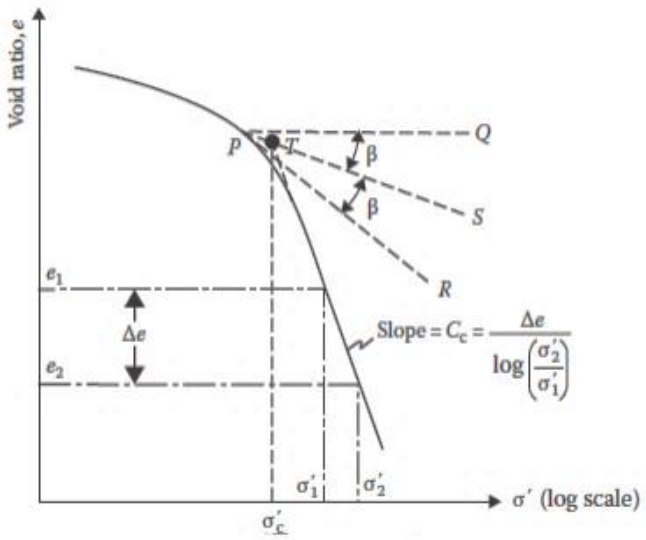

Figure 2.13. Pre-consolidation stress (DAS, 2013)

The pre-consolidation stress is lower than the current effective overburden pressure, that results in ground being consolidated. The volume of consolidated ground usually decreases with an increase in applying pressures as presented in Figure 2.14.

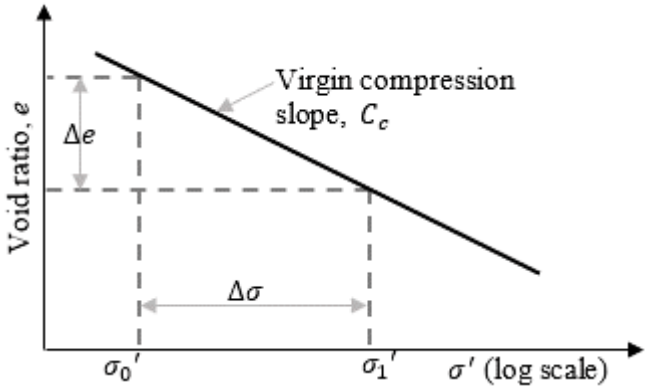

Figure 2.14. Void ratio-efficient pressure increase for ground (DAS, 2013)

When the present effectual pressure on the overburden is lower compared to the pre-consolidation stress, the ground was considered overconsolidated. The overconsolidation proportion is the ratio between the current functional pressure of overburden and the pre-consolidation stress Equation 2.23.

$$OCR = \frac{\sigma_c'}{\sigma_0'} \tag{2.23}$$

The cumulative difference in void ratio between recompression and virgin parts is used to calculate volume change in overconsolidated soils Figure 2.15.

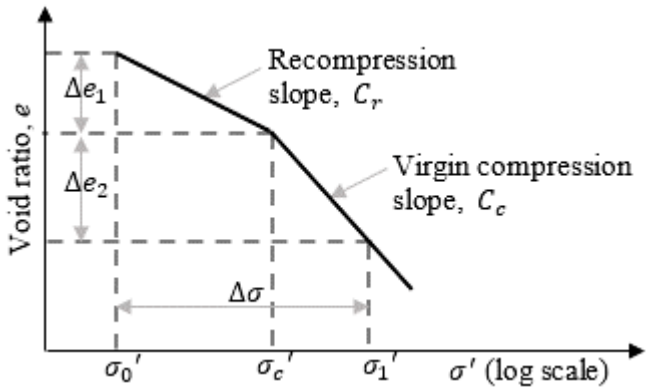

Figure 2.15. Efficient pressure development in recompression and virgin compressing (DAS,2013)

Compressibility Index

The compressibility index of the ground could be determined by the sloping of the recompression slope and the virgin compression slope in Figure 2.14. The compression indices represent the gradient of the undefined linear component of the e-log σ' plot.

$$C_c = \frac{\Delta e}{log\sigma_1{}' - log\sigma_0{}'} \tag{2.24}$$

$$C_r = \frac{\Delta e}{log\sigma_c{}' - log\sigma_1{}'} \tag{2.25}$$

Computation of Consolidated Settlements

The displacement is calculated through dividing the strain by the height of the ground. The ground's strain is defined by the overconsolidation proportion, pressure increment, and compression indices. Utilizing these parameters, three different approaches may be used for primary consolidation settlement estimation. For usually consolidated clays, the Compression Index (C_c) may also be utilized for calculating the settling of the H-layer.

Normally consolidated ground ($OCR \leq 1$) and increasing pressure in the scope of virgin compression areas by Figure 2.15.

$$S_c = \frac{C_c}{1 + e_0} log \frac{\sigma_1{}'}{\sigma_0{}'} H \tag{2.26}$$

Overconsolidated ground and pressure increases in the spectrum of recompression areas

$$S_c = \frac{C_r}{1 + e_0} log \frac{\sigma_1{}'}{\sigma_0{}'} H \tag{2.27}$$

Overconsolidated ground and pressure increases in the spectrum of compression areas

$$S_c = \frac{H}{1 + e_0} \left(C_c \, log \frac{\sigma_1{}'}{\sigma_c{}'} + C_r \, log \frac{\sigma_c{}'}{\sigma_0{}'} \right) \tag{2.28}$$

The three preceding formulations differ according to stress intensity. For constant stress levels, an average coefficient of volume compressibility (m_v) can be utilized in another formula. These formulas decrease the impact of nonlinearity (Das, 2014).

$$S_c = m_v \, H \, \Delta\sigma \tag{2.29}$$

2.5.4. Secondary Consolidation

Secondary compression probably originated in North America during the 1930s (Çelik, 2020). Secondary consolidation is a mechanism that initiates continuous volume change from

primary consolidation. Individual particles deforming and their relative movements with respect to one another are part of this mechanism.

Secondary compression is a process that is dependent on time and occurs after primary consolidation is completed. The ground structure depends on a steady reduction in EPP to assist maintain the embankment stress throughout primary consolidation while building an embankment. When the initial consolidation finishes, the surplus EPP is totally drained, and the real stress increase induced by the embankment weight is fully transmitted to the ground. Constant loading over time can result in extra secondary compression or creep because of the soil not relying on pore water pressure for structural support. Secondary settlement is often a minor fraction of the entire settlement, but it might be sufficient to generate long-term settlement concerns. The calculation of secondary compression settlement (S_s) can be done utilizing Equation 2.30, Equation 2.31, and Equation 2.32 (Das, 2011).

$$S_s = C_\alpha{}' H_c \, log\left(\frac{t_2}{t_1}\right) \tag{2.30}$$

$$C_\alpha{}' = \frac{C_\alpha}{1 + e_p} \tag{2.31}$$

$$C_\alpha = \frac{\Delta e}{log\left(\frac{t_2}{t_1}\right)} \tag{2.32}$$

Where, C_α is the secondary compression index, $C_\alpha{}'$ is the modified secondary compression index, H_c is the thickness of clay layer, t_1 is the time duration to complete initial consolidation, t_2 is the complete targeted time period, e_p is the void ratio at end of primary consolidation, Δe is the change in void ratio.

According to Figure 2.16, settling occurs at the conclusion of the initial consolidation (when extra pore water pressure has entirely gone) as a result of the ground fiber plastic correction. This phase of consolidation is known as secondary consolidation. Throughout secondary consolidation, the deformation-log of time *(log t)* plot is nearly linear. Figure 2.16 depicts the changes in the void ratio over time t for a particular load increase.

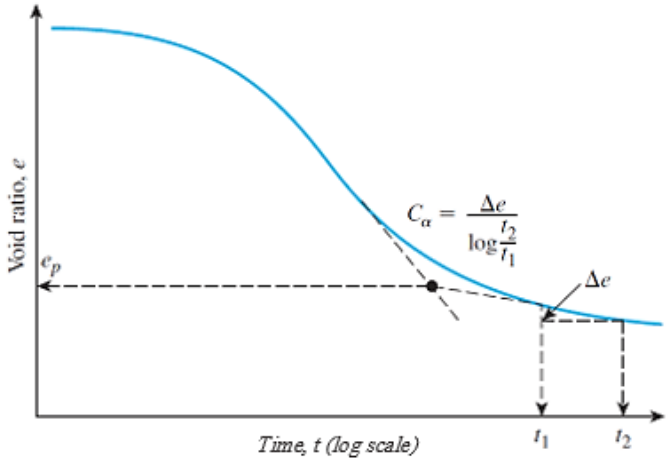

Figure 2.16. Change of *(e)* over (*log t)* during a certain load increase and determination of secondary consolidation index (Das et al., 2013)

2.5.5. Evolution of PVD consolidation theories

To enhance horizontal consolidation of soft ground using vertical drains, most analytical approaches devised employ the 'unit cell' concept. Considering the axisymmetric nature of water moving toward a vertical drain, the unit cell concept offers a fair and adequate solution to the issue. Many researchers have investigated hypotheses for horizontal consolidation surrounding a vertical drain, a few of which are described as follows:

Rendulic and Carillo adaptation hypothesis

In 1-D vertical displacement due to horizontal water movement, the following formula was formulated by Rendulic (1936):

$$\frac{\partial u}{\partial t} = c_h \left(\frac{\partial^2 u}{\partial r^2} + \frac{1}{r} \frac{\partial u}{\partial r} \right) \tag{2.33}$$

Where, *r* is the radius coordinate, c_h is the axial coefficient of consolidation. Carillo (1942) used Equation 2.33 to calculate the extra pore pressure ($u_{r,z}$).

$$\frac{\partial u}{\partial t} = c_h \left(\frac{\partial^2 u}{\partial r^2} + \frac{1}{r} \frac{\partial u}{\partial r} \right) + c_v \frac{\partial^2 u}{\partial z^2} \tag{2.34}$$

$$u_{r,z} = \frac{u_r \, u_z}{u_0} \tag{2.35}$$

Where, u_r and u_z are respectively the EPP due to horizontal and vertical water movement only and u_0 is the initial EPP.

$\overline{U}_z$ may be used to represent the mean amount of consolidation, whereas Terzaghi's equation and $\overline{U}_r$ can calculate the mean degree of consolidation in the vertical axis. Equation 2.35 may be utilized to replace the mean EPP for the mean amount of consolidation in a horizontal direction determined by Rendulic's formula.

$$(1 - \overline{U}) = (1 - \overline{U}_z)(1 - \overline{U}_r) \tag{2.36}$$

Where, $\overline{U}$ is the mean amount of consolidation of the soft ground at the given period *t* for coupled vertically and radially movement, whereas $\overline{U}_z$ and $\overline{U}_r$ are the mean degrees of consolidation at given period *t* for vertically and flow radially only. It needs to be mentioned that both Rendulic and Carill's systems are designed for perfect drains.

Suggestion of Barron (1948): Equivalent strain theory

Barron (1948) discussed the effect of well resistance and disturbed area on the efficiency of vertical drains, given the impossibility of perfect drainage. He used the smear impact in his method to consolidate with vertical drains. He presented closed-form approaches to two severe instances of horizontal drainage-induced consolidation in the soil layer, known as independent strain and identical strain, and established that the mean consolidation in both situations is almost identical. He

demonstrated that a soil cylinder could be combined by using the same assumptions as Terzaghi's theory, except for the drain, which had a perfect center vertical drain and an impermeable border excepting at the point of drainage. Equation 2.33 u_r was utilized to define EPP solution for horizontal movement while also accounting for the influence of smear.

$$u_r = \bar{u}_r \frac{1}{v}\left[l_n\left(\frac{r}{r_s}\right) - \frac{(r^2 - {r_s}^2)}{2R^2} + \frac{k_h}{{k_h}'}\left(\frac{n^2 - s^2}{n^2}\right) l_n(s)\right] \tag{2.37}$$

Where,

$$\bar{u} = u_0 \, exp\left(-\frac{8T_h}{v}\right) \tag{2.38}$$

Where, *r* is the radius of the drain; r_s is the radius of the disturbed area; *R* is the radius of the cylindrical ground; k_h is the radial permeability of the untouched ground; and ${k_h}'$ is the radial permeability in the disturbed area. The disturbed area aspect, ν, can be calculated by:

$$v = F(n, s, k_h, {k_h}') = \left[\frac{n^2}{n^2 - s^2} l_n\left(\frac{n}{s}\right) - \frac{3}{4} + \frac{s^2}{4n^2} + \frac{k_h}{{k_h}'}\left(\frac{n^2 - s^2}{n^2}\right) l_n(s)\right] \tag{2.39}$$

The distance proportion is specified as $n = R/r_w$, while the disturbed area extension factor is written as $s = r_s/r_w$. The mean amount of consolidation $\bar{U}_r$ can be calculated as follows:

$$\bar{U}_r = 1 - \frac{u}{u_0} = 1 - \, exp\left(-\frac{8T_h}{v}\right) \tag{2.40}$$

Where, T_h is the duration aspect of horizontal drainage and can be defined as follows:

$$T_h = \frac{c_h t}{{D_e}^2} \tag{2.41}$$

Figure 2.17 shows the curves for the mean degree of horizontal consolidation compared to the time factor T_h.

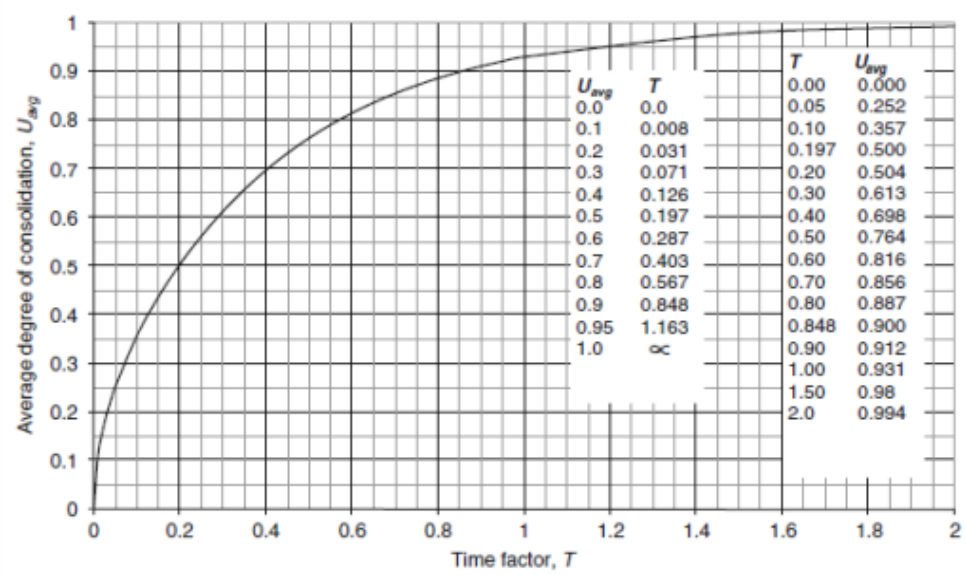

Figure 2.17. Relation between T and U_{avg} (Ameratunga et al, 2016)

Evaluation of well resistance and disturbed area

Hansbo (1981) presented an accurate approach of vertically drainage that takes into consideration both well resistance and disturbed region, founded on the 'equal strain' principle. He founded that horizontal flow $\overline{U}_{rz}$ has a mean degree of consolidation at profundity *z* as follows:

$$\overline{U}_{rz} = 1 - exp\left(-\frac{8T_h}{\mu}\right) \tag{2.42}$$

In which

$$\mu = \frac{n^2}{n^2-1}\left(l_n\left(\frac{n}{s}\right) + \left(\frac{k_h}{k_h{}'}\right) l_n(s) - 0{,}75\right) + \frac{s^2}{n^2-1}\left(1 - \frac{s^2}{4n^2}\right) + \frac{k_h}{k_h{}'}\frac{1}{n^2-1}\left(\frac{s^4-1}{4n^2} - s^2 + 1\right) + \pi z(2l-z)\frac{k_h}{q_w}\left(1 - \frac{1}{n^2}\right) \tag{2.43}$$

Alternatively, in the following form (ignoring the smallest importance terms):

$$\mu = l_n\left(\frac{n}{s}\right) + \left(\frac{k_h}{k_h{}'}\right) l_n(s) - 0{,}75 + \pi z(2l-z)\frac{k_h}{q_w} \tag{2.44}$$

The mean degree of consolidation $\overline{U}_{r,av}$ for every stratum could be achieved via exchanging the value of μ Equation 2.44 for:

$$\mu = l_n\left(\frac{n}{s}\right) + \left(\frac{k_h}{k_h{}'}\right) l_n(s) - 0{,}75 + \frac{2k_h\pi l^2}{3q_w} \tag{2.45}$$

3. MATERIAL AND METHOD

3.1. Finite Element Analysis

The utilization of computational simulation in geotechnical science grew dramatically in recent years, because of considerable increases in computational capacity and applications including PLAXIS. The software is beneficial for tackling a wide range of complicated issues with an emphasis on geotechnical solutions for engineers. This was utilized for computational simulation in the present study.

3.1.1. PLAXIS 2D Software Program

PLAXIS 2D is a 2D computational finite element software created by Delft University of Technology in the Netherlands. The tool was first created in collaboration with the Dutch Ministry of Public Works and Water Management to analyze 32 canal embankments on soft ground in Holland's lowlands (Brinkgreve, 2002). Subsequently, PLAXIS corporation was established in 1993, PLAXIS 2D first became available in 1998, and the program has grown into an effective instrument in a wide range of geotechnical tasks.

The Mesh option allows users to set mesh characteristics for discretization and converting the computational shape to a finite-element simulation. In regard to element distribution, mesh choices include very coarse, coarse, medium, fine, and extremely fine. When the mesh becomes finer, additional components are incorporated and dispersed across the model's computational design. Finer meshes can occasionally yield more exact results, but they can take longer to compute (Brinkgreve, 2002). The created mesh in PLAXIS is composed of triangular components with the choice of 6- or 15-node elements, as seen in Figure 3.1.

Nodes Stress points

a) 15-node triangle

Nodes Stress points

b) 6-node triangle

Figure 3.1. Positions of nodes and stress points in triangular elements (Brinkgreve, 2002)

To numerically simulate a system, an established constitutive relation has to be present that estimates the effect of stresses and strains. The designer chooses the constitutive model at their own discretion, however it frequently depends on decision and past experience. Furthermore, it is essential to know the differences and relevance of every indicative model for particular types of soils and loading situations. Certain models get more extensively used than others. In particular, Mohr Coulomb, Hardening-Soil, Soft Soil, Modified Cam-Clay and Soft Soil Creep constitutive models have seen extensive investigation and have been recognized as adequate models for characterizing the complicated connections among stress and strain in various ground (Brinkgreve, 2002). The above models are accessible in PLAXIS 2D. This section outlines the fundamental models accessible in PLAXIS and indicates which of them were employed in the present study.

3.1.2. Mohr-Coulomb Model

Mohr-Coulomb Model (MCM) is a linear elastic completely plastic model that is both basic and widely recognized, as illustrated in Figure 3.2, and can be utilized as an initial prediction of soil characteristic. Hooke's law of isotropic elasticity is used to determine the linear elastic part of MCM. Mohr-Coulomb failure criteria is the basis of the perfectly plastic part, which is expressed in a non-associated plasticity framework.

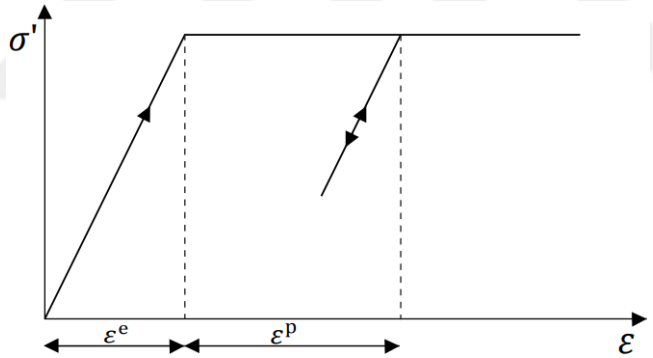

Figure 3.2. Fundamental notion of an elastic perfectly plastic model

MCM requires five parameters, all of which are common knowledge among geotechnical specialists, which might be acquired from standard ground sample testing. The parameters and their standard units are outlined in Table 3.1.

Table 3.1. Fundamental parameters of MCM

Item	Symbol	Unit
Young's modulus	E	$[\mathrm{kN/m^2}]$
Poisson's ratio	ν	[-]
Cohesion	c	$[\mathrm{kN/m^2}]$
Friction angle	φ	[°]
Dilatancy angle	ψ	[°]

Where E and ν are elastic stiffness parameters, whereas φ, ψ, and c are plastic strength parameters.

In primary stress space, Figure 3.3 shows a 3D illustration of Mohr-Coulomb yield surface for a cohesionless ground, apparently determined stated in PLAXIS.

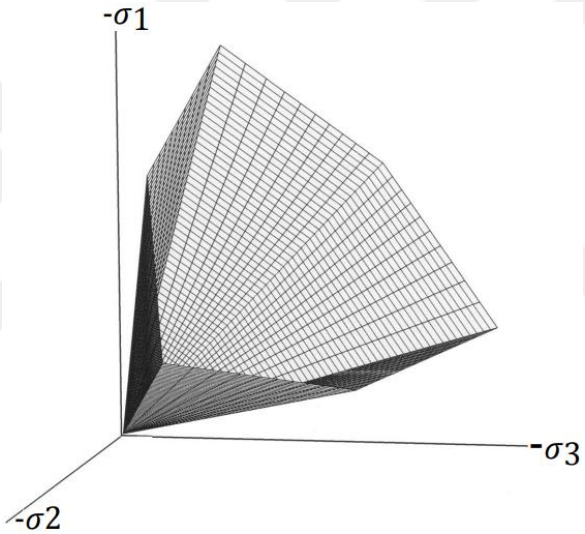

Figure 3.3. Mohr-Coulomb yielding area in primary stress region (c = 0) (Brinkgreve, 2002)

3.1.3. Hardening Soil model

Hardening Soil Model (HSM) was developed to be a further development of MCM that includes an area where the yield surface varies nonlinearly on plastic strain. (Schanz, 1998) describes HSM as a complicated structure model for capturing the characteristics of various soil types, including soft and stiff soils. In the same manner as PLAXIS creates MCM, the plastic strength or failure parameters for HSM are determined by *(φ)*, *(ψ)*, and *(c)*; however, soil stiffness is represented by three separate input stiffnesses, as illustrated in Figure 3.4 and described in Table 3.2.

Table 3.2. Fundamental parameters for stiffness of ground in HSM

Item	Symbol	Unit
Secant stiffness in standard drained triaxial test	E_{50}^{ref}	$[\mathrm{kN/m^2}]$

Tangent stiffness for primary oedometer loading	E_{oed}^{ref}	$[\mathrm{kN/m^2}]$
Unloading / reloading stiffness (default $E_{ur}^{ref} = 3E_{50}^{ref}$)	E_{ur}^{ref}	$[\mathrm{kN/m^2}]$
Power for stress-level dependency of stiffness	m	[-]

Note that HSM does not consider the stress-strain curve's initial slope, often known as the initial tangent modulus (E_i).

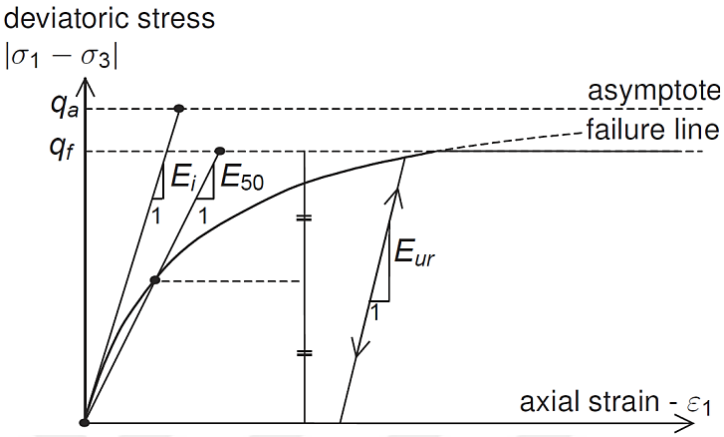

Figure 3.4. Hyperbolic stress-strain relationship in initial loading for a standard drained triaxial test (Brinkgreve, 2002)

Equation 3.1 calculates the triaxial secant stiffness (E_{50}) of a conventional drained triaxial test shown in Figure 3.4. In this equation, p^{ref} is the reference confining pressure, *m* measures the component's stress dependence and specifies the contours of the yielding loci, and E_{50}^{ref} the standard rigidity factor associated with the constraining pressure. PLAXIS sets to p^{ref} = 100 stress units. To represent the logarithmic compressive characteristic observed in moderate grounds, *m* could be considered to be equivalent to 1.0 (Janbu, 1963); whereas, for hard ground, *m* might be set to 0.5.

$$E_{50} = E_{50}^{ref}\left(\frac{c\cos\varphi - \sigma_3'\sin\varphi}{c\cos\varphi + p^{\mathrm{ref}}\sin\varphi}\right)^{\mathrm{m}} \tag{3.1}$$

In 3D, PLAXIS extends Mohr-Coulomb hexagonal cone yield area by adding a second type of yielding area to complete the elastic zone for compression stress pathways. The second yield surface is represented by Figure 3.5 as a yield cap.

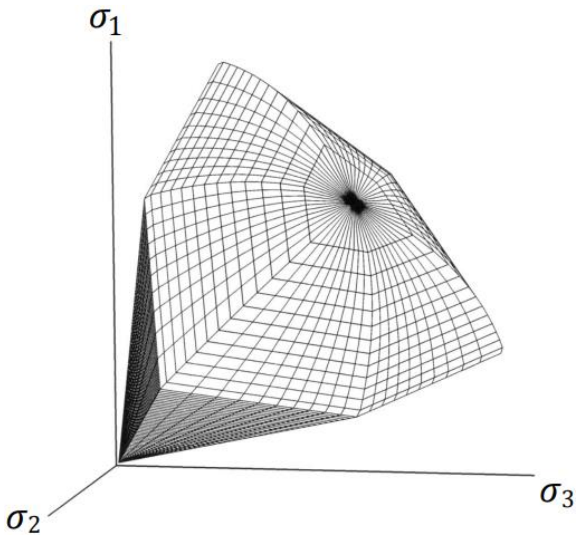

Figure 3.5. Principal stress space represents the total yield shape of HSM for cohesionless soil (Brinkgreve, 2002).

The hyperbolic relationship among vertical strain (ε_1) and deviatoric stress *(q)* in primary triaxial loading is a fundamental concept in the derivation of HSM. Standard drained triaxial measurements usually provide contours which might be characterized as follows:

$$-\varepsilon_1 = \frac{1}{E_i}\frac{q}{1 - q/q_a} \quad for: \; q < q_r \tag{3.2}$$

In this equation, q_a represents the approximate measure of the shear strength and E_i represents the desired starting stiffness.

E_i is connected to E_{50} through the following measures:

$$E_i = \frac{2E_{50}}{2 - R_f} \tag{3.3}$$

The final deviatoric stress, q_f, and the value q_a in Equation 3.2 are determined as follows:

$$q_f = (c\cot\varphi - \sigma_3')\frac{2\sin\varphi}{1 - \sin\varphi} \tag{3.4}$$

$$q_a = \frac{q_f}{R_f} \tag{3.5}$$

It is noted that σ_3' is frequently negative. The previous connection for q_f is obtained via the Mohr-Coulomb failure criteria, which includes the strength factors c and φ. shortly as $q = q_f$ the

collapse requirement is fulfilled and fully plastic area happens as MCM describes. For removing and adding stress pathways, alternate load-dependent stiffness parameter is employed:

$$E_{ur} = E_{\mathrm{ur}}^{ref}\left(\frac{c\cos\varphi - \sigma_3'\sin\varphi}{c\cos\varphi - p^{\mathrm{ref}}\sin\varphi}\right)^{\mathrm{m}} \tag{3.6}$$

Where, E_{ur}^{ref} represents the reference Young's modulus and reloading, which corresponds to the reference pressure p^{ref}.

In summary, HSM is substantially more efficient however more complicated than MCM; nevertheless, this ignores the potential for softness because of to ground dilatancy and the debonding impacts related to soft soil (Brinkgreve, 2002).

3.1.4. Modified Cam-Clay Model

Modified Cam-Clay Model (MCCM) is a commonly recognized model in worldwide ground (Brinkgreve, 2002). It was developed mainly for the simulation of almost generally consolidated ground. The above model was recently introduced in PLAXIS to enable comparison to other programs. The primary difference between MCCM and other soil models is that it takes into account the considerable volume change that happens when soft clays are compressed (Santamaria, 2015). MCCM is dependent on both strength and stiffness parameters, which are presented in Tables 3.3 and Table 3.4.

Table 3.3. Factors for stiffness of MCCM

Item	Symbol	Unit
Cam-Clay compression index	λ	[-]
Cam-Clay swelling index	K	[-]
Poisson's ratio	ν	[-]
Initial void ratio for loading / unloading	e_{init}	[-]

Table 3.4. Parameters for strength of MCCM

Item	Symbol	Unit
Tangent of the critical state line	M	[-]
Coefficient of lateral stress in normal consolidation derived from M	K_0^{nc}	[-]

As indicated in Equation 3.7 and Figure 3.6, MCCM assumes a logarithmic connection between void ratio *e* and mean stress effectiveness *p'* in virgin isotropic compression,

$$e - e^0 = -\lambda \, ln\left(\frac{P'}{P^0}\right) \quad \text{(virgin isotropic compression)} \tag{3.7}$$

Where, P^0 is the initial effective stress.

Furthermore, Equation 3.8 may be used to calculate the inclination of Figure 3.6's unloading-reloading line using Cam-Clay swelling index *(K)*.

$$e - e^0 = -K \, ln\left(\frac{P'}{P^0}\right) \text{ (isotropic unloading and reloading)} \tag{3.8}$$

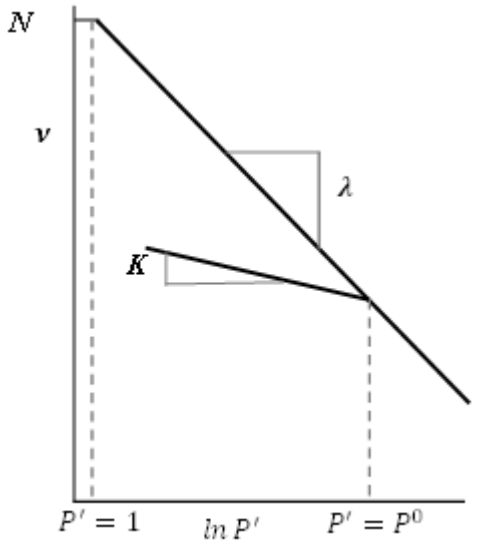

Figure 3.6. Cam-Clay linear normal compression and unloading-reloading lines (Brinkgreve, 2002)

Area function of MCCM is defined as follows:

$$f = \frac{q^2}{M^2} + P'(P' - P_P) \tag{3.9}$$

As seen in Figure 3.7, the yielding area *(f = 0)* is an elliptical in the *p′*-*q*-plane. The yielding area represents the limit area among elasticity stress regions. Stress routes inside this region only cause elastic strain stages, but stress lines which traverse it frequently cause simultaneous elastic and plastic strain increments (Brinkgreve, 2002). In the *p′*-*q′* plane, the highest point of the elliptical intersects an axis that may be represented as follows:

$$q = M\ P' \tag{3.10}$$

This line, known as the critical state line *(CSL)*, describes the relation among *p′* and ***q*** in a failure state. The value of the constant *M* is the tangent to the critical state line, determining how much the maximum deviatoric stress, *q*, relies on the effective stress, *p′*. Therefore, *M* might be considered as a friction constant. Furthermore, *M* defines the yielding area and effects the coefficient of lateral ground pressure K_0 in a properly consolidated stress state during 1-D compression.

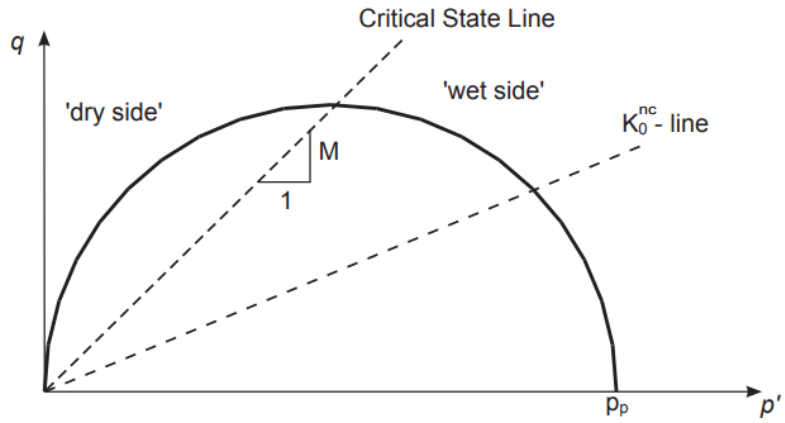

Figure 3.7. Yielding area of Modified Cam-Clay model in p'-q – plane (Brinkgreve, 2002)

To achieve the appropriate shear strength, the parameter *M* should be dependent on the friction angle *(φ)*. Therefore, the numerical value of *M* could be determined by *φ*:

$$M = \frac{6 \sin \varphi}{3 - \sin \varphi} \tag{3.11}$$

3.1.5. Soft Soil Model

Soft Soil Model (SSM) was designed for soil that is normally consolidated with significant compressibility, which include clays and peat (Brinkgreve, 2002). This model has its theory derived from Cam-Clay and Mohr-Coulomb Models. The failure pattern model is represented by Mohr Coulomb criteria and logarithmic relations, which are comparable to the Cam-Clay model. During basic stress conditions, the plastic characteristicr of SSM under general stress is determined by three compression yielding factors and three Mohr Coulomb yielding factors. The fundamental SSM parameters utilized by PLAXIS are summarized in Table 3.5. Modified compression and swelling indices are utilized to accurately represent soil stiffness characteristics. The relationship between modified compression and swelling indices can be established by using Equations 3.17 and Equations 3.18 or by using normalized compression index (C_C) and swelling index (C_S) according to Equations 3.19 and Equations 3.20. There are other advanced parameters that can be determined, nevertheless, they were not employed for the purpose of this study.

Table 3.5. Fundamentals parameter of SSM

Item	Symbol	Unit
Modified compression index	λ^*	[-]
Modified swelling index	K^*	[-]
Cohesion	c	$[\mathrm{kN/m^2}]$
Friction angle	φ	[°]
Dilatancy angle	ψ	[°]

SSM considers a logarithmic relationship among volumetric strain *(εv)* and effective stress (p'), as observed in Equation 3.12 and Figure 3.8.

$$\varepsilon_v - \varepsilon_v^0 = -\lambda^* \, ln\left(\frac{P'}{P^0}\right) \tag{3.12}$$

Where the modified compression index *(λ*)*, defined as the inline of the virgin compression alignment, determines the material's compressibility under first primary loading.

In SSM, the slope of the isotropic unloading-reloading alignment can be defined by calculating the modified swelling index of the soil *(K*)* because this parameter corresponds to volumetric strain, which can be described as follows:

$$\varepsilon_v^e - \varepsilon_v^{e0} = -K^* \, ln\left(\frac{P'}{P^0}\right) \tag{3.13}$$

SSM can simulate soil characteristics in general conditions of stress. To clarify, this part restricts to triaxial loading settings when $\sigma_2' = \sigma_3'$. The yield function *(f)* describes in Equation 3.14, and Figure 3.9 shows how it is physically expressed.

$$f = \bar{f} - P_P \tag{3.14}$$

Where, $\bar{f}$ represents the stress state $(P', \tilde{q})$, and P_P represents the pre-consolidation stress, that is affected by plastic strain.

$$\bar{f} = \frac{\tilde{q}^2}{M^2(P' + c\cot\varphi)} + P' \tag{3.15}$$

$$P_P = P_P^0 \exp\left(\frac{-\varepsilon_v^P}{\lambda^* - K^*}\right) \tag{3.16}$$

Where, $\tilde{q}$ is identical deviatoric stress quantity as described for the cap yielding area in HSM.

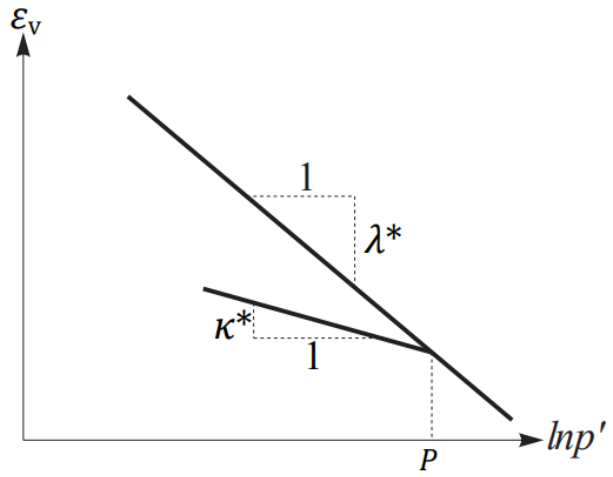

Figure 3.8. Logarithmic relationship among volumetric strain and mean effective stress (Brinkgreve, 2002)

As SSM is somewhat aaccording to Mohr-Coulomb collapse criteria, failure is not always connected to critical state, however more importantly to the strength factors of friction angle and cohesion, that deviate from the alignment created by *M* parameter (Brinkgreve, 2002). Modifications based on pre-consolidation stress are then done by setting a yield threshold. Consider the yielding cap and the expansion that is permitted in primary compression as shown in Figure 3.9 when contrasted with the yielding limit created in HSM.

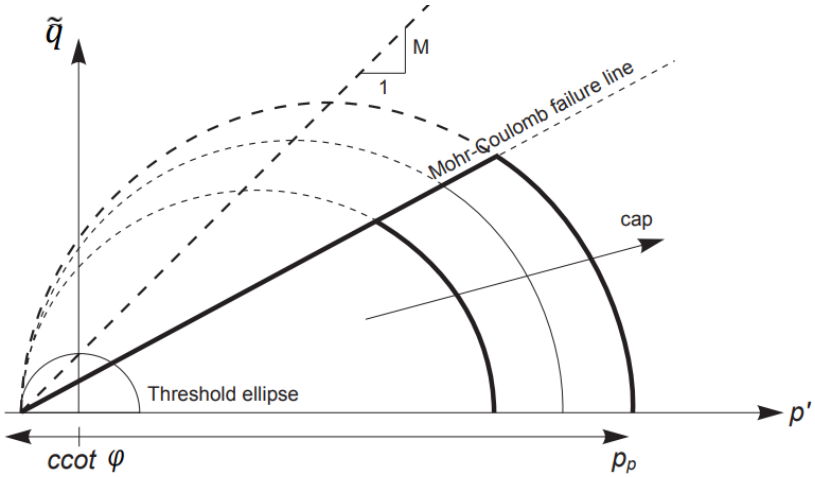

Figure 3.9. Yield surface of SSM in p'- q-plane (Brinkgreve, 2002)

Finally, the full SS yield curve in 3-D main stress area as illustrated in Figure 3.10 demonstrating the possibility of application of an extended limit to represent soft ground throughout initial compression.

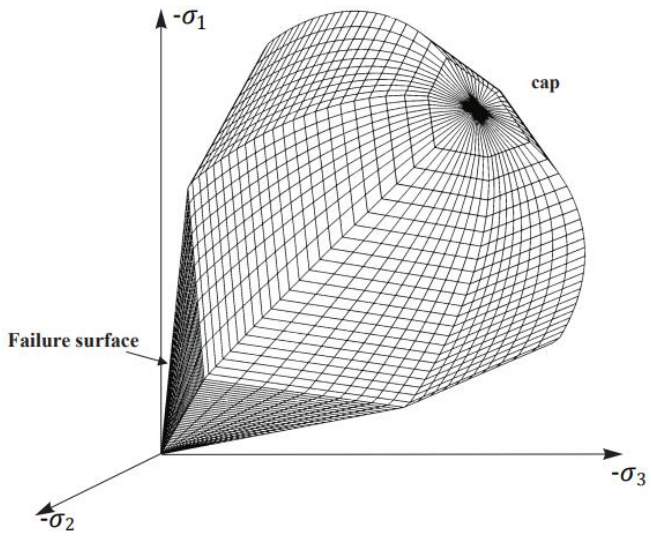

Figure 3.10. Overall yielding curve of SSM in major stress area (Brinkgreve, 2002)

$$\lambda^* = \frac{\lambda}{1+e} \tag{3.17}$$

$$K^* = \frac{K}{1+e} \tag{3.18}$$

$$\lambda^* = \frac{C_C}{2.3\ (1+e)} \tag{3.19}$$

$$K^* = \frac{2C_S}{2.3\ (1+e)} \tag{3.20}$$

3.1.6. Soft Soil Creep Model

As the name indicates, Soft Soil Creep Model (SSCM) is a modified version of SSM that takes into consideration creep. Creep is defined as continuous displacement with uniform pressure, which is closely connected to secondary compression and, as a result, has time-dependent characteristic. Soils that are soft and/or overconsolidated are especially susceptible to this type of behavior. Soft ground with high initial compression can often contain a substantial number of secondary compression, which is sometimes considered to represent a proportion of primary compression. This is particularly true for clays, silts, and peat that are typically consolidated beneath embankment stress.

The stiffness and strength characteristics of SSM apply to SSCM, through the inclusion of the modified creep index *(μ^*)* to describe the time-dependent secondary compression of ground. To calculate the modified creep index, it is necessary to combine the normalized secondary compression index (C_α) and the void ratio obtained from oedometer experimental using Equation 3.21.

$$\mu^* = \frac{C_\alpha}{2.3(1+e)} \tag{3.21}$$

In conclusion, the constitutive models accessible in PLAXIS can be employed for a variety of objectives and applications; nevertheless, the model's performance and effectiveness depends on the user's knowledge of fundamental theory.

3.2. Methodology: matching Methods

As mentioned previously, throughout consolidation of soil with PVD, water moves horizontally and vertically, demanding 3D numerical modeling to estimate the impacts of PVDs (Yildiz, 2009). Nevertheless, 3D modeling takes an extensive period of time and requires a powerful computer. Fort his reason, number of studies have developed matching approaches to transform 3D to 2D PVD analysis using the unit cell idea. Matching approaches could be accomplished through changing the system's geometry or permeability of the ground. The concept of these matching methods are discribed below:

3.2.1. Method I

Shinsha et al. (1982) became the initial researchers to offer a valid matching technique for converting an axisymmetric module to plane strain settings. They presented a method for comparing the mean degree of horizontally consolidation which develops under axisymmetric settings with what is seen in a plane strain assessment for a specific level of consolidation. The identical value of permeability was determined assuming that the duration needed to accomplish 50% consolidation in the two designs was identical. They presented the following matching formula:

$$\frac{k_{pl}}{k_{ax}} = \left(\frac{B}{D_e}\right)^2 \frac{T_{hp50}}{T_{h50}} \tag{3.22}$$

Where, *B* is the half of drain distance in the plane strain, k_{pl} is the permeability in plane-strain state, k_{ax} is the permeability in axisymmetric circumstance, T_{h50} is the time factor for 50% consolidation of an axisymmetric because of the impact of PVD, that is available to be determined using Equation 3.23, and T_{hp50} = 0.197 is an unrestricted time factor for 50% consolidation calculated by 1-D consolidation concept of Terzaghi.

$$\bar{U}_{hp} = 1 - \frac{\bar{u}}{u_0} = 1 - \ exp\left(-\frac{8T_h}{\mu}\right) \tag{3.23}$$

Where,

$$\mu = l_n\left(\frac{n}{s}\right) + \frac{k_h}{k_s} l_n(s) - \frac{3}{4} + \pi z(2L - z)\frac{k_h}{q_w} \tag{3.24}$$

The impact of disturbed area simply is expressed as:

$$\mu = l_n\left(\frac{n}{s}\right) + \frac{k_h}{k_s} l_n(s) - \frac{3}{4} \tag{3.25}$$

The impact of well resistance simply is provided through:

$$\mu = l_n(n) - \frac{3}{4} + \pi z(2L - z)\frac{k_h}{q_w} \tag{3.26}$$

When both disturbed are and well resistance are neglected, the following factors become:

$$\mu = l_n(n) - \frac{3}{4} \tag{3.27}$$

3.2.2. Method II

Through modifying Hansbo's (1981) concept for the plane strain situation, Hird et al. (1992) demonstrated that the mean rates of consolidation *U*, any given deep and period in the two-unit structures were conceptually similar in without the presence of well resistance assuming

$$\frac{k_{pl}}{k_{ax}} = \frac{2B^2}{3R^2\left[l_n\left(\frac{R}{r_s}\right) + \left(\frac{k_{ax}}{k_s}\right) l_n\left(\frac{r_s}{r_w}\right) - \frac{3}{4}\right]} \tag{3.28}$$

While the abbreviations *ax* and *pl* represent axisymmetric and plane-strain circumstances, correspondingly.

Matching could be accomplished by changing drain distance and/or permeability of the ground. Equation 3.28 is used to compute the identical plane-strain permeability k_{pl} when a predetermined amount of *B* has been chosen. It should be noted that geometrical matching may be established by inserting $k_{ax} = k_h$ in Equation 3.28, while permeability matching could be accomplished by replacing *B* = *R*.

3.2.3. Method III

Bergado et al. (1994) proposes transformed permeability under disturbed area impact, according to the requirement for an equivalent rate of discharge in the two systems, using the idea that the coefficient of permeability is not dependent of the degree of water seepage. Within this method, the permeability of the ground along drain walls in the 2-D design is changed to achieve the identical discharge in the actual situation. The upward circulation in both approaches could be considered to be similar. Following that, just the radial flow must be transformed.

$$k_m = \frac{\pi(1-a_s)D}{2S\, l_n(\alpha\, n)}k \tag{3.29}$$

Wherein, $n = D/d$; $\alpha = D_e/D$; $S = D$ and $\alpha = 1.05$ for rectangular design; $S = 0.866D$ and $\alpha = 1.13$ for triangular design.

When the disturbed area impact is considered, the numerical value of *k* in Equation 3.29 could be substituted by k_e, in which k_e represents an identical permeability with disturbed area impacts.

$$k_e = \frac{k\, l_n(\alpha\, n)}{l_n\left(\frac{\alpha D}{d_s}\right) + R_s l_n\left(\frac{d_s}{d_w}\right)} \tag{3.30}$$

Where, $R_s = k/k_s$, k and k_s are the radial permeabilities in the untouched and disturbed area, correspondingly; a, n, and D have already been determined, and the remaining values are presented in Figure 3. 14. Changing *k* in Equation 3.25 with the amount of k_e from Equation 3.30 yields the quantity of radial transformed permeability for the 2-D approach, k_m, as a function of the radial permeability of natural ground, *k*, as following illustrated.

$$k_m = \frac{\pi D(1-a_s)k}{2S\left[l_n\left(\frac{\alpha D}{d_s}\right) + R_s\, l_n\left(\frac{d_s}{d_w}\right)\right]} \tag{3.31}$$

3.2.4. Method A

Indraratna et al. (1997) changed the permeability of the interactions to convert the vertical drain scheme shown in Figure 3.11 become a parallel drain wall. They assumed that the half-widths of unit cell *B*, drains b_w, and disturbed area b_s are the same like their axisymmetric radius *R*, r_w and r_s, respectively. They suggested a certain correlation among k_{hp} and k_{sp}:

$$\frac{k_{sp}}{k_{hp}} = \frac{\beta}{\frac{k_{hp}}{k_h}\left[l_n\left(\frac{n}{s}\right) + \left(\frac{k_h}{k_s}\right) l_n(s) - 0.75\right] - \alpha} \tag{3.32}$$

Where, $n = D_e/d_w$ and $s = r_s/r_w$ as D_e, d_w and r_s are the identical sizes of the unit cell, the drain, and the radius disturbed area, correspondingly, k_h the radial permeability of the ground in its natural state k_s is the radial permeability of disturbed ground, and the symbol p indicates the plane-strain situation.

The constraints α and β can be connected as follows:

$$\alpha = \frac{2}{3} - \frac{2b_s}{B}\left(1 - \frac{b_s}{B} + \frac{{b_s}^2}{3B^2}\right) \tag{3.33}$$

$$\beta = \frac{1}{B^2}(b_s - b_w)^2 + \frac{b_s}{3B^3}\left(3{b_w}^2 - {b_s}^2\right) \tag{3.34}$$

Nevertheless, the appropriate part of Equation 3.32 consists of the expression (k_{hp}/k_h), consequently obtaining the quantity of k_{hp}, requires a certain form of estimate. They presented an additional assumption of (k_{hp}/k_h), which ignores both the disturbed area impact and well resistance:

$$\frac{k_{hp}}{k_h} = \frac{0.67}{[l_n(n) - 0.75]} \tag{3.35}$$

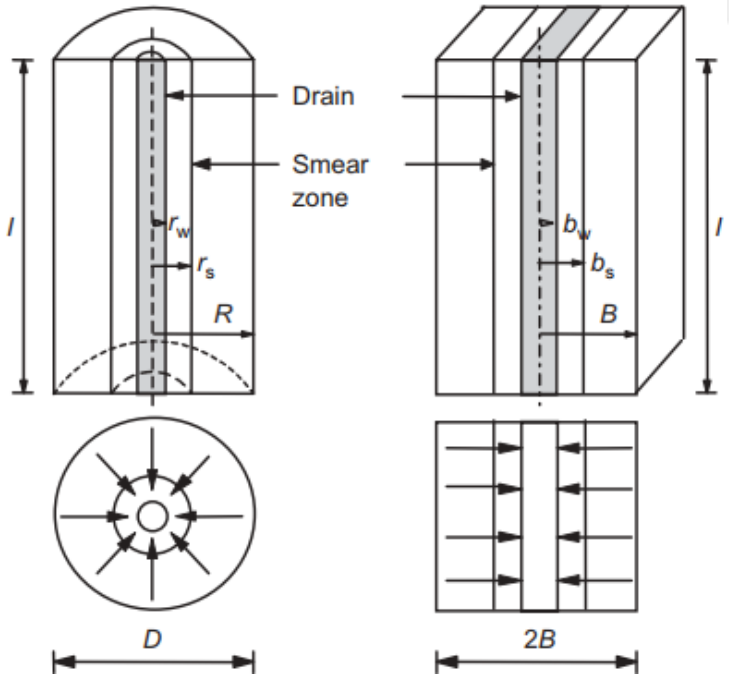

(a) (b)

Figure 3.11. Matching approach concept. (a) Axisymmetric; (b) Plane-strain (Indraratna et al. 1997)

3.2.5. Method B

Chai et al. (2001) provided an affordable estimation approach for analyzing the effects of PVD. This method produces a prediction of vertically permeability that approximately captures both the upward flow of natural ground and the horizontal permeability caused by PVD (Chai et al., 2001). The corresponding vertical permeability (k_{ve}) was computed utilizing the same typical degree of consolidation as in the 1D situation. The identical vertically permeability k_{ve} could be expressed using the following formula:

$$k_{ve} = \left(1 + \frac{2.5l^2}{\mu {D_e}^2}\frac{k_h}{k_v}\right)k_v \tag{3.36}$$

Where, k_v is the vertical permeability, l is the length of the drain, and, D_e is the identical size of the unit cell. The significance of μ is defined as follows:

$$\mu = l_n\left(\frac{n}{s}\right) + \frac{k_h}{k_s}l_n(s) - \frac{3}{4} + \frac{\pi 2l^2 k_h}{3q_w} \tag{3.37}$$

Where, $n = D_e/d_w$ (drain equivalent diameter), $s = d_s/d_w$ (identical size of the disturbed area) and L is length of the drain.

3.2.6. Method C

Ba-Phu (2019) provided an analogous plane-strain (2D) model for PVD-reinforced soil that accounted for the effects of the disturbed area. He determines the equivalent radial permeability of the soft ground using the plane-strain theory outlined below:

$$k_{hp} = -\frac{\pi B \bar{U}_h k_h}{8 T_h} \tag{3.38}$$

Where, $\bar{U}_h$ is the amount of horizontal consolidation of the soft ground, B is the half width of the plane-strain unit cell, k_h is the radial permeability of natural ground, and T_h is the time factor of radial consolidation, that was found utilizing the method of Hansbo (1979). Equation 3.37 describes the magnitude of μ. The time factor T_h was developed as follows:

$$T_h = -\frac{\mu}{8} l_n (1 - \bar{U}_h) \tag{3.39}$$

Where, by replacing Equation 3.39 into Equation 3.38 yields the corresponding radial permeability of ground in 2D could be described as following:

$$k_{hp} = -\frac{\pi B \bar{U}_h k_h}{\mu l_n (1 - \bar{U}_h)} \tag{3.40}$$

3.3. Experimental of large-scale consolidometer

Saowapakpiboon et al. (2011) developed a consolidometer experimental to investigate the effect of a PVD on soft ground. The research employed ground specimens collected in the Second Bangkok International Airport (SBIA) region, that is situated around 30 kilometers south of Bangkok. Specimen were retrieved at a depth of 3.0 to 4.0 meters below an empty crust stratum. The ground specimens generated in this manner were determined to be roughly 0.7 m in thickness, as illustrated in Figure 3.12. Throughout the consolidation assessment, 100 kPa stress was put on directly to the soil's surface and time-varying settlements were recorded. Nevertheless, as stated by Bergado (2013), a shaft was put in the middle and upper portion of the cylinders, and the actual normal pressure produced on the simulated area was roughly 95 kPa. Throughout consolidation, outflow was permitted only on the top layer, with the bottom side restricted to drainage systems.

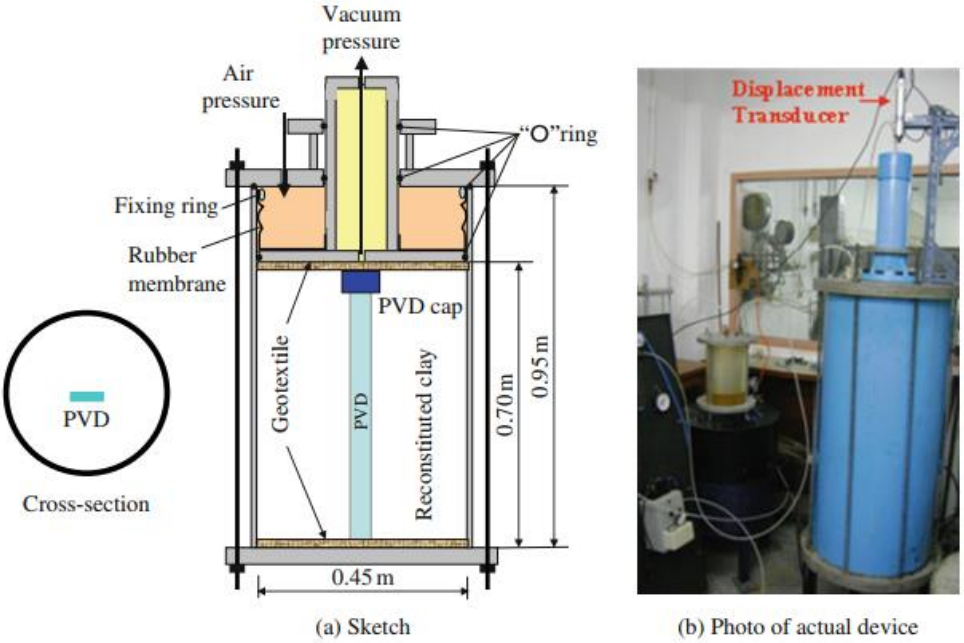

Figure 3.12. Consolidometer experimental of PVD (Saowapakpiboon et al., 2011).

3.3.1. Characteristics of the ground and experimental methodologies

Table 3.6 displays the ranking parameters of the ground utilized in the consolidometer investigation conducted in the laboratory. Throughout the consolidometer test, CeTeau's CT-D911 type PVD items was employed. Table 3.7 illustrates the parameters of PVD material utilized in the experimental.

Table 3.6. Properties of soft ground utilized (Saowapakpiboon et al., 2011)

Characteristics	Measure
Liquid limit (%)	102.24
Plastic limit (%)	39.55
Water content (%)	112.69
Plasticity index	62.69
Unit weight (kN/m³)	14.70
Specific gravity	2.66

Table 3.7. Properties of the core used (Saowapakpiboon et al., 2011)

Drainage	Polypropylene
Channels	44
Filter	Polypropylene
Weight (g/m)	78
Width, W (mm)	100
Thickness, td (mm)	3.5

3.3.2. Parameters of the ground model and characteristics of PVD

The ground specimen has been simulated utilizing an advanced modeling known as SSM. Table 3.8 presents the model values obtained from experimental results, while Table 3.9 provides PVD properties. The experiment and corresponding permeability in plane strain conditions are described in Table 4.1 below.

Table 3.8. SSM parametric utilized in FEA (Saowapakpiboon et al., 2011)

H (m)	γ (kN/m³)	K*	λ*	ν	e_0
0.70	14.70	0.0167	0.173	0.3	2.29

Table 3.9. Properties of PVD utilized throughout consolidation (Saowapakpiboon et al., 2011)

Parameters	Symbol	Unit	Measure
Equivalent diameter of PVD	d_w	m	0.0268
Diameter of disturbed are	d_s	m	0.087
Discharging capacity	q_w	m³/year	100
Ratio of k_h to k_s	k_h/k_s	–	3

Table 3.10. Contrast of soft ground permeability in plane-strain and in the experimental setting

		Identical permeability in plane-strain			
Experimental		Method A		Method B	Method C
k_h (m/day)	k_v (m/day)	k_{pl} (m/day)	k_m (m/day)	k_m (m/day)	k_m (m/day)
6.30×10^{-5}	6.30×10^{-5}	2.04×10^{-5}	4.18×10^{-6}	1.49×10^{-4}	7.26×10^{-6}

3.4. Case study 1

The case study 1 investigated in this study is situated in eastern China, namely Hangzhou-Ningbo. Hangzhou-Ningbo (HN) road goes across the southern sea of Hangzhou Bay. It starts in Hangzhou, capital of Zhejiang, and concludes in Ningbo, the province's major coastal city. HN road is approximately 145 kilometers long, with approximately 92 kilometers running in soft ground. As reported by Wang (1998), 12 full test embankments having a total length of 3.15 km were built and researched in order to obtain reliable natural data. As a result, this study represents one of these test embankments that were built on top of PVD-reinforced soft ground.

3.4.1. Properties of the ground embankment

According to Ba-Phu (2019), the structure of the ground of the eastern China embankment could be characterized by the following characteristics: the highest strata of ground comprised of a thinly weathered crusted (TC) which varied from 1 to 1.5 m high over a 4 m thick silty clay stratum (SC1). The next level is extremely soft mucky clay (MC), having a total measurement of around 10 m. The following layer is also a soft clay, which is called mucky-silty clay (MSC), having a typical depth of around 4 m The next layer down is an average to stiff silty clay stratum (SC2) that is approximately 3 to 5 m deep. Beneath the previous level, that is found an additional of clayey sand. Before embankment building, the ground surfaces were slightly to highly consolidated. The top crust exhibited an overconslidated ratio (OCR) of approximately 5. The level of groundwater was around 1,5 m below the ground area. Figure 3.13 depicts the sectional shape and composition of the ground of embankment using PVD-reinforced subsurface. The soft ground was layered via 0,5 m thin sandy material, followed by stone fill material that have a unit weight of roughly 20 kN/m^3. The embankment has an altitude of 5.88 meters. PVD was built in a triangle layout approximately 1,5 m spacing for a total depth of 19 m.

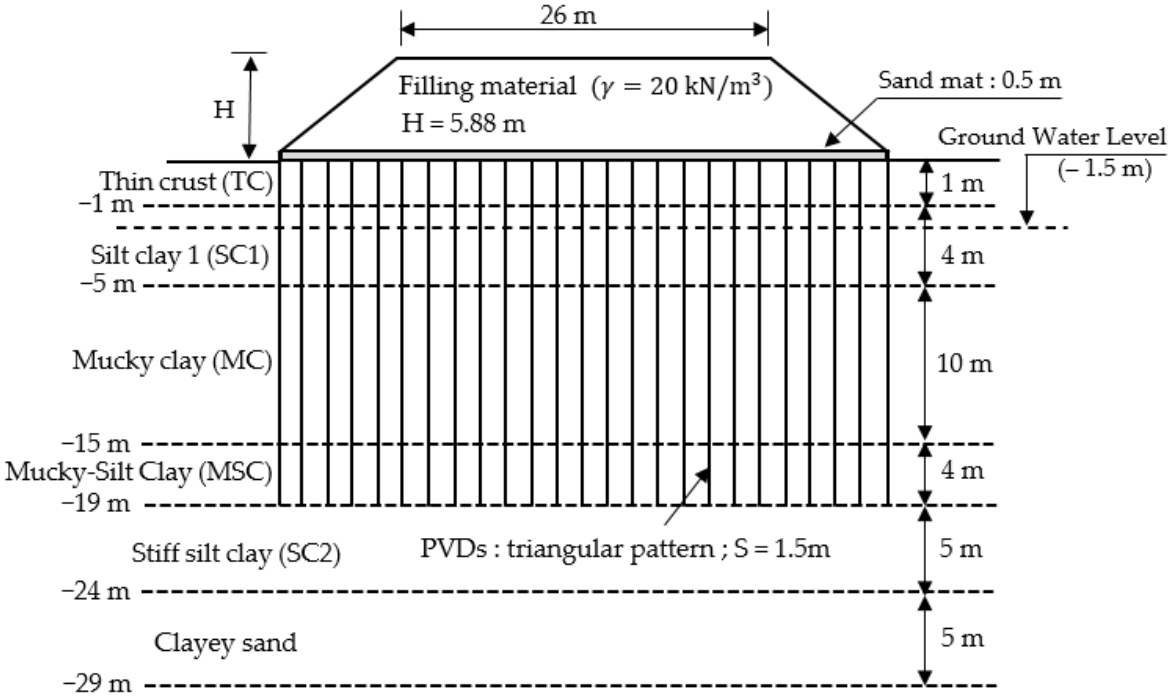

Figure 3.13. Cross-sectional of embankment with the location of PVD (Ba-Phu, 2019)

3.4.2. Model settings of soft ground, PVD properties and equivalent permeability

Soft grounds were simulated with SSM as indicated in Table 3.10 using PLAXIS 2D Version 8.6 (Brinkgreve, 2002) program. The fill material was represented utilizing MCM with Young's modulus E = 30000 kPa and Poisson's ratio 0.2. Table 3.11 presents the parameters of PVD utilized in the test embankment. Table 4.2 summarizes the identical permeability in plane-strain and field values obtained from Ba-Phu (2019).

Table 3.11. Model settings of ground clay strata (Ba-Phu, 2019)

Layer	H (m)	E (kPa)	γ_{sat} (kN/m³)	K*	λ*	ν	e_0	C_k	OCR
TC	1	–	19.3	0.004	0.044	0.3	0.81	0.365	5
SC1	4	–	18.5	0.008	0.077	0.35	1.07	0.482	1
MC	10	–	17.3	0.012	0.119	0.35	1.36	0.612	1
SMC	4	–	17.9	0.009	0.086	0.35	1.1	0.495	1
SC2	5	–	19.3	0.006	0.055	0.3	0.81	0.365	1
CS	5	25 000	19.5	–	–	0.25	–	–	–
Fill	5.88	30 000	20	–	–	0.2	–	–	–

Table 3.12. PVD characteristics employed for test embankment (Ba-Phu, 2019)

Item	Symbol	Unit	Measure
Equivalent diameter of PVD	d_w	m	0.053
Diameter of influencing area	d_e	m	1.58
Spacing of PVD	S	m	1.5
Diameter of disturbed area	d_s	m	0.355
Ratio of k_h over k_s on site	$(k_h/k_s)f$	–	13.8
Longer of PVD	L	m	19
Discharge capacity	q_w	m^3/year	100

Table 3.13. Contrast of soft ground permeability in plane-strain and in the field

			Identical permeability in plane-strain			
	Field		Method A		Method B	Method C
Layers	k_h (m/day)	k_V (m/day)	k_{hP} (m/day)	k_{sp} (m/day)	k_{ve} (m/day)	k_{hp} (m/day)
TC	3.03×10^{-3}	3.03×10^{-3}	7.68×10^{-4}	3.56×10^{-5}	3.41×10^{-2}	1.46×10^{-4}
SC1	5.60×10^{-4}	2.24×10^{-4}	1.42×10^{-4}	6.57×10^{-6}	7.36×10^{-2}	3.34×10^{-5}
MC	2.54×10^{-3}	1.69×10^{-3}	6.44×10^{-4}	2.98×10^{-5}	2.88×10^{-2}	1.27×10^{-4}
SMC	2.06×10^{-3}	1.03×10^{-3}	5.22×10^{-4}	2.42×10^{-5}	2.39×10^{-2}	1.07×10^{-4}
SC2	3.90×10^{-4}	1.82×10^{-4}	–	–	–	–
SC	2.60×10^{-2}	2.60×10^{-2}	–	–	–	–
Fill	2.0×10^{-1}	2.0×10^{-1}	–	–	–	–

3.5. Case study 2

The case study 1 investigated in this study is the full test embankment in Dover New Hampshire. In 2012, New Hampshire Department of Transportation constructed full embankment in Dover, NH, employing PVD to stabilize weak ground. The presentation of Dover point test embankment is shown in Figure 3.14. Before starting construction, University of New Hampshire (UNH) carried out field vane, flat plate dilatometer, and piezocone investigation, as well as soil sample collection for laboratory consolidation experiments, to analyze the field and evaluate the parameters of the soft ground (Getchell, 2013; Santamaria, 2015). Field measurement and laboratory tests are used in this thesis to analyze the efficiency and performance of matching methods.

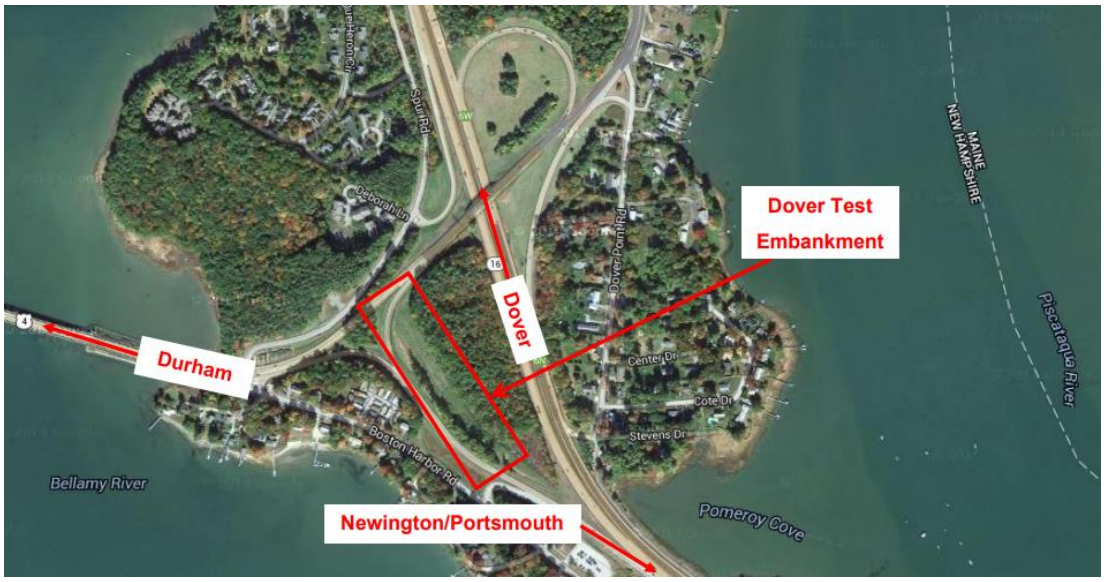

Figure 3.14. Presentation of Dover Point the test embankment in Dover, NH (Santamaria, 2015)

3.5.1. Geometry and characteristics of the embankment

The construction of the Newington-Dover project's embankment was built with PVDs to speed up the vertical displacement of the underlying clay. Test embankment was built with 5 different segment geometries and varying PVD spacing. The length of every segment is approximately 61 m and they have a fill height of 3.7 m with inclination of 2H:1V, and only difference being of Segment 4, that features a fill material of 5.5 m and inclination of 1.5H:1V. The distances of PVDs between the embankment segments are not uniform; Segment 1 has a spacing of roughly 1.8 m, whereas Segments 2, 3, and 4 each maintain a spacing of 3 m. In comparison, Segment 5 has a larger spacing of 4.2 m. This examination focuses particularly on three segments: Segment 1, Segment 4, and Segment 5, due to their distinct characteristics concerning spacing and fill height, which are notably different from one another.

The soil conditions discovered in the field borings constitute the following types of layers: fill, alluvium, upper marine deposit, lower marine deposit, and glacial till. Figure 3.15 presents the soil profile and related thicknesses of each segment determined by geologists at the NHDOT (Getchell, 2013; Santamaria, 2015). The upper and lower marine layers, which comprise of soft and very soft silty clay, are the most important to settlement. Table 4.3 and Table 4.4 summarizes SSCM and MCCM model parameters which are calculated from SSCM.

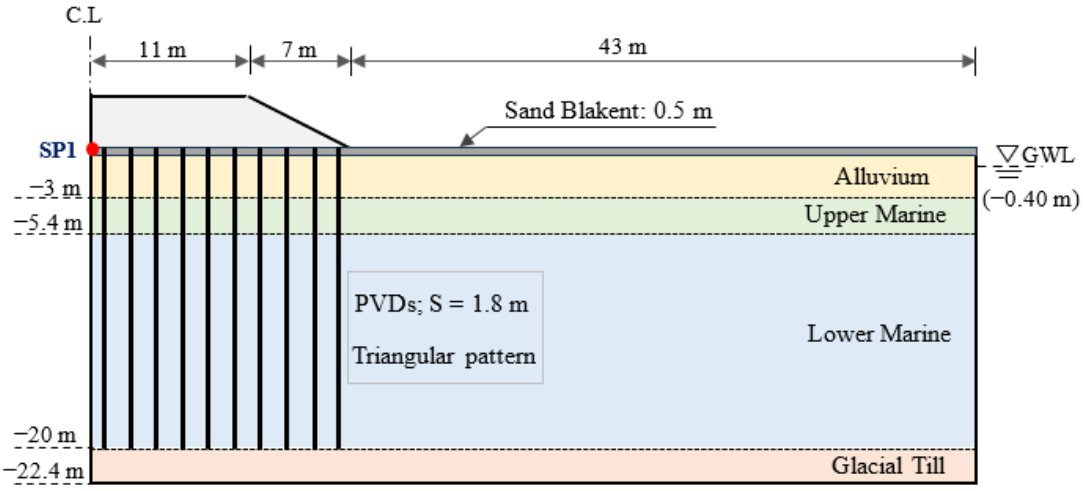

(a)

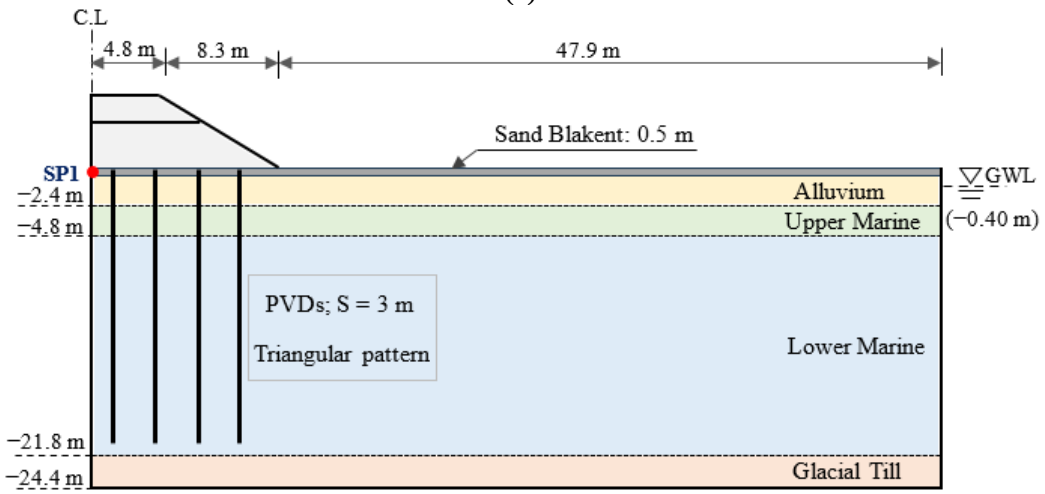

(b)

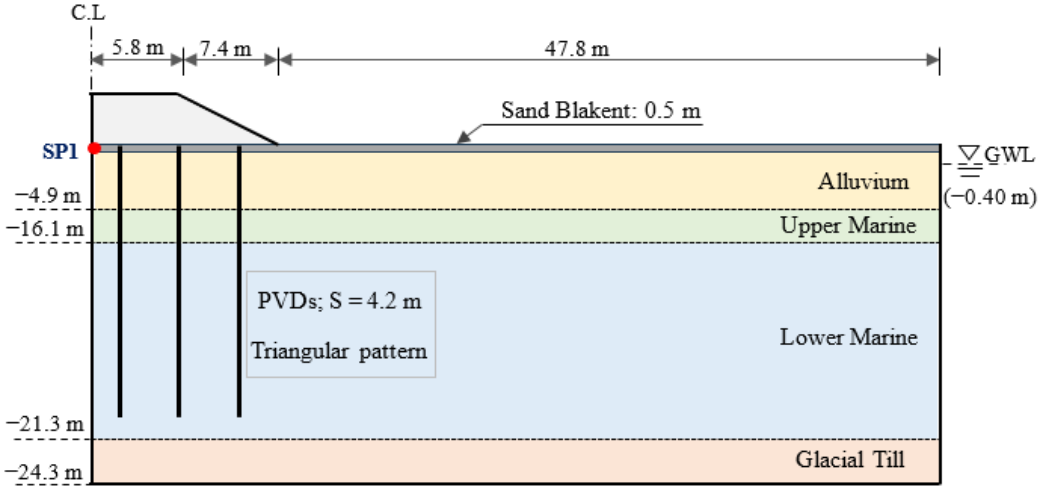

(c)

Figure 3.15. Cross-Section of test embankment for the Newington-Dover for all segment geometries. (a) Segment 1, (b) Segment 4, (c) Segment 5.

Table 3.14. Model parameters of soft clay in numerical analysis (Getchell, 2013; Santamaria, 2015)

Layers	γ_{sat} (kN/m^3)	λ^*	k^*	μ^*	φ (°)	ψ (°)	c (kN/m^3)	e_0	OCR	E_{50}	E_{oed}	E_{ur}
Lower Marine	17.3	0.36	0.05	1.976×10^{-3}	22.5	–	0.048	1.2	1.2	–	–	–
Apper Marine	18.5	0.33	0.05	2.070×10^{-4}	25	–	0.240	1.1	3.7	–	–	–
Alluvium	20	–	–	–	37.5	7.5	–	0.5	6	35000	35000	104858
Sand Blanket	20	–	–	–	35	5	–	0.5	1	30021	30021	90015
Glacial Till	20	–	–	–	40	10	–	0.5	6.2	39980	39980	120179
Fill	18.85	–	–	–	40	10	–	0.5	1	39980	39980	120179

Table 3.15. MCCM parameters of soft clay in numerical analysis

Layers	γ_{sat} (kN/m^3)	λ	K	φ (°)	ψ (°)	c (kN/m^3)	e_0	OCR	E_{50}	E_{oed}	E_{ur}
Lower Marine	17.3	0.156	0.044	22.5	–	0.048	1.2	1.2	–	–	–
Apper Marine	18.5	0.143	0.0441	25	–	0.240	1.1	3.7	–	–	–
Alluvium	20	–	–	37.5	7.5	–	0.5	6	35000	35000	104858
Sand Blanket	20	–	–	35	5	–	0.5	1	30021	30021	90015
Glacial Till	20	–	–	40	10	–	0.5	6.2	39980	39980	120179
Fill	18.85	–	–	40	10	–	0.5	1	39980	39980	120179

3.5.2. Characteristics of PVD utilized in test embankment and equivalent permeability

The characteristics of PVD utilized for test embankment is presented in Table 3.12. The equivalent unit cell diameter (d_e) and drain spacing ratio (n) of the test embankment are summarizes in Table 3.13. Table 4.6, Table 4.7 and Table 4.8 summarizes the field and equivalent permeability values for three distinct matching approaches for each Segment.

Table 3.16. Characteristics of PVD used for test embankment (Getchell, 2013; Santamaria, 2015)

Item	Symbol	Unit	Measure
Width	a	m	0.101
Thickness	b	m	0.003
Equivalent Drain diameter	d_w	m	0.066
Diameter of disturbed area	d_s	m	0.49
Ratio of k_h over k_s in field	k_h/k_s	–	3
Discharge capacity	q_w	m^3/year	100

Table 3.17. Equivalent unit cell diameter and drain spacing ratio of test embankment

Spacing of PVD triangular pattern	S	1.8	3	4.2	[m]
Equivalent unit cell diameter	d_e	1.89	3,15	4.41	[m]
Equivalent unit cell radius	r_e	0.945	1.575	2.25	[m]
Drain spacing ratio	n	28.6 4	47.73	66.8 2	[-]

Table 3.18. Field and identical permeability of soft ground for segment 1

			Identical permeability of ground		
	Field		Method I	Method II	Method III
Layers	k_h (m/day)	k_v (m/day)	k_{pl} (m/day)	k_{pl} (m/day)	k_m (m/day)
Lower Marine	6.10×10^{-6}	4.57×10^{-5}	4.75×10^{-7}	6.15×10^{-7}	2.69×10^{-6}
Upper Marine	1.22×10^{-5}	2.15×10^{-4}	9.51×10^{-7}	1.23×10^{-6}	5.38×10^{-6}
Alluvium	2.48×10^{-1}	2.48×10^{-1}	1.93×10^{-2}	2.50×10^{-2}	1.09×10^{-1}
Sand Blanket	1.00×10^{0}	1.00×10^{0}	7.80×10^{-2}	1.01×10^{-1}	4.41×10^{-1}
Glacial Till	6.00×10^{-1}	6.00×10^{-1}	–	–	–
Fill	12×10^{-2}	12×10^{-2}	–	–	–

Table 3.19. Field and identical permeability of soft ground for segment 4

		Identical permeability of ground		
	Field	Method I	Method II	Method III

Layers	k_h (m/day)	k_v (m/day)	k_{pl} (m/day)	k_{pl} (m/day)	k_m (m/day)
Lower Marine	6.10×10^{-6}	4.57×10^{-5}	4.41×10^{-7}	5.71×10^{-7}	4.26×10^{-6}
Upper Marine	1.22×10^{-5}	2.15×10^{-4}	8.83×10^{-7}	1.14×10^{-6}	8.52×10^{-6}
Alluvium	2.48×10^{-1}	2.48×10^{-1}	1.79×10^{-2}	2.32×10^{-2}	1.73×10^{-1}
Sand Blanket	1.00×10^{0}	1.00×10^{0}	7.24×10^{-2}	9.36×10^{-2}	6.99×10^{-1}
Glacial Till	6.00×10^{-1}	6.00×10^{-1}	–	–	–
Fill	12×10^{-2}	12×10^{-2}	–	–	–

Table 3.20. Field and identical permeability of soft ground for segment 5

			Identical permeability of ground		
	Field		Method I	Method II	Method III
Layers	k_h (m/day)	k_v (m/day)	k_{pl} (m/day)	k_{pl} (m/day)	k_m (m/day)
Lower Marine	6.10×10^{-6}	4.57×10^{-5}	4.21×10^{-7}	5.45×10^{-7}	5.76×10^{-6}
Upper Marine	1.22×10^{-5}	2.15×10^{-4}	8.43×10^{-7}	1.09×10^{-6}	1.15×10^{-5}
Alluvium	2.48×10^{-1}	2.48×10^{-1}	1.71×10^{-2}	2.22×10^{-2}	2.34×10^{-1}
Sand Blanket	1.00×10^{0}	1.00×10^{0}	6.91×10^{-2}	8.93×10^{-2}	9.45×10^{-1}
Glacial Till	6.00×10^{-1}	6.00×10^{-1}	–	–	–
Fill	12×10^{-2}	12×10^{-2}	–	–	–

4. RESULTS AND DISCUSSIONS

4.1. FEA for consolidometer experimental

Throughout the numerical simulation, the bottom of the system was fixed for horizontal and vertical movement ($u_x = u_y = 0$). Moreover, radial movements were closed along the right and left borders ($u_x = 0$) as shown in Figure 4.1a. The bottom side was closed to water flow, and the lower limit defines the level of groundwater as illustrated through Figure 4.1c.

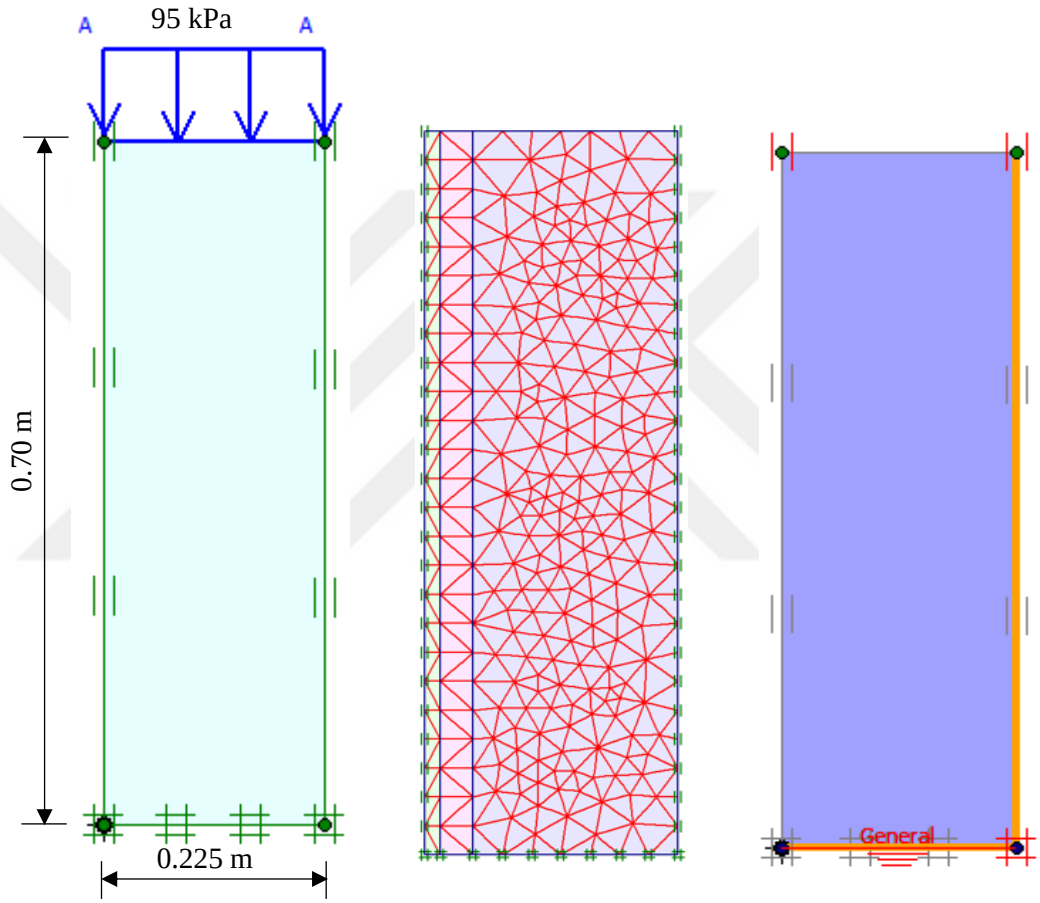

Figure 4.1 Numerical simulation of consolidometer experimental. (a) Profil; (b) axisymmetric mesh; (c) initial conditions

4.1.1. Parametric study of OCR and C_k

All parametric models utilized in this consolidometer experimental were available in the literature except for the value of OCR and change of permeability (C_k). Therefore, this part is analyzed using FEA to evaluate the number of the OCR and C_k factors, and the findings are presented in Figure 4.2 and Figure 4.3.

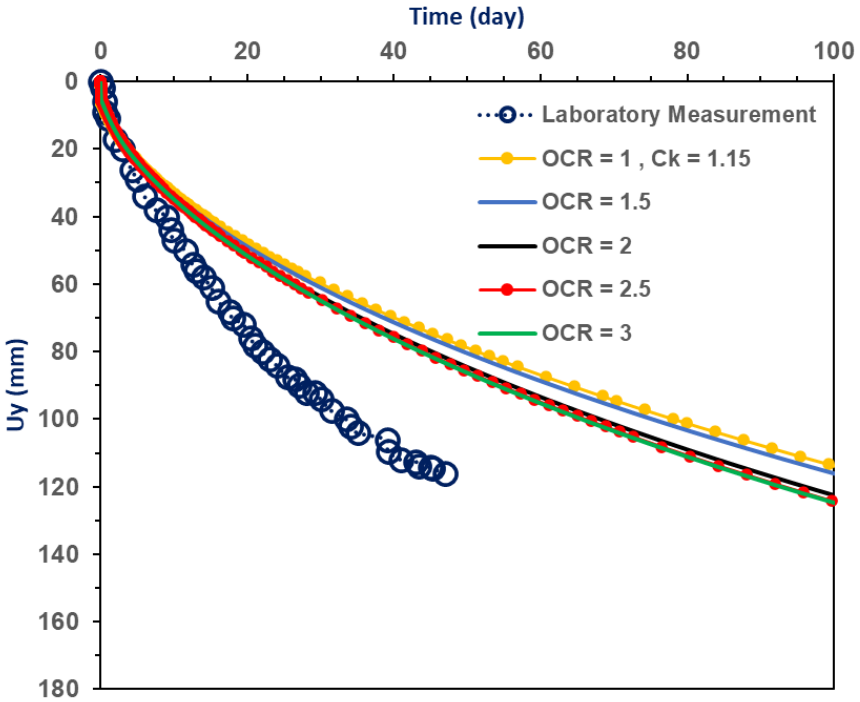

(a)

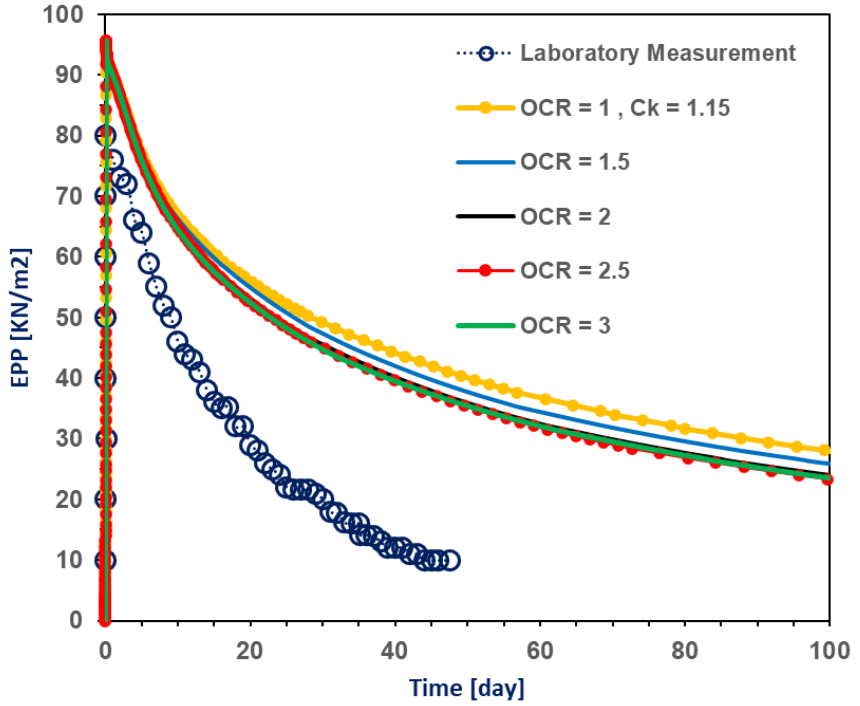

(b)

Figure 4.2. Parametric Study for OCR in FEA. (a) Settlement, (b) excess pore pressure

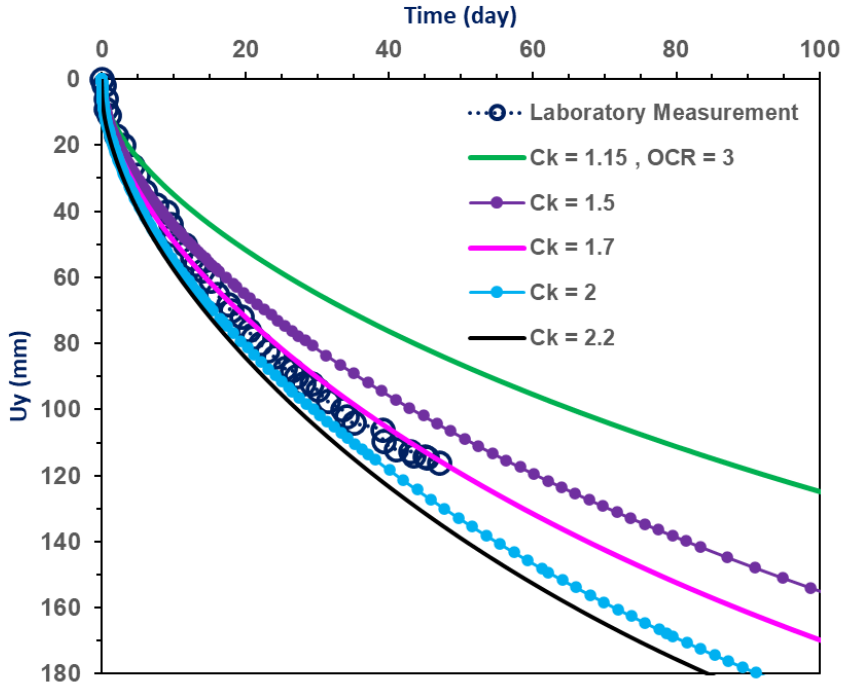

(a)

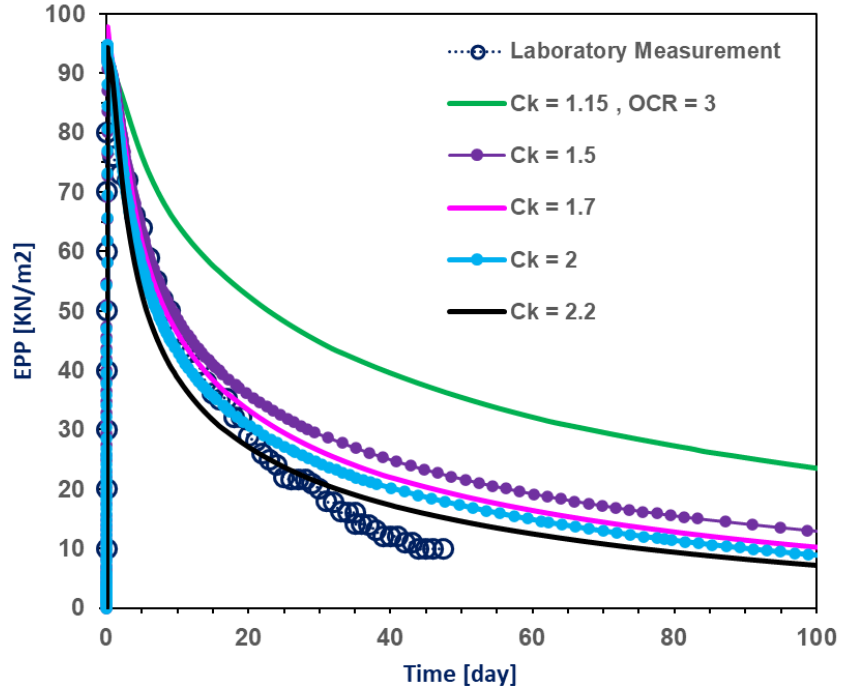

(b)

Figure 4.3. Parametric Study for C_k in FEA. (a) Settlement, (b) excess pore pressure

These results show that varying values of the OCR parameter have a small influence on consolidation behavior. However, the C_k parameter showed considerable differences in consolidation behavior. Based on these findings, we can determine OCR and C_k values of 3 and 1.7, respectively, which will be employed in the following section of the study.

4.1.2. Unit cell in plane-strain condition using different matching methods

This part investigates three alternative matching approaches to evaluate their performance and effectiveness, that are Method A developed by Indraratna et al. (1997), Method B developed by Chai et al. (2001), and Method C developed by Ba-Phu (2019). The concept of these approaches was detailed before in the methodology part.

Figure 4.4a depicts the estimated vertical settlement of axisymmetric and plane-strain unit cells using FEA and experimental data. As shown that, for axisymmetric FEA, time-varying vertical displacement measure was about 119 mm at the end of 47 days, whereas the laboratory data value was roughly 120 mm. This is evident that FEA findings and laboratory measurements are quite similar. Furthermore, EPP vs time for consolidometer of axisymmetric in FEA finding and experimental data are shown in the same figure. Despite the models somewhat overstated EPP values, numerical analysis mostly agreed to the observations. As shown that, FEA results and laboratory data are in excellent agreement, following then, they considerably after 20 days. Based on (Rujikiatkamjorn, 2005), this is not unexpected that there is an EPP difference among FEA and experimental. This is due to the experimental EPP was set up close to PVD, indicating that the highest EPP near to PVD during consolidation was significantly lesser than the level close to the cell boundary, and EPP considerable drop caused by the permeable membrane of PVD. The findings indicated that the simulation characteristic of PVD on soft ground can be effectively predicted in a FEA software.

Furthermore, the plane strain findings presented in Figure 4.4 show that, although the real characteristic of consolidation of soft ground deposits reinforced by PVD is in 3D, two-dimensional plane-strain settings utilizing matching approaches can estimate vertical displacement and EPP in FEA. Overall, it is clear that, despite some changes, all estimated vertical deplacements of matching approaches are agree well with the axisymmetric finding and the laboratory data. The difference among Method A and axisymmetric was 6% at the initial phase of the consolidation, but it had been reduced to 1.5% by the end of the 47th day, as seen in Figure 4.5. In the case of Method B, the difference was around 4.15% at the 47th day of consolidation, but Method C indicated a 4% discrepancy at the same time. According to Method B, Chai et al. (2001) indicated that the disparity was caused by the basic estimation technique, that integrates the influence of both vertically and horizontal flows to vertically drainage. Note that the vertical deformation, horizontal deformation and EPP numerical output of experimental in plane strain situations are presented in Appendix B.

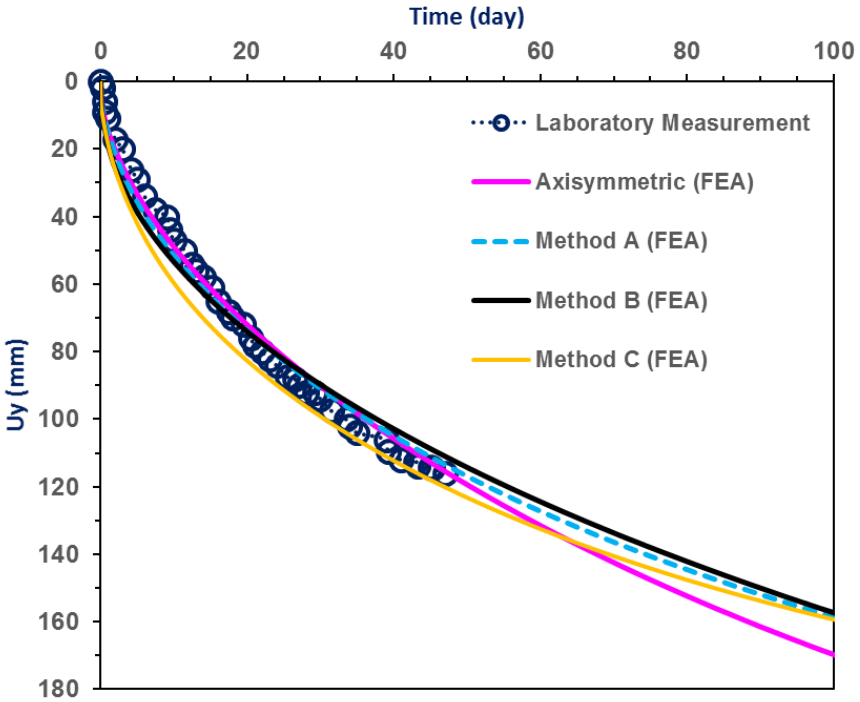

(a)

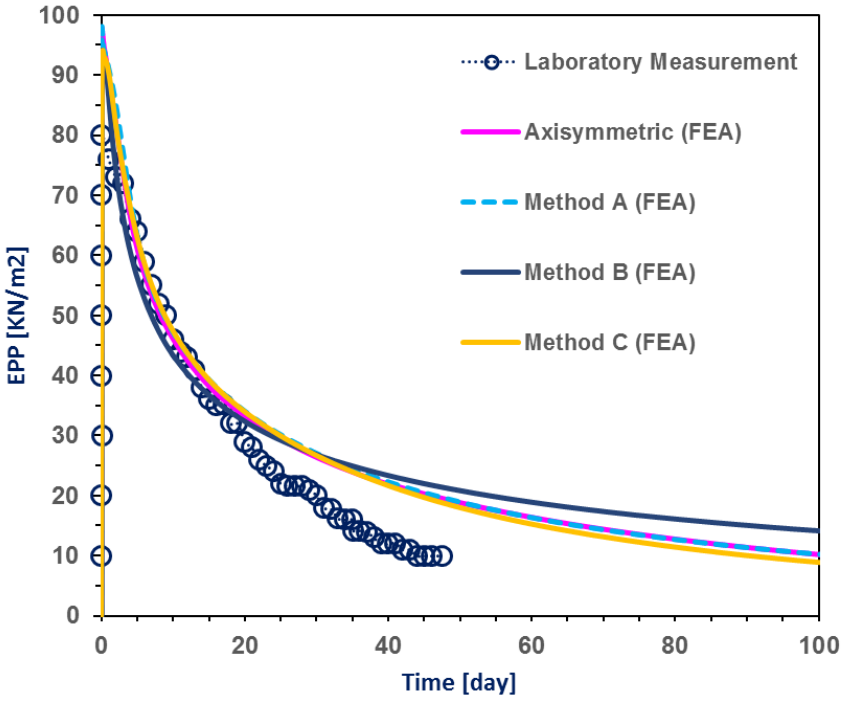

(b)

Figure 4.4. FEA of three matching approaches, axisymmetric and laboratory data. (a) Vertical displacement; (b) EPP.

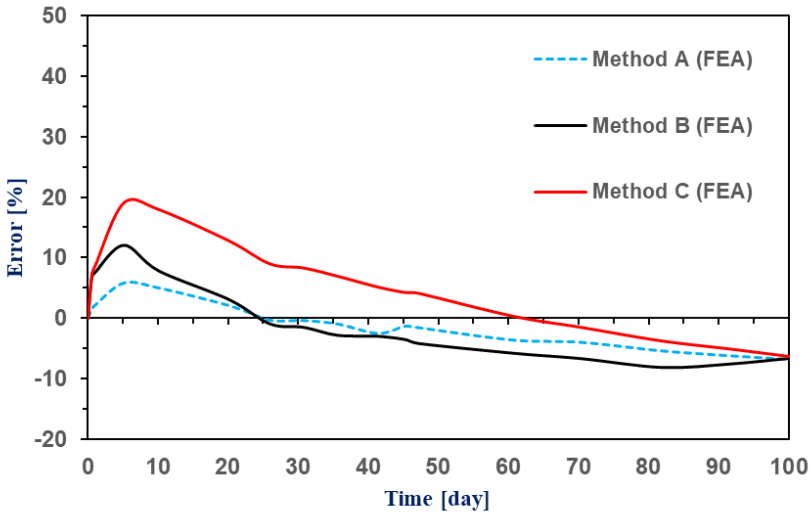

Figure 4.5. Errors in the numerical findings for three matching approaches

4.2. FEA of case study 1

As previously indicated, this part examines 2D FEA in 2D for a full embankment constructed with many vertical drains as multi drain characteristic is ignored in the concept. To determine the characteristic of PVDs, the full embankment in eastern China was examined utilizing the same matching approach employed in large-scale consolidators. Bottom boundary displacements cannot occur in both directions during consolidation. Radial displacements are prohibited on the left and right edges, and restricted to the consolidation limit. During the numerical simulation, the bottom of the system was fixed for horizontal and vertical movements ($u_x = u_y = 0$) during consolidation. Furthermore, radial movement had limitations at the right and left edges ($u_x = 0$). Figure 4.6 shows the finite element mesh for three distinct matching approaches under plane-strain circumstances.

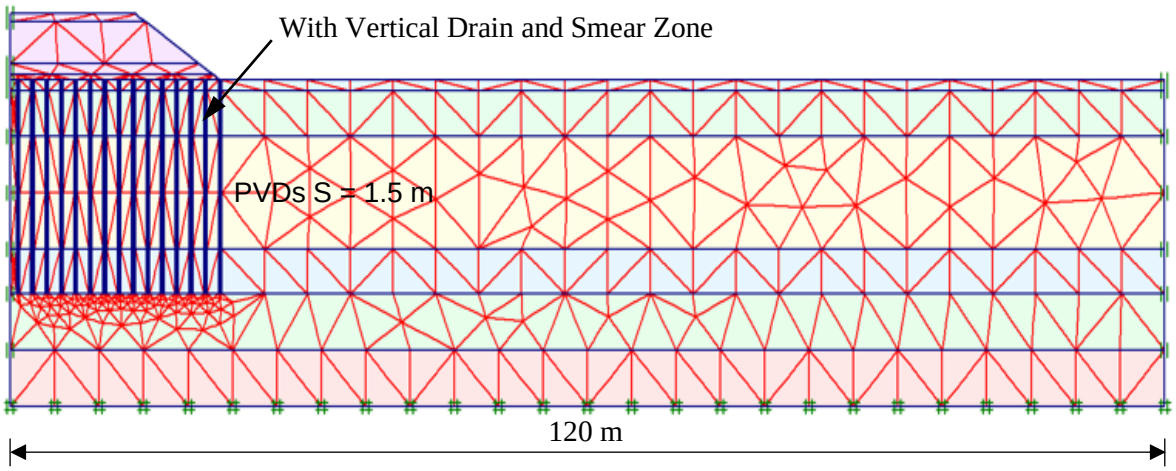

(a)

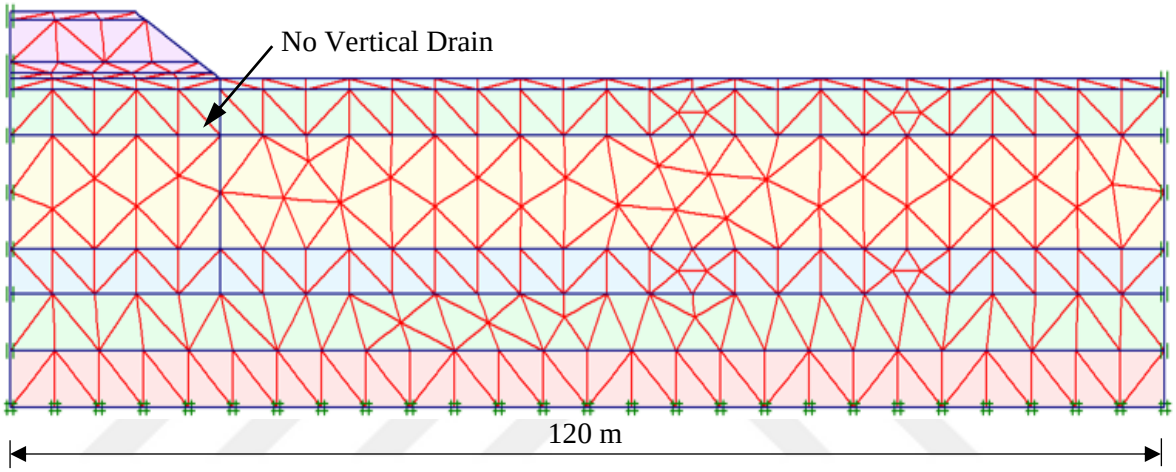

(b)

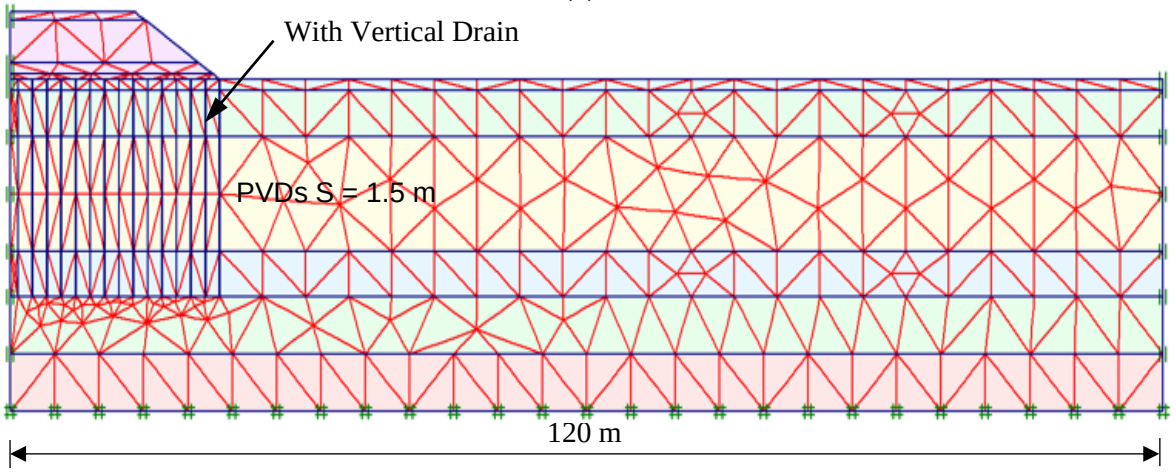

(c)

Figure 4.6. FEA mesh for three matching approaches in plane-strain. (a) Method A; (b) Method B; and (c) Method C

Figure 4.7 shows that, despite being predicated on a unit cell using only one vertical drain, matching approaches can accurately estimate vertical displacement and EPP in a full embankment. Furthermore, while the true characteristic of consolidation of soft ground reinforced by PVDs is in three-dimensional, two-dimensional plan-strain employing matching techniques can estimate

vertical displacement and EPP in FEA. In addition, despite the fact that each of these methods are totally opposed, their FEA findings were highly similar and closely matched the field data. As shown in Figure 4.7a, the variable in time displacement for all matching approaches reached approximately 200 cm following 900 days. Nevertheless, there exists some discrepancy between anticipated results and observed data in the beginning phases (from 0 to roughly 120 days). In the words of Leroueil et al. (1990), the displacements are tiny because the subsurface ground was overconsolidated during the initial stages of operation, causing it to act quasielastically and stiffly.

Method A produced an extremely precise estimated vertical displacement in contrast to other approaches through observed data. Nevertheless, the adoption of this method necessitates difficult since the disturbed area around each vertical drain has to be described in the computational simulation, and the values of radial permeabilities in the disturbed area and natural ground have to be specified individually for every stratum. As demonstrated by Method B, FEA yielded a slightly lower consolidation. Nevertheless, his technique is easier and neglects the modeling of vertical drains. Because of the ease of use, this technique is less difficult to use in practical problems. Method C produced a considerably quicker vertical displacement. But the distinctions among both of the other approaches are minimal. This method has a modest benefit with regard to Method A as the model does not include the disturbed area around every single vertical drain.

Furthermore, as seen in Figure 4.7b, the generated EPP is contrasted to observed data. In overall, accurately predicting EPP is somewhat difficult than predicting vertical displacement (Indraratna et al., 2000). It can be shown that the estimated EPP were in satisfactory agreement from beginning until about 280 days, following which they overestimated the observed data. The huge disparities among computations and observed might be attributed to mistakes in piezometric assessment (Indraratna et al., 2000). Piezometers are frequently employed for measuring EPP in deep ground. Such piezometers may become blocked when ground particles enter into the pore. As a result, piezometers capture some extra pore pressure (Chai et al., 1999; Shen et al., 2005). Moreover, physical inconsistencies among the computations utilizing plane-strain and the field situation, which is 3D may have explained the disparity (Russell, 1995). In the opinion of (2023), EPP estimation error might be related to creep impacts in the stage, since the volume of water-filled holes reduces as ground particles reorganize. Based on these findings, the matching approaches were capable to estimate the vertical displacement and EPP in FEA. These methods prove helpful in practice as engineers because they enable modeling of the characteristics of PVD-reinforced ground. In any event, we have to do a 3D model to assess the characteristics of PVD-improved ground. Nevertheless, because of the complexity of 3D assessments, using them to a real embankment project having a large number of vertical drains involves a substantial amount of computer work. Note that the vertical deformation, horizontal deformation and EPP numerical output of test embankment are shown in Appendix C.

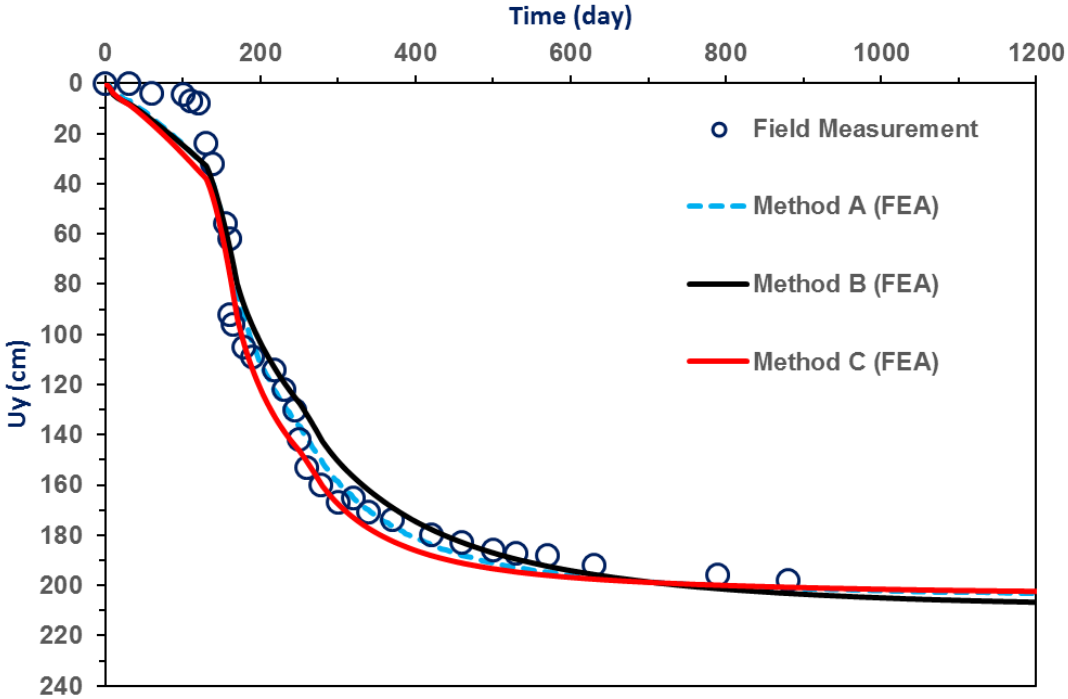

(a)

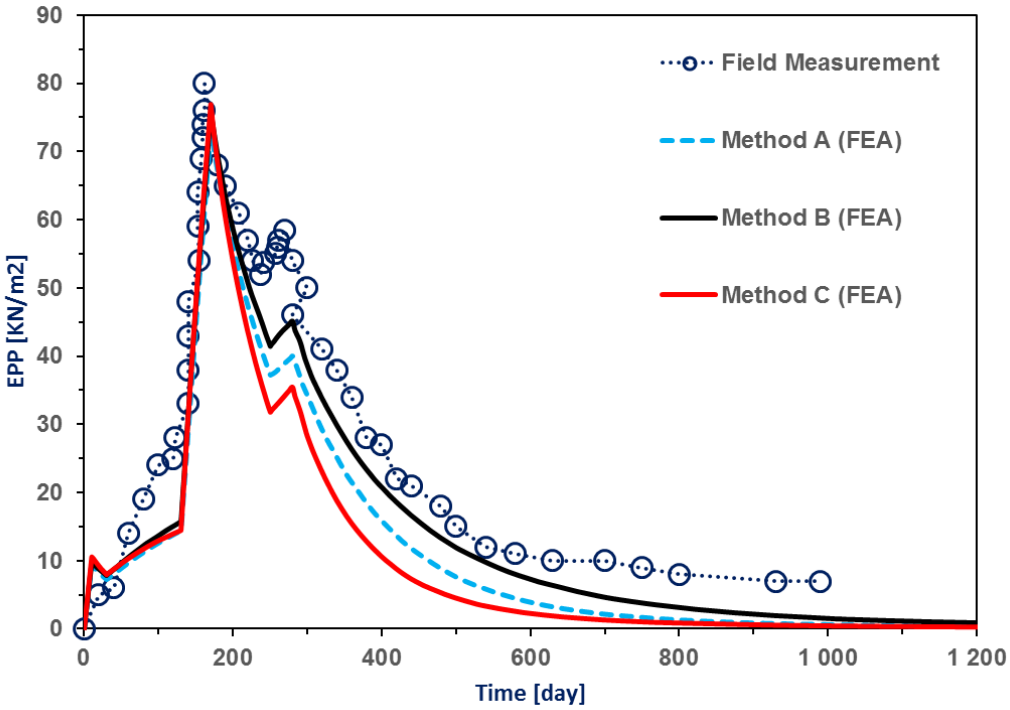

(b)

Figure 4.7. FEA of three matching approaches and observed data. (a) Vertical displacement; (b) EPP, at a depth of 14.05 m

4.3. FEA of case study 2

Throughout the consolidation process, bottom edge movements in both directions are not allowed ($u_x = u_y = 0$). Radial movements are not permitted on the right and left borders ($u_x = 0$), which are close to the consolidation edge. Every single model were discretized employing a fine

mesh distribution. The fine mesh was selected because it produced good results without additional refining.

4.3.1. Comparison for three different simulation model

In this section, three different constitutive models (SSCM, SSM, and MCCM) are examined to determine the most appropriate model for this test embankment. The computational findings are contrasted and discussed with the observed data. As previously stated, the top and lower marine layers, which consist of soft and extremely soft silty clay, are the most crucial for settlement. During simulation, SSM uses the identical model parameters as SSCM. The construction process employed for every segment is summarized in Table 4.5, and settlement field measurements data for test embankment segment is illustrated in Figure 4.8. Finite element mesh for each segment of the test embankment in Dover, NH under plane strain conditions is shown in Figure 4.9.

Table 4.1. Construction process employed for every segment (Getchell, 2013; Santamaria, 2015)

Calculation Phase	Segment 1	Segment 4	Segment 5	Units
Sand and PVDs	3	3	3	days
Waiting Time	13	10	9	days
Embankment [3,7 m]	40	40	40	days
Waiting Time	–	45	–	days
Embankment [1,8 m]	–	7	–	days
Minimum EPP	1	1	1	kN/m^2

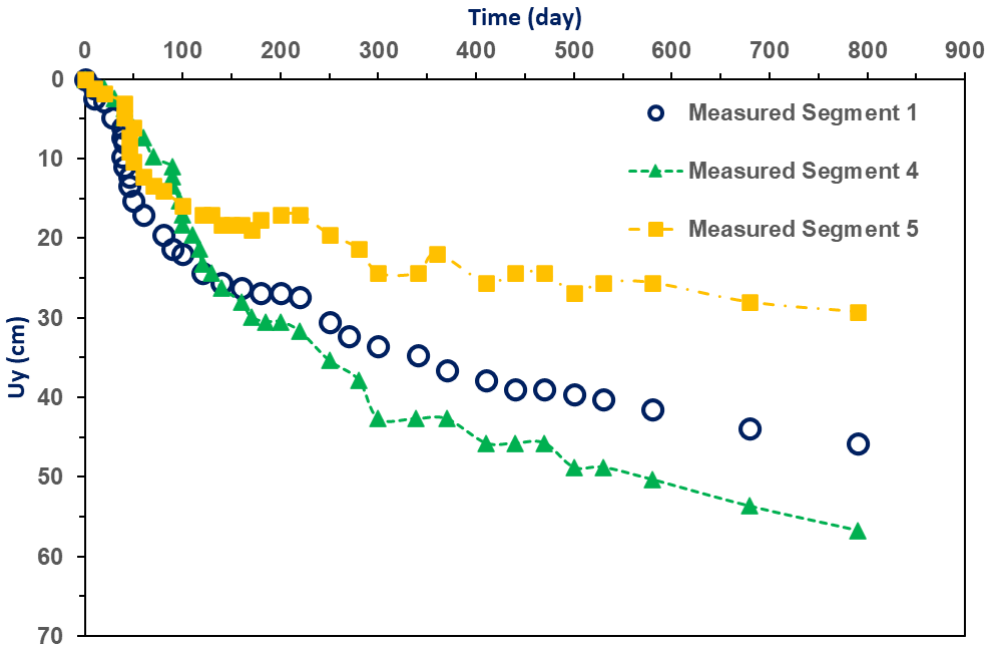

Figure 4.8. Field data measurements of Settlement for 3 Segments in Dover New Hampshire test embankment

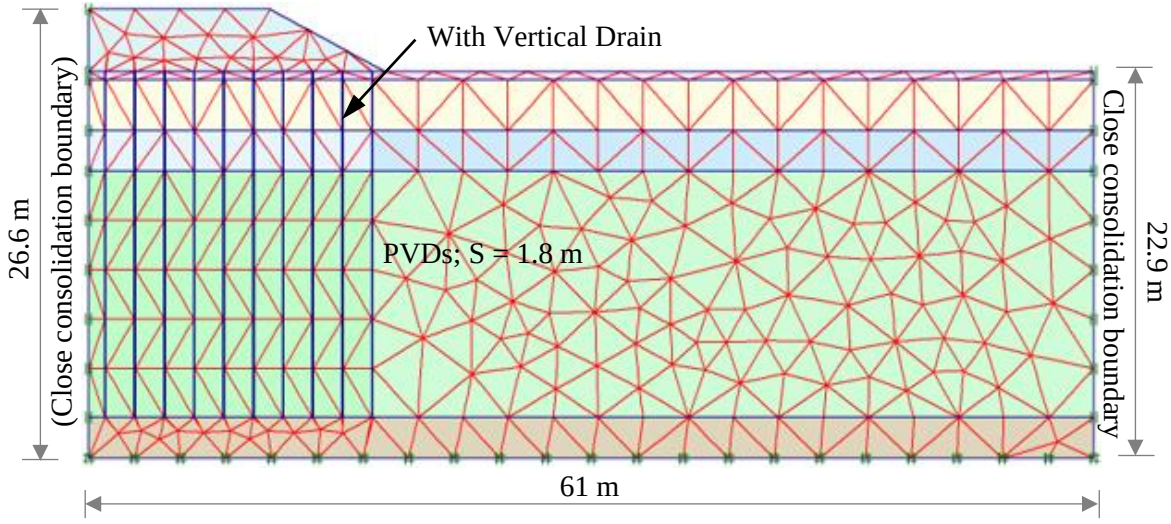

(a)

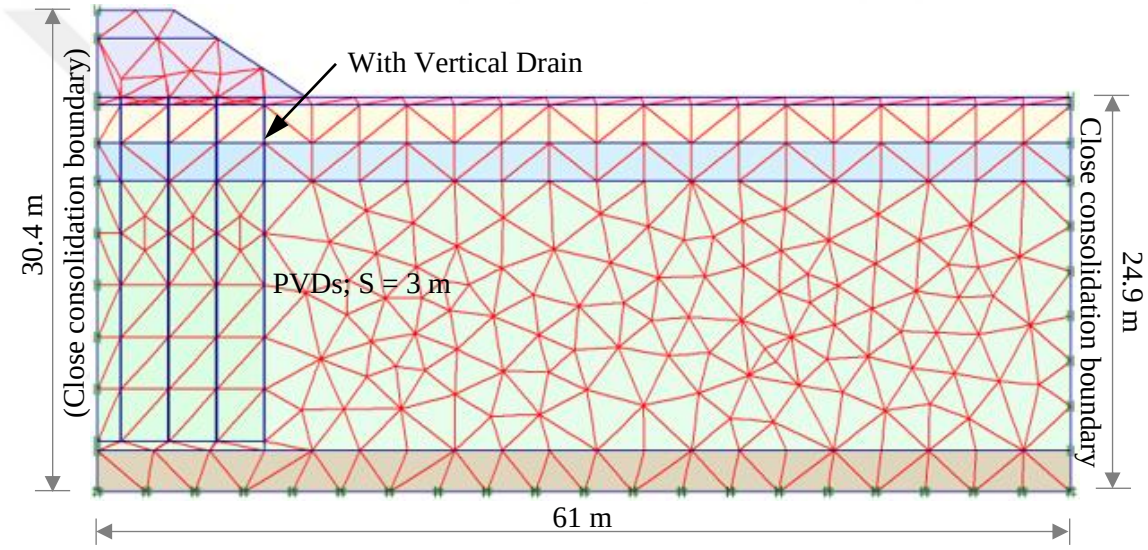

(b)

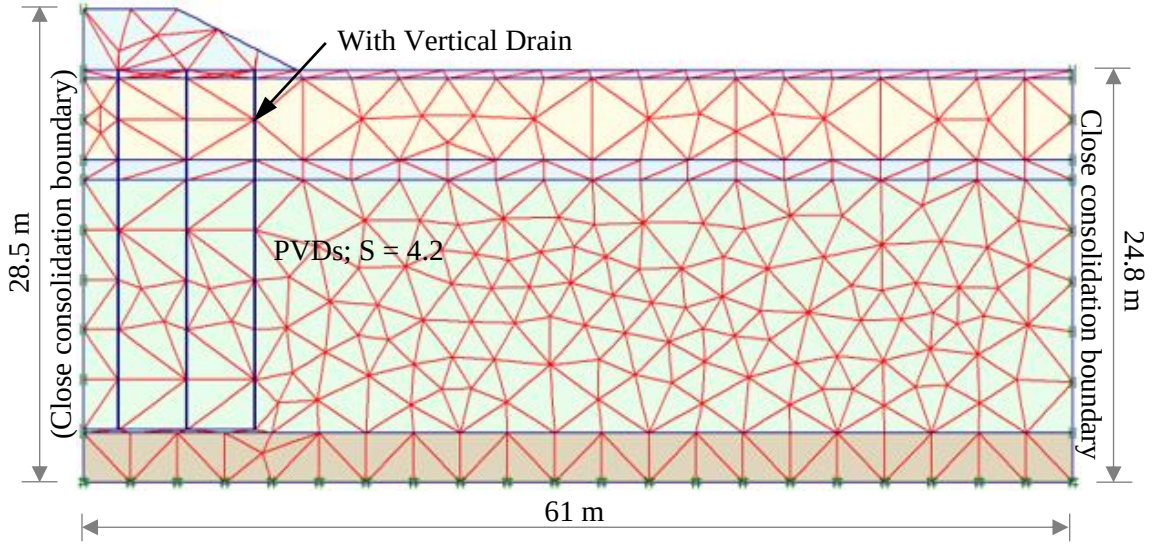

(c)

Figure 4.9. Finite element mesh of test embankment in Dover NH in plane strain conditions. (a) Segment 1, (b) Segment 4, (c) Segment 5

The comparison of the settlements of Segment 1 test embankment for three constitutive models and field measurement is shown in Figure 4.10. As can be shown, estimated vertical settlement for all three models stays relatively comparable after around 60 days of installation and provides an accurate estimate for field measurement. However, after 60 days, SSM and MCCM significantly underestimate settlements, but SSCM is very similar to field observations. It illustrates that the model can provide better simulation for complicated conditions in which soil strata include both undisturbed and disturbed sections, as well as drainage aspects. The field measurement settlement beneath the embankment's centerline is 47 cm after around 800 days of consolidation, with a maximum settlement of 49 cm reported by SSCM. Moreover, SSM estimates a settlement of about 33 cm with 800 days of consolidation beneath the embankment's centerline, whereas the MCCM predicts a vertical displacement of around 34 cm. The findings show that the creep model gives a better estimate of settlements.

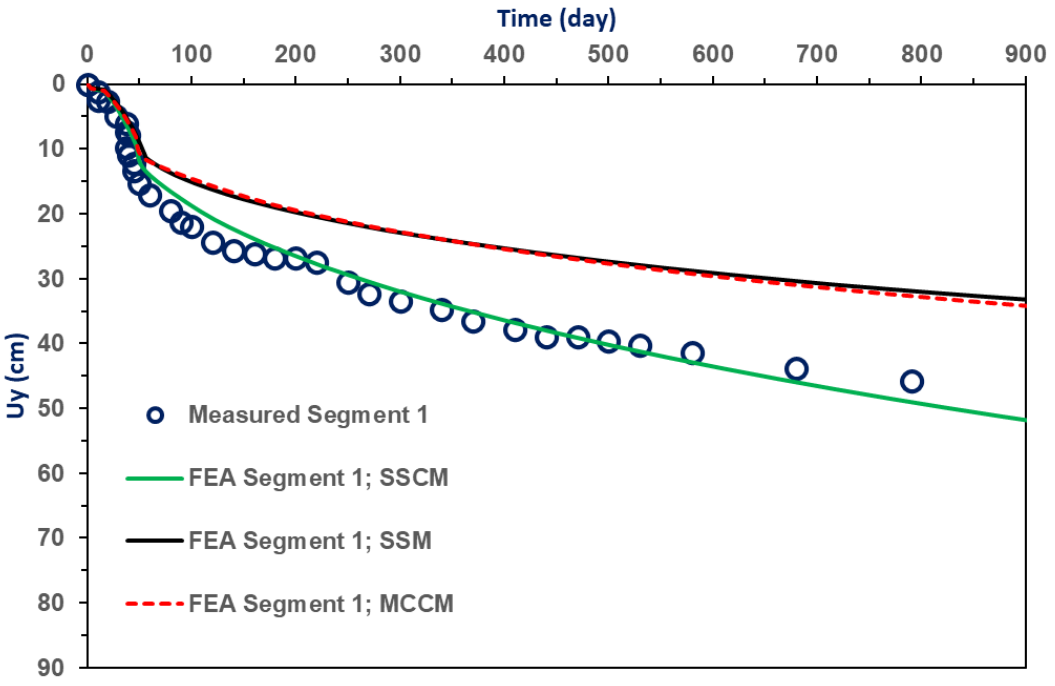

Figure 4.10. Comparison of FEA result and field measurement for three different simulation model for Segment 1

With regard to Segment 4 in Figure 4.13, up to 150 days following execution, field vertical displacement measurement values are significantly more comparable with SSM and MCCM expected settlements than SSCM. However, after roughly 150 days, SSCM is in agree well with the vertical displcement of field measurement, nevertheless both SSM and MCCM estimate a decrease of settlement throughout the simulation, making their predictions less accurate than SSCM. After 800 days of consolidation, the highest measured vertical displacement at the embankment's center was around 58 cm. SSM and MCCM predict a maximum settlement of 37 cm and 40 cm, respectively

after 800 days of consolidation, however the SSCM estimates a maximum vertical displacement of 58 cm.

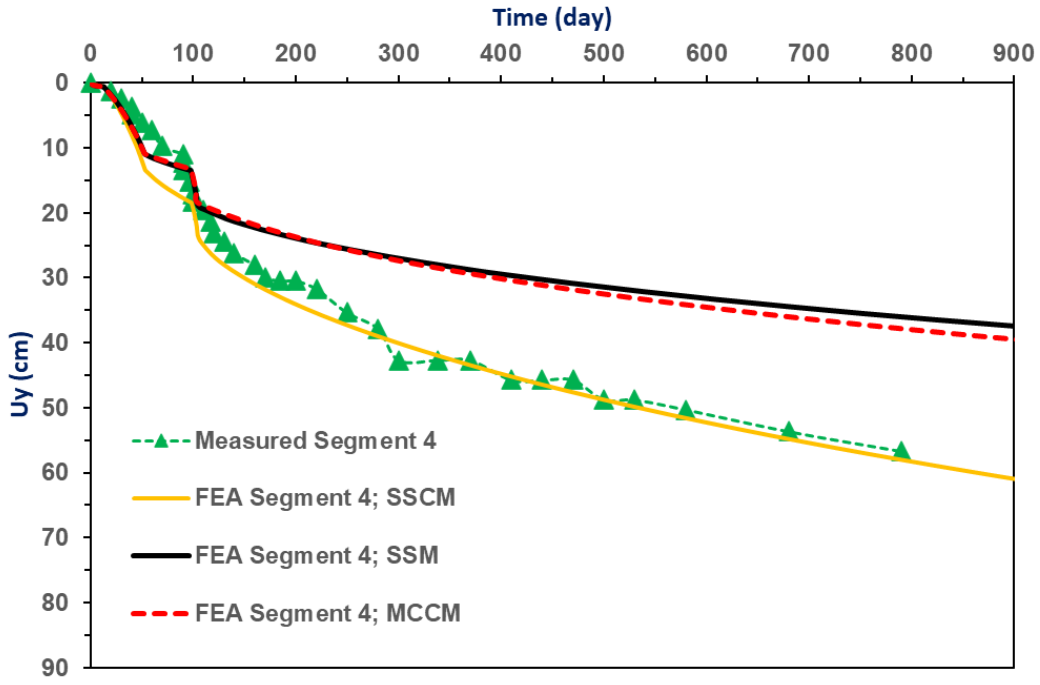

Figure 4.11. Comparison of FEA result and field measurement for three different simulation model for Segment 4

Figure 4.14 shows how the settlements of Segment 5 predicted by three constitutive models (SSCM, SSM, and MCCM) match to field measurement data. The results demonstrate that differences among the three models are generally inadequate for beginning of 50 days after embankment execution, and that field measurement is agree well with estimated vertical displacement, however afterwards differences was found throughout consolidation. After about 800 days of consolidation, the field measurement settlement under the embankment's centerline measures 30 cm. Again, SSCM agrees with the field measurement centerline settlements. It estimates a highest vertical displacement of 30 cm at the end of 800 days of consolidation time. SSM estimates a vertical displacement of roughly 18 cm after 800 days of consolidation beneath the embankment's centerline, whereas the MCCM predicts a settlement of around 19 cm. The vertical deformation, horizontal deformation and EPP numerical output for all segments of test embankment are shown in Appendix D to Appendix H.

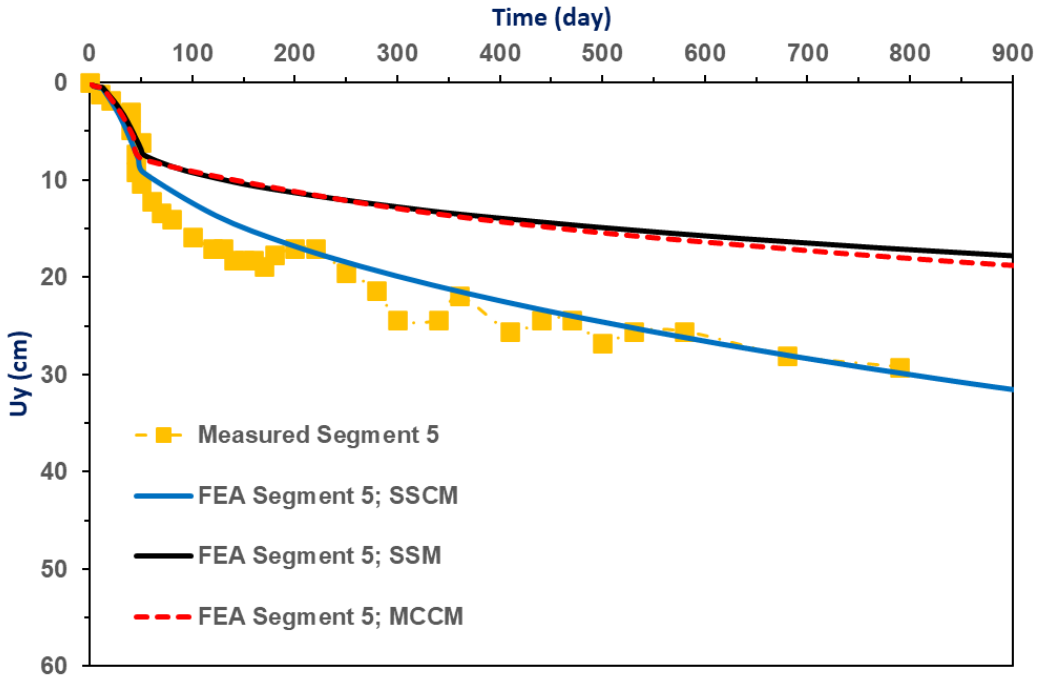

Figure 4.12. Comparison of FEA result and field measurement for three different simulation model for Segment 5

4.3.2. Comparison of three distinct matching approaches

As earlier indicated, many different researchers developed matching approaches in the literature. In this part, another matching methods were investigated in Dover test execution in FEA, which are Method I developed by Shinsha et al. (1982), Method II developed by Hird et al. (1992), and Method III developed by Bergado et al. (1994). The concept of these methods have explained previously in the methodology.

Three matching methods and field measurements are compared in Figure 4.15 to show the comparison of FEA results for the settlement under the test embankment of Segment 1. This result shows that the two matching procedures are comparable to field measurement. The findings showed that for Segment 1 of the test embankment, the field measurement estimated a maximum settlement of 47 cm after 800 days of consolidation. Based on Method I, the maximum settlement after 800 days of consolidation is approximately 49 cm, whereas Method II yields a maximum settlement of approximately 50 cm. However, Method III predicts a maximum settlement of around 56 cm after 800 days of consolidation. This result shows that this method is expected to settle faster than Method I and Method II. The explanation for this is most likely that the smear zone factor is not given enough consideration in the method's design.

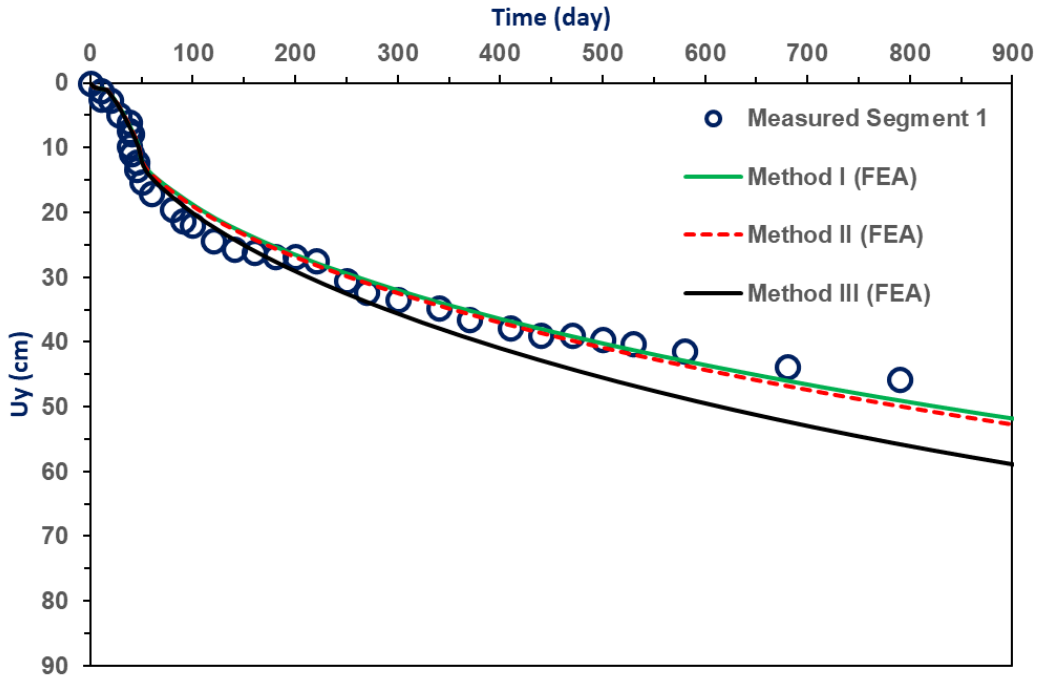

Figure 4.13. Comparison of FEA results Settlement of three matching methods and field measurement for test embankment Segment 1

Moreover, Figure 4.16 also shows EPP over time for the Segment 1 of test embankment in FEA results and field measurements. Despite the models somewhat overstated EPP values, numerical analysis largely agreed with the observed value. As demonstrated, the numerical analysis and field measurements coincide fairly well. Following that, they differentiated significantly over 60 days. Based on Rujikiatkamjorn (2005), the difference in EPP among numerical analysis and field measurement is unsurprising. This can be explained since EPP field measurement is located close PVD, that indicates the highest EPP near to PVD during consolidation load was significantly lower, and EPP close the drain was greatly lowered as a consequence of the permeability of PVD (Rujikiatkamjorn, 2005). These findings show that the consolidation characteristic of PVD on soft marine ground was quite well predicted in FEA utilizing the matching approach with SSCM. The errors among field measurements and all three matching methods for the test embankment of Segment 1 were compared in Figure 4.17. It is noted that the difference between Method I and field measurement is 10% at the initial stage of the consolidation, but it was reduced to 5.6% by the 800th day. With regard to Method II, the error margin was around 7.5% at the end of the 800th day of consolidation, but Method III indicated a 15.8% discrepancy at the end of the 800th day.

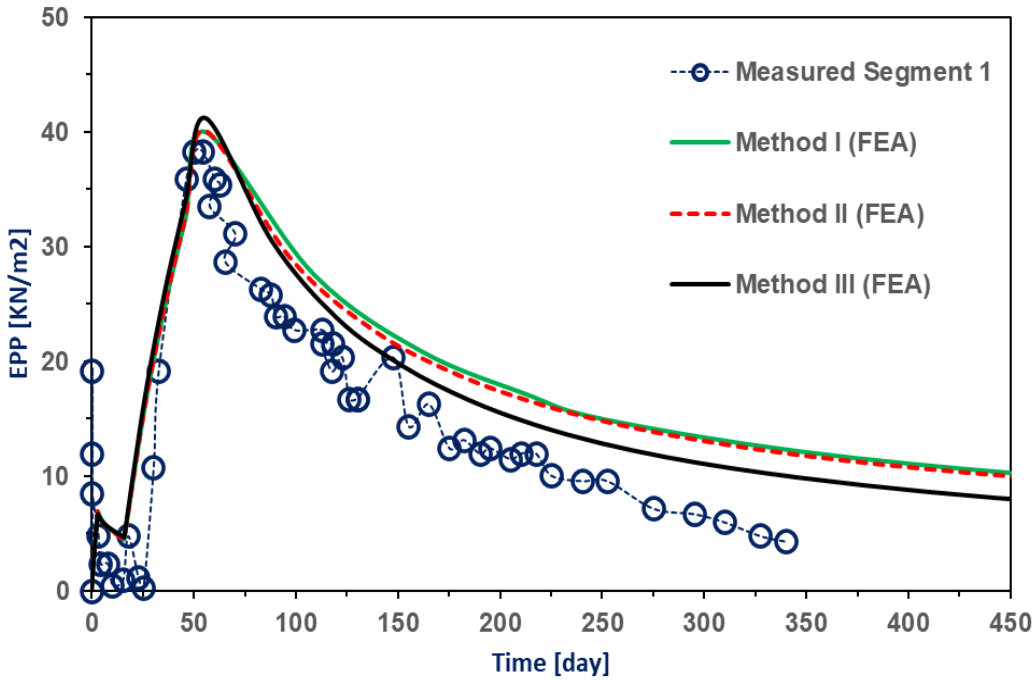

Figure 4.14. Contrast of FEA results EPP of three matching methods and field measurement for test embankment Segment 1

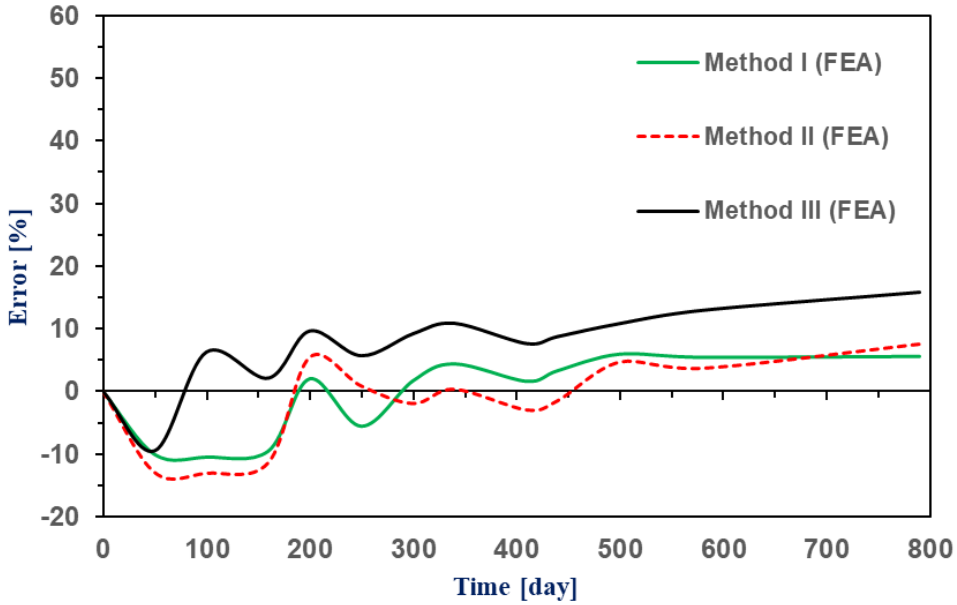

Figure 4.15. Errors between FEA results of three different matching Methods and field measurement for test embankment Segment 1

Figure 4.22 compares three matching methods and observed data to demonstrate FEA findings for settlement beneath Segment 4 of test embankment. This result demonstrates that the two matching methods are similar to field measurement. The results indicated that for Segment 4 of the test embankment, the field measurement predicted a maximum settlement of 58 cm after 800 days of consolidation. According to Method I, the maximum settlement after 800 days of consolidation is roughly 58 cm, whereas Method II produces a maximum settlement of approximately 60 cm.

Nevertheless, Method III estimates a maximum settlement of around 64 cm after 800 days of consolidation. This result indicates that this approach is going to settle faster than Methods I and II. The probable explanation for this have explained previously.

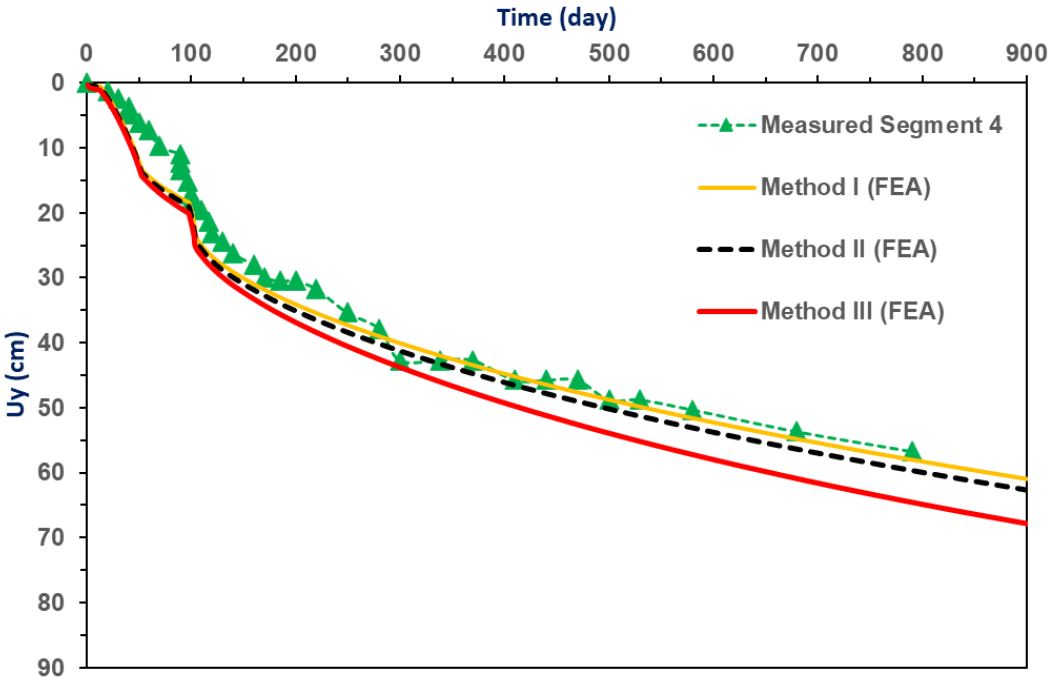

Figure 4.16. Comparison of FEA results Settlement of three matching methods and field measurement for test embankment Segment 4

Furthermore, the computed of EPP for Segment 4 of the test embankment is compared to field data in Figure 4.23. In most cases, predicting of EPP is more difficult than predicting settlement (Indraratna, 2000). This can be observed that the projected EPP were in perfect match from the beginning of consolidation; nevertheless, they later overestimated the field measurement by around 150 days. The huge disparities between numerical calculations and observations might be caused by error in piezometric measurement (Indraratna, 2000). Piezometers are often used for measuring pore water pressure in profond soil. Hence, these piezometers can become clogged when soil particles enter the filter's pores. Hence, some sort of EPP is trapped in the piezometers (Chai et al., 2001; Shen, 2005).In addition, geometric discrepancies among the computational studies, which used plane strain, and the field situation, which was 3D, may have explained the difference (Russell, 1995). As indicated by Sundström (Sundström, 2023), the mistake in EPP estimate might be related to layer creep, since the volume of water-filled gaps reduces when soil particles reorganize. Figure 4.24 compares the errors in field measurements and the three matching approaches to Segment 4 of test embankment. It is reported that the gap between Method I and field measurement was 15.5% at the start of the consolidation, but it had been decreased to 2.3% by the 800th day. The error margin for Method II was about 4.8% at the conclusion of the 800th day of consolidation, but Method III showed a 10.5% disparity.

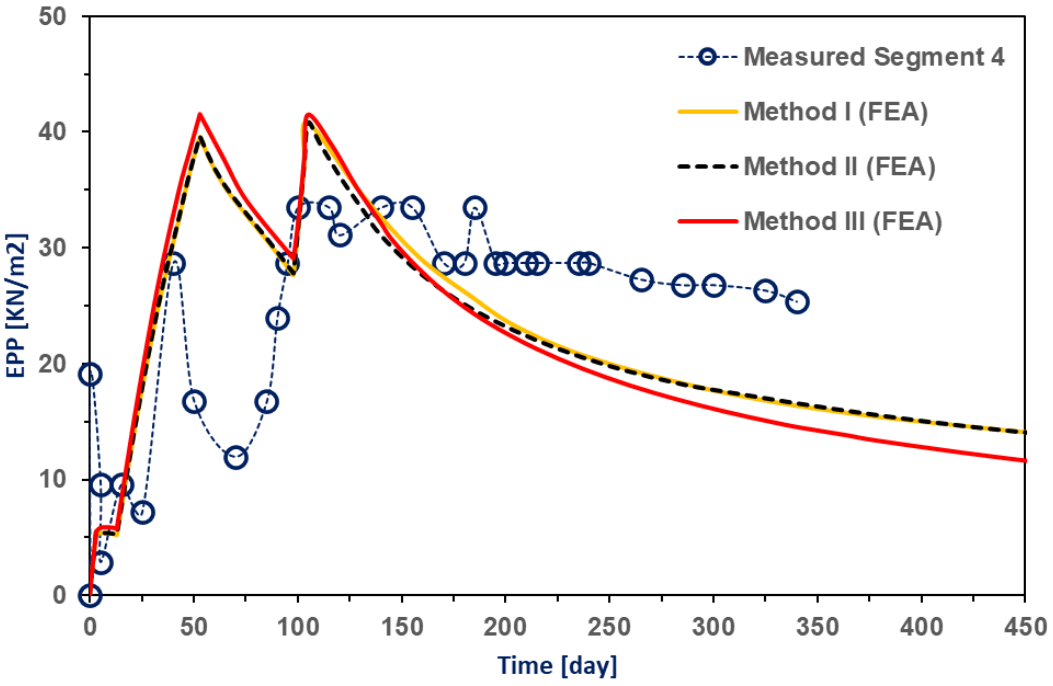

Figure 4.17. Comparison of FEA results EPP of three matching approaches and observed data for test embankment Segment 4

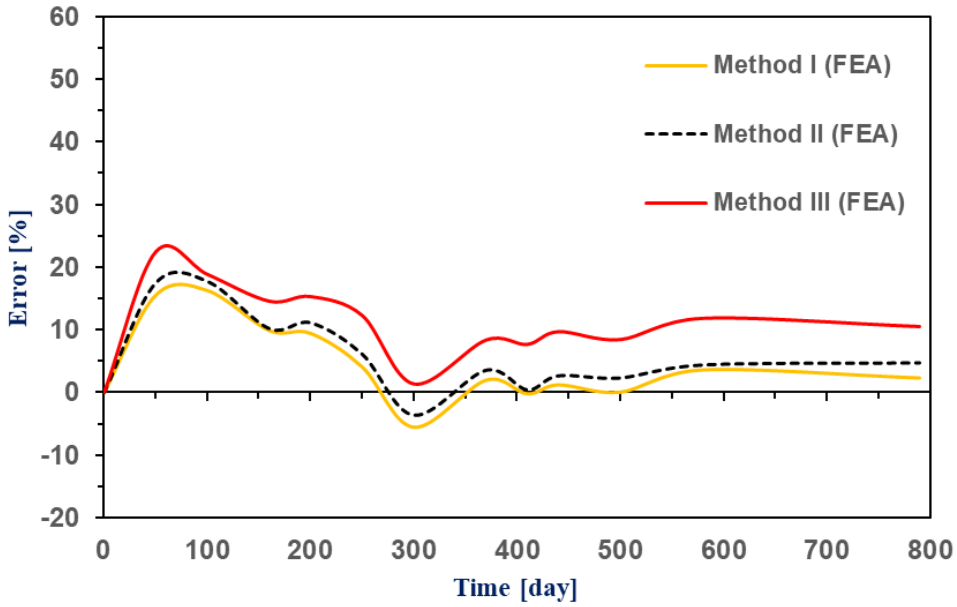

Figure 4.18. Errors between FEA results of three different matching Methods and field measurement for test embankment Segment 4

Three matching methods and field measurements are compared in Figure 4.25 to show the contrast of FEA for the settlement under the test embankment of Segment 5. This result shows that the two matching procedures are comparable to field measurement. The findings showed that for Segment 5 of the test embankment, the field measurement estimated a maximum settlement of 30 cm after 800 days of consolidation. Based on Method I, the maximum settlement after 800 days of

consolidation is approximately 30 cm, whereas Method II yields a maximum settlement of approximately 31 cm. However, Method III predicts a maximum settlement of around 35 cm after 800 days of consolidation. This result shows that this method is expected to settle faster than Method I and Method II. The probable explanation for this have explained earlier. The errors among field measurements and all three matching methods for the test embankment of Segment 5 were compared in Figure 4.26. It is noted that the difference between Method I and field measurement is 9.3% at the initial stage of the consolidation, but it was reduced to 6.6% by the 800th day. With regard to Method II, the error margin was around 9.7% at the end of the 800th day of consolidation, but Method III indicated a 19.5% discrepancy at the end of the 800th day.

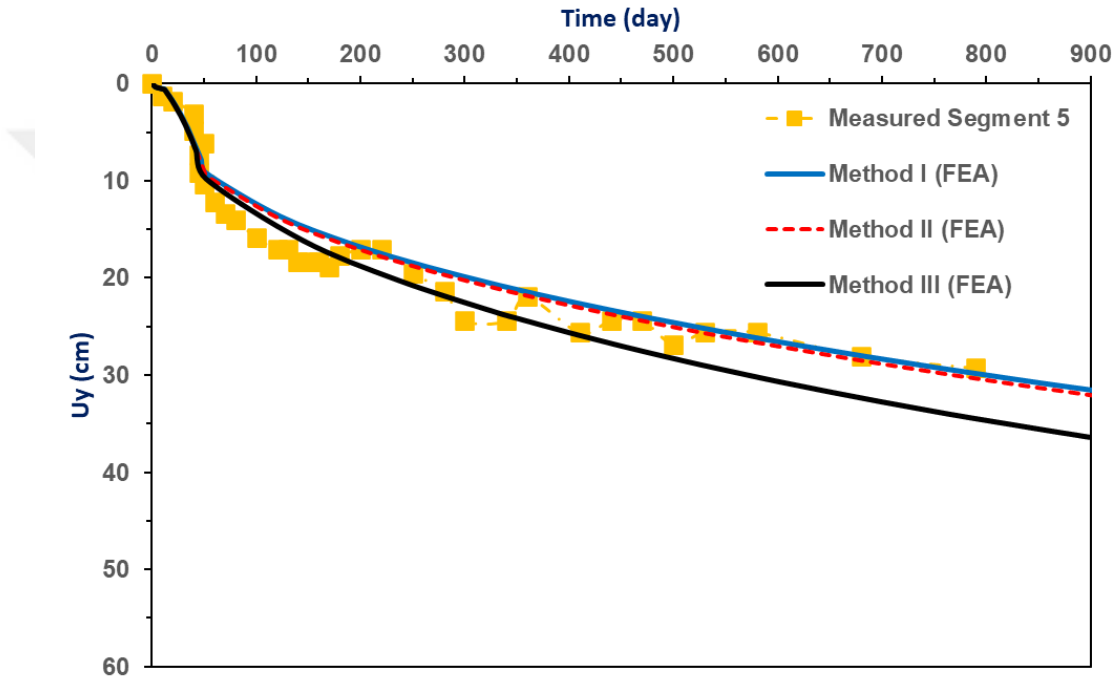

Figure 4.19. Contrast of FEA results Settlement of three matching methods and field measurement for test embankment Segment 5

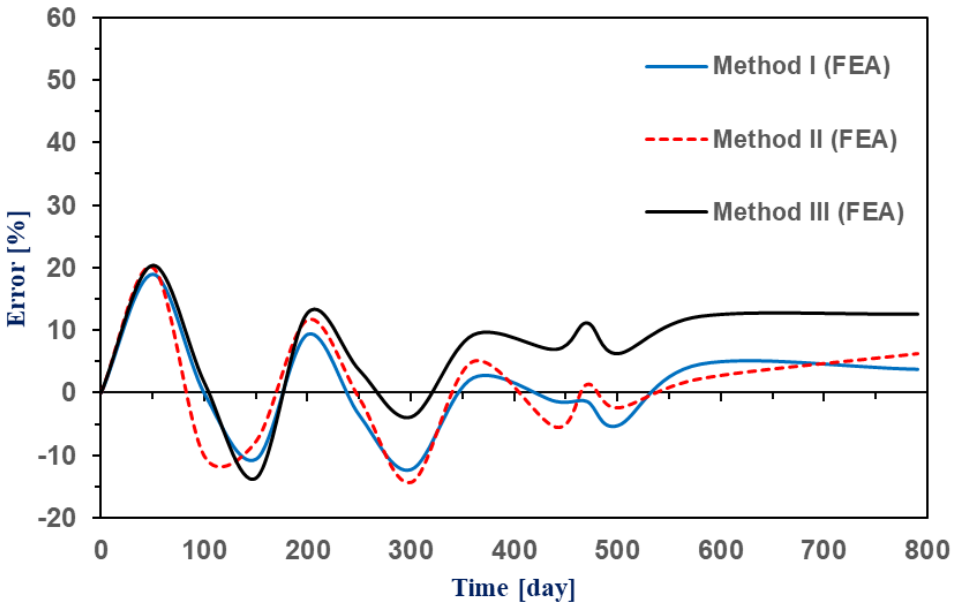

Figure 4.20. Errors between FEA results of three distinct matching approaches and field measurement for test embankment Segment 5

5. CONCLUSIONS

This present study was evaluated the performance and effectiveness of matching methods in 2D numerical analysis of consolidation of soft soil improved by PVDs. To assess the effectiveness and reliability of these approaches, a large-scale experimental, full embankment in eastern China and 5 segments test embankment in Dover, New Hampshire were investigated. Method A, Method B and Method C were used in large-scale unit cell and full embankment in eastern China, whereas Method I, Method II and Method III were performed for all 5 segments test embankment in Dover NH. The computational investigation was conducted utilizing PLAXIS 2D program and the smear zone was included during the consolidaiton. To validate the model, FEA results of settlements and EPP were compared to the field measurement values.

According to the consolidometer experimental, settlement in FEA findings and experimental data are quite similar. Despite the models somewhat overstated EPP of axisymmetric values, numerical analysis mostly agreed with the observations. Moreover, while the true characteristic of consolidation of soft ground deposits reinforced by PVD is in 3D, 2D in plane-strain utilizing matching approaches can estimate vertical displacement and EPP. It was clear that all estimated vertical displacements of matching approaches were in agree well with the axisymmetric finding and the laboratory data.

Based on full test embankment in eastern China, while the matching approaches are built on unit cells using only one vertical drain, they are able to estimate vertical displacement and EPP in full embankments. Method A produced an extremely precise estimated vertical displacement agreement when contrasted to other approaches with observed data. Nevertheless, the adoption of this method necessitates challenging tasks since the disturbed area surrounding every vertical drain has to be described in the computational study, and the measurements of radial permeabilities in the disturbed area and natural soil have to be specified individually for every stratum. Based on Method B, FEA yielded a slightly lower consolidation process. Nevertheless, his approach is easier and does not involve the representation of vertical drains. Because of its simplicity, this method is easier to use in practical work. Method C produced a considerably quicker vertical displacement process. Nevertheless, the distinctions among both of the other approaches are minimal. This method has a modest benefit beyond Method A as the model does not include the disturbed area around every vertical drain.

In accordance with full test embankment in Dover NH, the comparisons between numerical and field measurements showed that the settlements estimated by SSCM agree well with the field measurement. However, both SSM and MCCM underestimate dependent on time settlements beneath the embankment. According to the findings, it can be stated that SSM containing creep estimates vertical settlement much better than SSM without creep. Generally, both SSM and MCCM are acceptable for simulating PVD performance on soft clay when creep represents a small effect.

However, SSCM should be used when creep is likely to play a significant impact. Moreover, another matching methods were also investigated in FEA in this test embankment. The simulation results showed that the settlements predicted by Methods I and Method II were adequate and in agree well with the observed data. Nevertheless, Method III somewhat underestimates the observed settlement; but stil maintains a maximum error of 19.5% at the end of 800 days of consolidation in Segment 3. The results indicated that, although being developed through unit cell concept with one vertical drain, the matching approaches can accurately estimate settlement in a full-scale embankment. These methods prove helpful in practice for engineers and can help simplicity the study of the characteristic of PVD reinforced ground. Alternatively, we must do a 3D simulations to investigate the behaviour of PVD reinforced ground. Nevertheless, 3D studies are quite complicated and demand a significant powerfull computer hen used to a full embankment construction over a large number of PVDs.

The following findings have been determined from the conducted study:

- While the real characteristic of consolidation of soft ground enhanced by PVD is in 3D, 2D plane-strain using matching methods may predict vertical displacement and EPP in FEA.
- Despite the fact that the matching approaches are developed on unit cells using one vertical drain, they are able to estimate vertical displacement and EPP in full embankments. These methods prove helpful in practice for engineers and can help simplicity the study of the characteristic of PVD enhanced subsoil.
- In general, both SSM and MCCM are acceptable for simulating PVD efficiency on soft clay where creep plays a minor effect. However, SSCM should be used when creep is likely to play a significant impact.
- The rate of disturbance inside the disturbed area, given as the k_h/k_s ratio, had no significant affect on settling behaviour at k_h/k_s= 2-5, as advised in the literature.

REFERENCES

Aboshi, H. (1992). Applied Ground Improvement Techniques, Workshop. *Southeast Asian Geotechnical Society (SEAGS), Asian Institute of Technology, Bangkok, Thailand, 40 p.* .

Aboshi, H. (1967). A study in the consolidation process affected by well resistance in the vertical drain method. *Soils and Foundations, 17(4)*, pp.38-58.

Akagi, T. (1977). *Effect of Mandrel-Driven Sand Drains on Strength.* Paper presented at the Proc. 9th International Conference on Soil Mech. and Found, Eng., Tokyo, Vol. 1, pp. 3–6.

Akagi, T. (1981). *Effect of Mandrel-driven sand drains on soft clay.* Paper presented at the Proc. 10th Int. Conf. Soil Mech. and Found. Eng, Stockholm, pp. 581-584.

Ali, F. H. (1991). The Flow Behavior of Deformed Prefabricated Vertical Drains. *Geotextiles and Geomembranes, 10*, 235-480 Elsevier. Web. 232 Apr. 2014.

Ali, P.P. (2014). *Analysing Ground Deformation Data to Predict Characteristics of Smear Zone Induced by Vertical Drain Installation for Soft Soil Improvement.* (Ph.D. Thesis), University of Technology, Sydney.

Almeida, M. S. S. (1993). *Field in situ and laboratory consolidation parameters of a very soft clay.* Paper presented at the Predictive Soil Mechanics, Proc. Of the Worth Memorial Symposium, Thomas Telford, London, pp .73-93.

Ameratunga, J., Sivakugan, N., and Das, B. M. (2016). Correlations of soil and rock properties in geotechnical engineering. *Springer*, pp. 8-9.

Atkinson, M. S., and Eldred, P. J. (1981). Consolidation of soil using vertical drains. *Geotechnique, 31(1)*, 33-43.

Barron, R.A. (1948). Consolidation of fine-grained soils by drain wells. *Transactions of the American Society of Civil Engineers, 113: 718–724*, Paper No. 2346.

Bell and Hicks, R. G. (1980). Evaluation of Test Methods and Use Criteria forGeotechnical Fabrics in Highway Applications - Interim Report. *U.S. Department of Transportation, Federal Highway Administration, Report No. FHWA/RD-80/021, Washington, DC, USA, June 1980*, 190 p.

Bergado, D.T. (1991). Smear effects of vertical drains on soft Bangkok clay. *Journal of Geotechnical Engineering, 117(10)*, 1509-1530.

Bergado, D.T., Chai, J.C., and Shui-Long, S. (2013). Modelling prefabricated vertical drain improved ground in plane strain analysis *Gound Improvement, 166* (G12).

Bergado, D. T. (1994). *Numerical analysis of embankment on subsiding ground improved by vertical drains and granular piles.* Paper presented at the Proc. 13th ICSMFE, New Delphi, India, pp. 1361-1366.

Bergado, D. T., and Redena., B. (1996). Proposed Criteria for Discharge Capacity of Prefabricated Vertical Drains. *Geotextiles and Geomembrances, 14*, 481-505.

Bo, M. (2004). Discharge capacity of prefabricated vertical drain and their measurements. *Geotextiles and Geomembranes, 22*, 37-48.

Brinkgreve, R. B. J. (2002). *PLAXIS, Finite Element Code for Soil and Rock Analyses, 2D-Version 8, Balkema, Rotterdam, Netherlands.*

Carillo, N. (1942). Simple two and three dimensional cases in the theory of consolidation of soils. *Journal of Mathematics and Physics, 21(1)*, 1-5.

Çelik, G. (2020). *Assessment of Consolidation Settlements in Karacabey Soft Clays : Estimated and Monitored Behaviour.* (Doctor of Philosophy), Middle East Technical University.

Chai, J-C., Miura, N. and Bergado, D-T. (2001). Simple method of modeling PVD improved subsoil. *Journal of Geotechnical and Geoenvironmental Engineering, ASCE 127(11)*, 965–972.

Chai, J.C. and Miura, N. (2001). Investigation of factors affecting vertical drain behaviour. *Journal of Geotechnical Engineering, 125(3), 216-226*.

Cholachat, R. (2005). *Analytical and Numerical Modelling of Soft Clay Foundation Improvement via Prefabricated Vertical Drains and Vacuum Preloading.* (Doctor of Philosophy), University of Wollongong, Wollongong.

Das, B. (2013). Principles of geotechnical engineering. *Eighth Edition, SI. Global Engineering, Christopher M. Shortt.*

De Jager, W. F. J. (1990). *Systematic quality control of vertical drains.* Paper presented at the Proceeding 4th International conference on Geotextiles, Geomembranes and Related Products. The Hague, pp.321-326.

Den Hoedt, G. D. (1981). *Laboratory testing vertical drains*. Paper presented at the Proceedings. 10th Intern. Conference on SMFE, Stockholm, pp.627-630.

Fellenius, B. H., and Castonguay, N. G. (1985). The efficiency of band-shaped drains: a full scale laboratory study. *Report to National Research Council and the Industrial Research Asistance Programme*.

Fox, G. (2014). Prefabricated vertical drains. *Geoengineer, DOI*, pp. 1-23.

Getchell, A. (2013). *Geotechnical Test Embankment on Soft Marine Clay in NewingtonDover, New Hampshire.* (Thesis Presented in Partial Fulfillment of the Requirements for the Master of Science Degree), University of New Hampshire, Durham, New Hampshire.

Giroud, J. P. (1982). Filter Criteria for Geotextiles. *Proceedings of the Second International Conference on Geotextiles, IFAI, Vol. 1*(Las Vegas, Nevada, USA, August 1982), pp. 103-108.

Hansbo, S. (1979). Consolidation of clay by band shaped prefabricated drains. *Ground Engineering, 12(5)*, 16-25.

Hansbo, S. (1997). Aspects of vertical drain design: Darcian or non-Darcian flow. *Geotechnique, 47(5)*, 983–992.

Hansbo, S. (1981). Consolidation of fine-grained soils by prefabricated drains. *Proceedings of 10th International Conference on Soil Mechanics and Foundation Engineering, v. 3, pp. 677-682*.

Hansbo, S. (1987). Design aspects of vertical drains and lime column installation. *Proc. 9th Southeast Asian Geotechnical Conference, Vol. 2*, No. 8, pp. 1-12.

Hird, C.C. (1992). Finite element modelling of vertical drains beneath embankments on soft ground. *Geotechnique, 42(3), 499-511*.

Hird, C.C., Pyrah, I.C., Russell, D., and Cinicioglu, F. (1995). Modelling the effect of vertical drains in two-dimensional finite element analyses of embankments on soft ground. *Canadian Geotechnical Journal, 32*, 795-807.

Hird, C.C. (2000). Model study of seepage in smear zones around vertical drains in layered soil. *Geotechnique, 50 (1)*, 89-97.

Holtz, R.D. (1987). Preloading with prefabricated vertical strip drains. *Geotextiles and Geomembranes,, v. 6(1-3),*, p. 109-131.

Holtz, R.D. (1991). Prefabricated vertical drains: design and performance. *CIRIA ground engineering report : ground improvement. Butterworth-Heinemann Ltd, UK, UK, 131 p.*

Holtz, R.D., William, D.K. and Thomas C.S. (2011). An Introduction to Geotechnical Engineering. *Upper Saddle River, NJ: Pearson*.

Holtz, R.D. (1987). Characteristics of Prefabricated Drains for Accelerating Consolidation. *Proceedings of the Ninth European Conference on Soil Mechanics and Foundation Engineering, Balkema, Vol. 2, Dublin, Ireland, August 1987*, pp. 903-906.

Holtz, R.D. (1973). *Excavation and Sampling Around Some Sand Drains at Ska-Edeby*. Paper presented at the Sweden, Proceedings of Specialty Conference on Performance on Earth and Earth supported Structure, Purdue University, Vol. 1, pp 435–464.

Holtz, R. D., Lancellota, R. and Pedroni, S. (1989). *Behavior of bent prefabricated vertical drains.* Paper presented at the Proc. 12th Int. Conf. Soil Mech. and Found. Eng., Rio de Janeiro, Vol. 3, pp. 1657-60.

Indraratna, B. and Redana, I.W. (1998). Laboratory determination of smear zone due to vertical drain installation. *J. Geotechnical and Geoenvironmental Eng., ASCE, Vol. 125, No. 1*, pp. 96-99.

Indraratna, B., and Rujikiatkamjorn, C. (2010). Review of methods of analysis for the use of vacuum preloading and vertical drains for soft clay improvement. *Geomechanics and Geoengineering: An International Journal, 5(4)*, 223-236.

Indraratna, B., Balasubramaniam, A.S. and Ratnayake, P. (1994). Performance of embankment stabilized with vertical drains on soft clay. *J. Geotech. Eng., ASCE, v. 120:2*, p. 257-273.

Indraratna, B., Bamunawita, C., Redana, I., and McIntosh, G. (2003). Modelling of geosynthetic vertical drains in soft clays. *Journal of Ground Improvement, 7(3)*, 127-138.

Indraratna, B. and Redana, I. W. (1997). Plane strain modeling of smear effects associated with vertical drains. *J. Geotech. Eng, 123(5)*, 474-478.

Indraratna, B. and Redana, I.W. (2000). Numerical modeling of vertical drains with smear and well resistance installed in soft clay. *Canadian Geotechnical Journal, 37*, 132-145.

Jamiolkowski, M., Lancellotta, R. and Wolski, W. (1983). *Precompression and speeding up consolidation*. Paper presented at the Pro. 8th European Conf. Soil Mech. And Found. Eng., Helsinki, Vol. 3, Spec. Session No. 6, pp. 1201-1226.

Jamiolkowski, M. L., R. (1981). *Consolidation by Vertical Drains.* Paper presented at the Panel Discussion, Proceedings of the 10th International Conference on Soil Mech. and Found, Eng., Stockholm, Vol. 1, pp 345–451.

Janbu, N. (1963). *Soil compressibility as determined by oedometer and triaxial tests*.

Jardine, R. D., and Hight, D.W. (1987). *The behaviour and analysis of embankments on soft clay. The Public Works Research Center of Greece, Athens.*

Jemal, J. M. P., Alemayehu T., and Aydin, Ö. (2020). Settlement of a railway embankment on PVD-improved Karakore soft alluvial soil. *Engineering Science and Technology, 23 (2020) 1015–1027*.

Johnson, S. J. (1970). Foundation precompression with vertical sand drains. *Soil Mechanics and Foundation Division, ASCE.*

Lee, S.R. and Kim, Y. T. (1997). An equivalent model and back-analysis technique for modelling in situ consolidation behavior of drainage-installed soft deposits. *Computers and Geotechnics, 20(2)*, 125–142.

Kjellman, W. (1948). *Accelerating consolidation of fine grain soils by means of cardboard wicks*. Paper presented at the in: 2nd Int. Conf. Soil Mech. Found. Eng., Rotterdam, 1948: pp. 302–305.

Koda, E., Szymanski, A. and Wolski, W. (1989). *Behaviour of Geodrains in organic subsoil.* Paper presented at the Proc. 11th Inte. Conf. on SMFE, Rio de Janeiro, Vol2, pp.1377-1380.

Kremer, R., de Jager, W., Maagdenberg, A., Meyvogel, I. and Oostveen, J. (1982). *Quality standards for vertical drains*. Paper presented at the Proceedings, 2nd International Conference on Geotextile, Las Vegas, pp.319-324.

Kremer, R., Oostveen, J., Van Weele, A.F., de Jager, W. and Meyvogel, l. (1983). *The quality of vertical drainage.* Paper presented at the Proceedings, 8th European Conference on SMFE., Helsinki, vol.2, pp.721-726.

Lawrence, C. A. (1988). Flow behaviour of kinked strip drains. *Proc. of Symposium on Geosynthetics foe Soil Improvement, Geotechnical Special Publication No. 18, ASCE, pp.22-39*.

Leroueil, S., Magnan, J-P. and Tavenas, F. (1990). Embankment on soft clays. Ellis Horwood Limited. *Chichester, UK*.

Leroueil, S., Magnan, J., and Tavenas, F. (1985). *Remblais sur argiles molles. Technique te Documentation Lavoisier, Paris.*

Lin, D. G., Kim, H.K. and Balasubramaniam, A.S. (2000). Numerical modelling of prefabricated vertical drain. *Geotechnical Engineering Journal, Southest Asian Geotechnical Society, 31 (2)*, 109-125.

Long, R. P., and Covo, A. (1994). Equivalent diameter of vertical drains with an oblong cross-section. *Journal of Geotechnical Engineering Division, ASCE, 120(9)*, 1625-1630.

Madhav, M., Park, Y.M. and Miura, N (1993). Modelling and study of smear zone around band shaped drains. *Soils and Foundations, Vol.33, No.4*, pp.135-147.

McGown, A. (1976). Properties and Uses of Permeable Fabric Membranes. *Proceedings of the Workshop on Materials and Methods for Low Cost Road, Rail and Reclamation Works, Lee, Ingles and Yeaman, Eds., published by the University of New South Wales, Leura, Australia, September 1976*, pp. 663-710.

Mesri, G. (1991). *Field performance of prefabricated vertical drains.* Paper presented at the Proceeding International Conference on Geotechnical Engineering for Coastal Development-Theory to Practice, Yokohama, Japan, Vol. 1, pp. 231-236.

Miura, N. and Chai, J.C. (2000). Discharge capacity of prefabricated vertical drains confined in clay. *Geosynth. Int., vol. 7, no. 2*, pp. 119-135.

Nguyen, Ba-Phu. (2019). *Consolidation Analysis of PVD-Installed Soft Deposits Considering Soil Disturbance and Discharge Capacity Reduction* (Doctor of Philosophy), Pukyong National University South Korea.

Nguyen, N. T. (2020). Applying the Equivalent Plane Strain solution to design the soft soil improvement by vertical drains. *Journal of Mining and Earth Sciences, Vol. 61*(Issue 3 (2020) 28 – 37). doi:DOI: 10.46326/JMES.2020.61(3).01

Onoue, A. (1988). Consolidation by vertical drains taking well resistance and smear into consideration. *J. Soils and Foundations, Vol. 28*, No. 4, pp. 165-174.

Parsa-Pajouh, A. (2014). *Analysing Ground Deformation Data to Predict Characteristics of Smear Zone Induced by Vertical Drain Installation for Soft Soil Improvement.* (Doctor of Philosophy), University of Technology, Sydney.

Perera, D., Indraratna, B., Leroueil, S., Rujikiatkamjorn, C., and Kelly, R. (2017). Analytical model for vacuum consolidation incorporating soil disturbance caused by mandrel-driven drains. *Canadian Geotechnical Journal, 54(4). 547-560.*

Pradhan T. B. S, Murata T., Kamon M. and Suwa S. (1993). Experiment study on the equivalent diameter of a prefabricated band-shaped drain. *Proceedings of the 11th Southeast Asian Geotechnical Conference, 1*, 391–396.

Quang Dong Pham1, The Viet T., Minh, T.T. (2022). Evaluation of Asaoka and Hyperbolic Methods for Settlement Prediction of Vacuum Preloading Combined with Prefabricated Vertical Drains in Soft Ground Treatment. *J. Eng. Technol. Sci., Vol. 54, No. 5, 2022, 220501*.

Reiner, A.-N.B. (2022). Application of artificial intelligence in geotechnical engineering. . *Earth-Science*. doi:10.1016/j.earscirev.2022.103991

Rendulic, L. (1936). *Relation between void ratio and effective principal stress for a remoulded silty clay*. Paper presented at the Proceedings of the 1st International Conference on Soil Mechanics and Foundation Engineering, 3, s. 48-51. Cambridge.

Rixner, J., Kramer, S., and Smith, A. (1986). Prefabricated vertical drains. *Federal Highway Administration, Washington D.C., Vol.s I, II and III : Summary of Research Report : Final Report*.

Rufaizal, C.M., A. K., Siti, F.M.R. (2019). Comparative Analysis of Settlement and Pore Water Pressure of Road Embankment on Yan soft soil Treated with PVDs. *Civil Engineering Journal, Vol. 5, No. 7*.

Rujikiatkamjorn, C. (2005). *Analytical and Numerical Modelling of Soft Clay Foundation Improvement via Prefabricated Vertical Drains and Vacuum Preloading.* (Ph.D. Thesis).

Rujikiatkamjorn, C. I., Buddhima; and Chu, Jian (2008). 2D and 3D Numerical Modeling of Combined Surcharge and Vacuum Preloading with Vertical Drains *International Journal of Geomechanics*.

Russell, D., and Hird, C.C. (1995). Discussion of Performance of embankment stabilized with vertical drains on soft clay, by B. Indraratna, A. S. Balasubramaniam, and P. Ratnayake. J. *Geotech. Engrg., ASCE, 121(4)*, 389-391.

Santamaria, A. J. (2015). *Finite Element Analysis of PV Drains for a Test Embankment on Soft Clay.* (Master of Science), University of New Hampshire. (1591829)

Saowapakpiboon, J.B. D., Voottipruex, P., Lam, L.G., and Nakakuma, K. (2011). PVD improvement combined with surcharge and vacuum preloading including simulations. *Geotext Geomembrane*, 29:74–82.

Sathananthan, I. (2005). *Modeling of vertical srains with smear installed in soft clay.* (M.Sc. Thesis), University of Wollongong, Wollongong, New South Wales, Australia.

Schanz, T. (1998). *Zur Modellierung des Mechanischen Verhaltens von Reibungsmaterialen*.

Sengul, T., Edil, T., and Özaydın, K. (2013). Determination of the factors affecting the discharge capacity of prefabricated vertical drains. *İMO Teknik Dergi*, s. 6529-6557.

Sharma, J., and Xiao, D. (2000). Characterization of a smear zone around vertical drains by large scale laboratory tests. *Canadian Geotechnical Journal, 37(6)*, 1265-1271.

Shen S-Li, Hong, Z-S., and Cai, F-X. (2005). Analysis of field performance of embankments on soft clay deposit with and without PVD-improvement. *Journal of Geotextiles and Geomembranes, 23*, 463–485.

Shinsha, H.H.H., Abe, Y., and Tanaka, A. (1982). Consolidation settlement and lateral displacement of soft ground improved by sand drains. *Tsuchi-to-Kiso, Japanese Soc Soil Mech Found Eng, 30(5)*, 7–12.

Sloan, A. M. L. (2019). Finite element modelling of prefabricated vertical drains using 1D drainage elements with attached smear zones. *Computers and Geotechnics, 107*, 235-254.

Stamatopoulos, A. C. (1985). *Soil Improvement by Preloading*: John Willey, p.261.

Sundström, S. (2023). *Numerical Analyses of a PVD-Improved Embankment on Soft Soil.* (Doctor of Philosophy), Chalmers University of Technology, Chalmers.

Taylor, D. W. (1948). *Fundamentals of Soil Mechanics*. New York.

Terzaghi, K. (1925). *Erdhaumechanik auf bodenphysikalischer grundlage*. Leipzig und Wein, 399 pp.

Tran TA, M. T. (2008). Equivalent plane strain modelling of vertical drains in soft ground under embankment combined with vacuum preloading. *Computers and Geotechnics, 35(5)*, 655–672.

Van Zanten, R. (1986). *The guarantee of the quality of vertical drainage systems.* Paper presented at the Proceedings 3rd International conference on Geotextile, Vienna, Vol.3., pp.651-655.

Wang ZM, X.L., and Jiang, Z.H. (1998). *Field experimental study on the soft ground treatment of Hongzhou-Niingbo (HN) expressway foundation.* Paper presented at the In: Cai TL (ed) Soft ground treatment in Hangzhou-Ningbo expressway, Hongzhou Press, Hongzhou in Chinese, pp 183–222

Xiao, D. (2001). *Consolidation of soft clay using vertical drains.* (PhD thesis), Nanyang Technological University, Singapore. P.301.

Yosouff., R. C. and Mamat, A.R. (2022). Numerical Simulation and Field Measurement Validation of Road Embankment on Soft Ground Improved by Prefabricated Vertical Drains: A Comparative Study. *Appl. Sci. 2022, 12, 8097.* https://doi.org/10.3390/app12168097.

Yildiz, A., and Karstunen, M. (2009). Three-dimensional analyses of PVD-improved soft soils. *Geotechnics of soft soils: focus on ground improvement, 197-203*.

Yoshikuni, H., and Nakanodo, H. (1974). Consolidation of Fine-Grained Soils by Drain Wells with Finite Permeability. *Japan Soc. Soil Mech. and Found. Eng., Vol. 14*, No. 2, pp. 35-46.

Zeng, G.X. (1989). *New development of the vertical drain theories.* Paper presented at the Proceedings of the 12th International Conference on Soil Mechanics and Foundation Engineering Rotterdam 2: 1435-1438.

CURRICULUM VITAE

Personal Information

Surname, Name : Abrasse Théodore SOAVINJANAHARY :
e-mail

Education

Degree	Institution	Graduation Year
Postgraduate	Cukorova University	2024
Undergraduate	Antsiranana University	2018
High School	Technical High School	2015

Experience

Year	Work Place	Title
2003-Present	Madagascar	Teacher

Publications

1. 2D Numerical Analysis of PVDs Using Different Matching Methods

APPENDICES

APPENDIX A

NUMERICAL OUTPUT OF LARGE SCALE IN AXISYMMETRIC

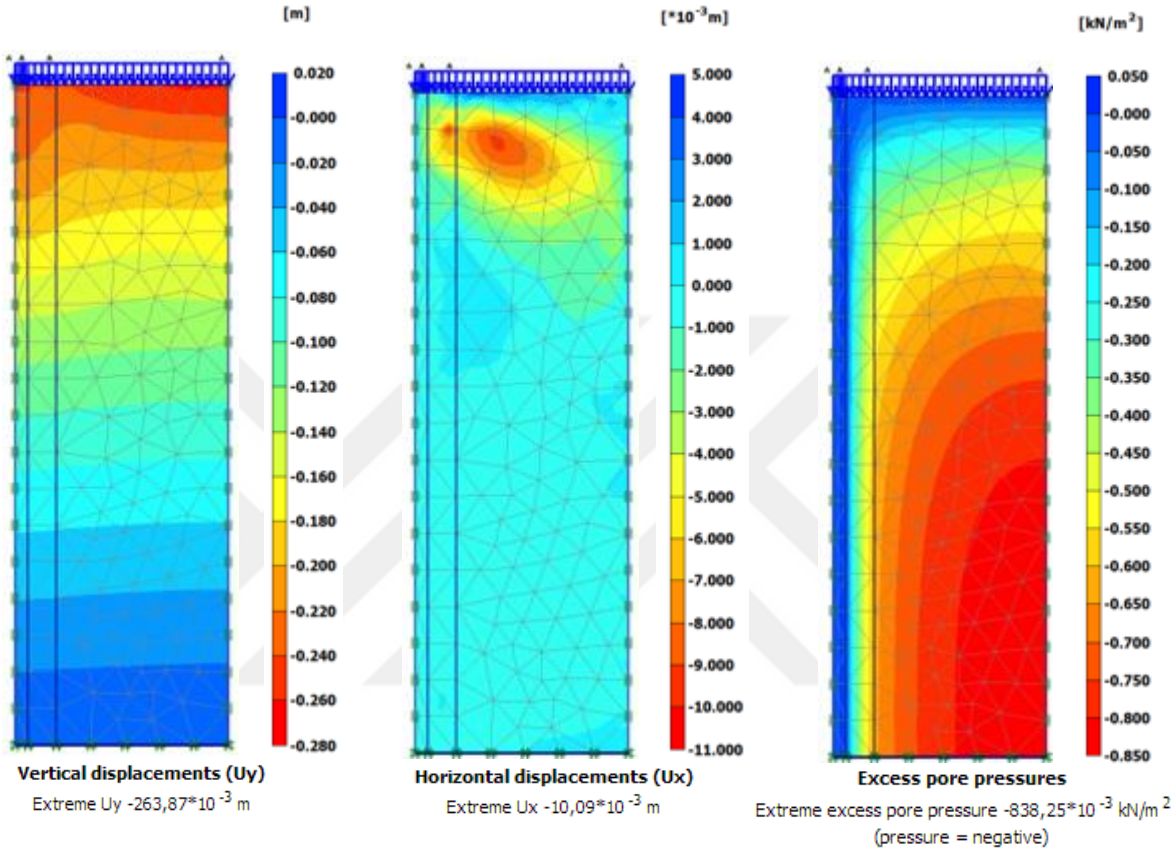

Figure A. 1 Large-scale deformations in axisymmetric

APPENDIX B

NUMERICAL OUTPUT OF LARGE SCALE IN PLANE STRAIN CONDITIONS

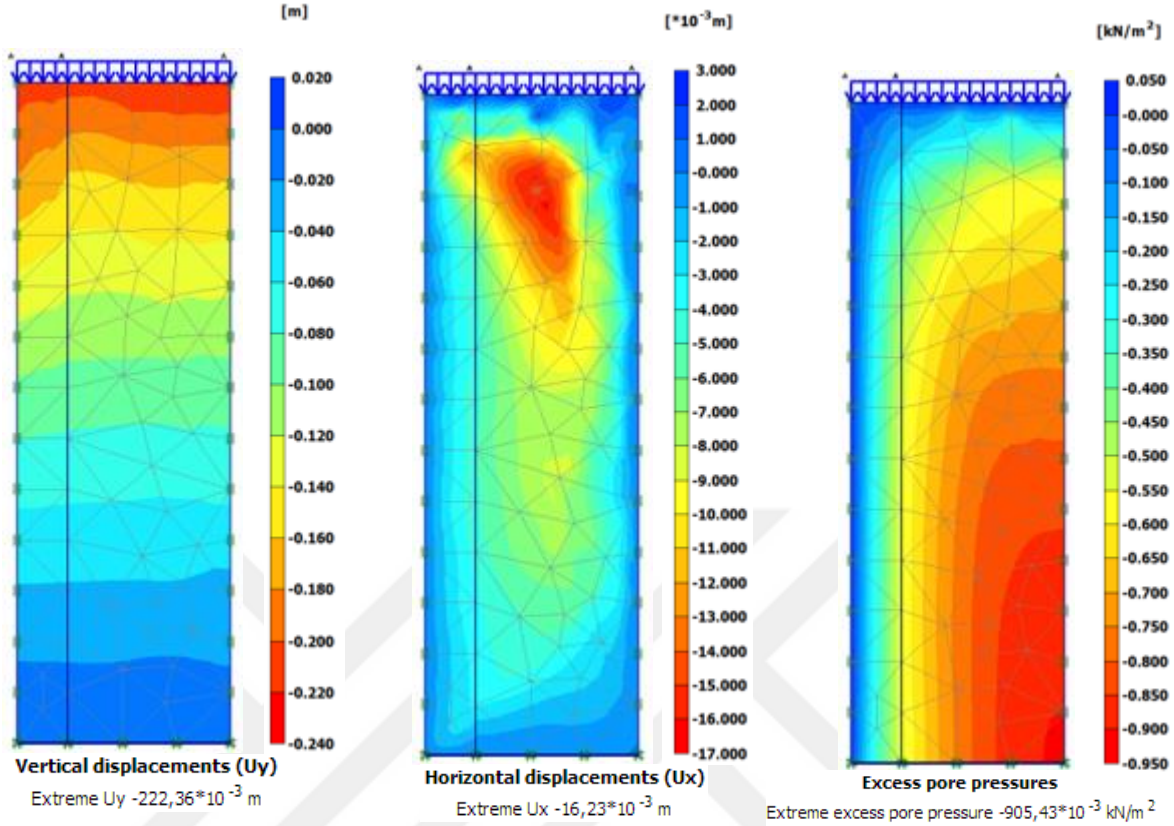

Figure B. 1 Large-scale deformations in plane strain Method A

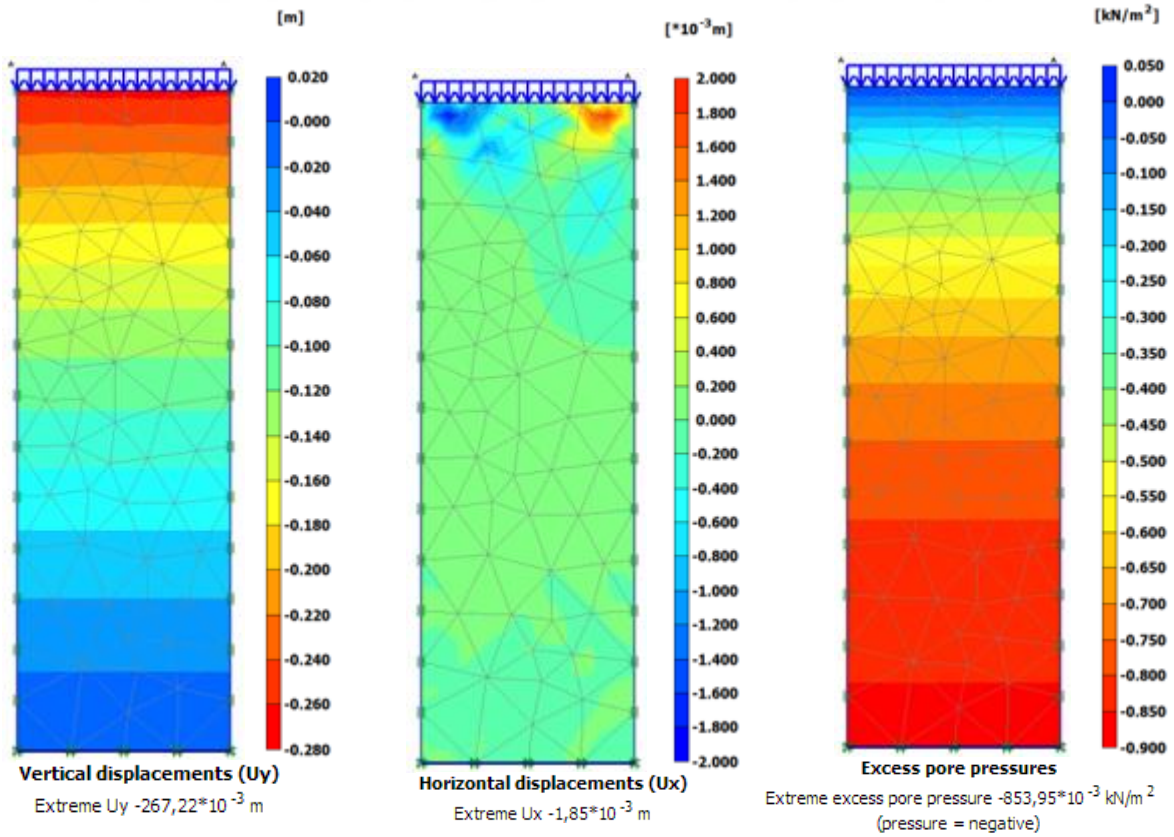

Figure B. 2 Large-scale deformations in plane strain Method B

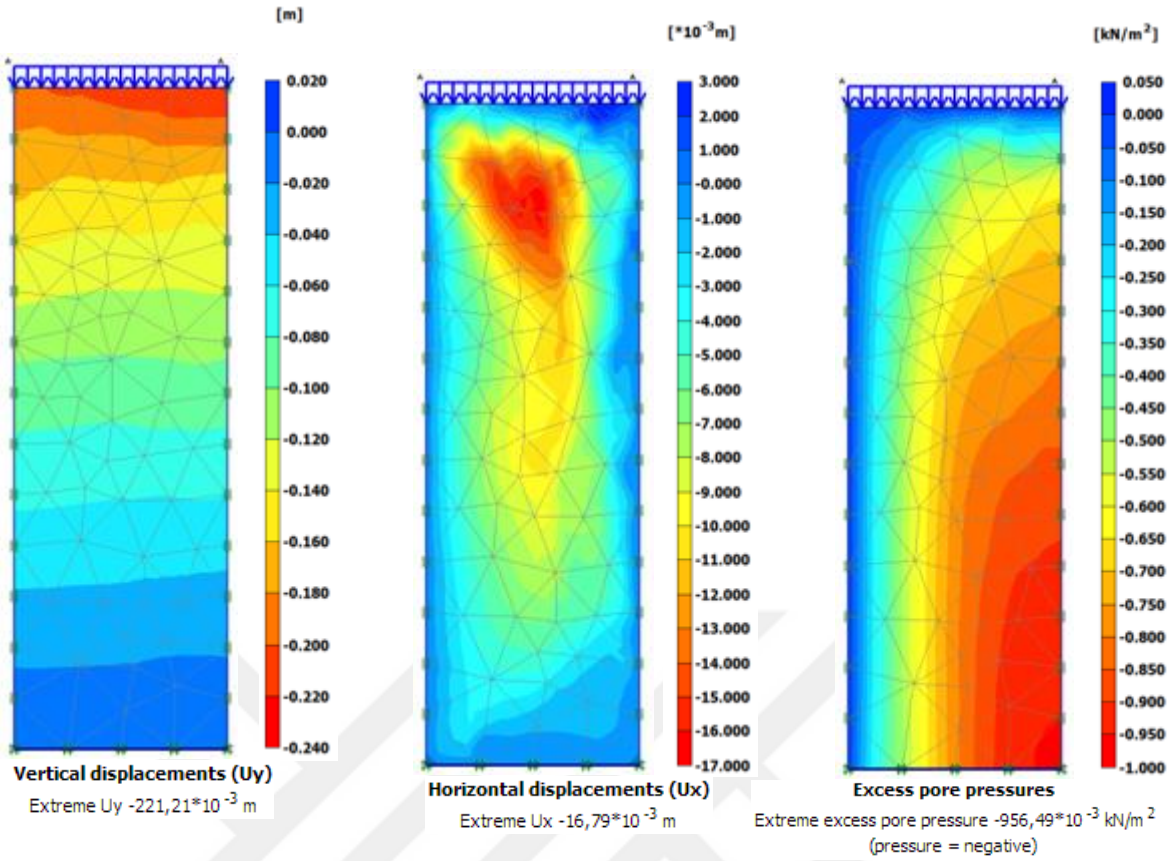

Figure B. 3 Large-scale deformations in plane strain Method C

APPENDIX C

NUMERICAL OUTPUT OF FULL TEST EMBANKMENT IN EASTERN CHINA

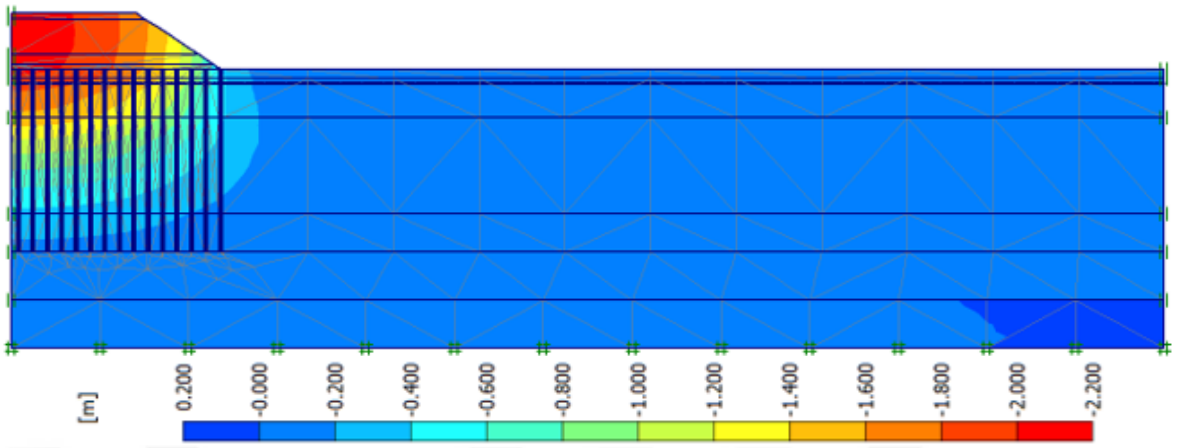

Figure C. 1 Vertical deformation of test embankment in eastern China for Method A

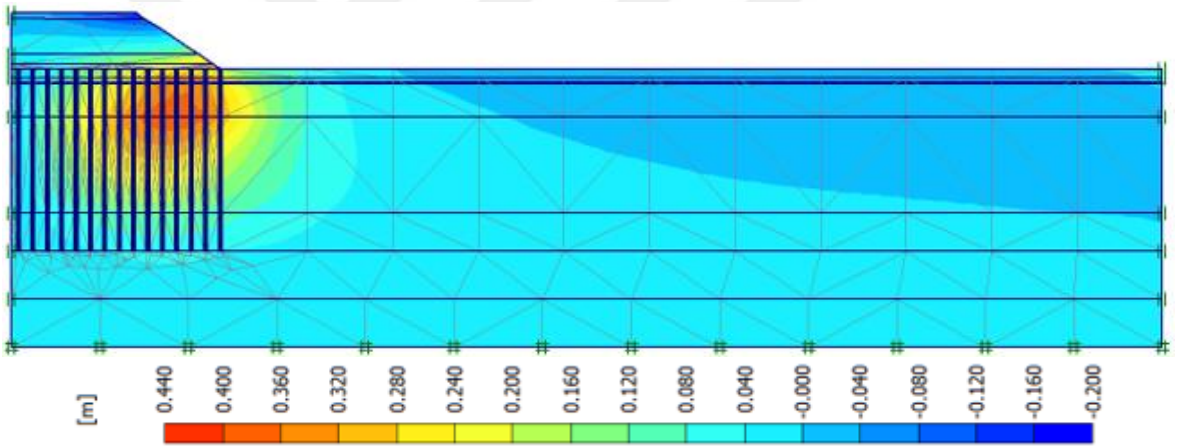

Figure C. 2 Horizontal deformation of test embankment in eastern China for Method A

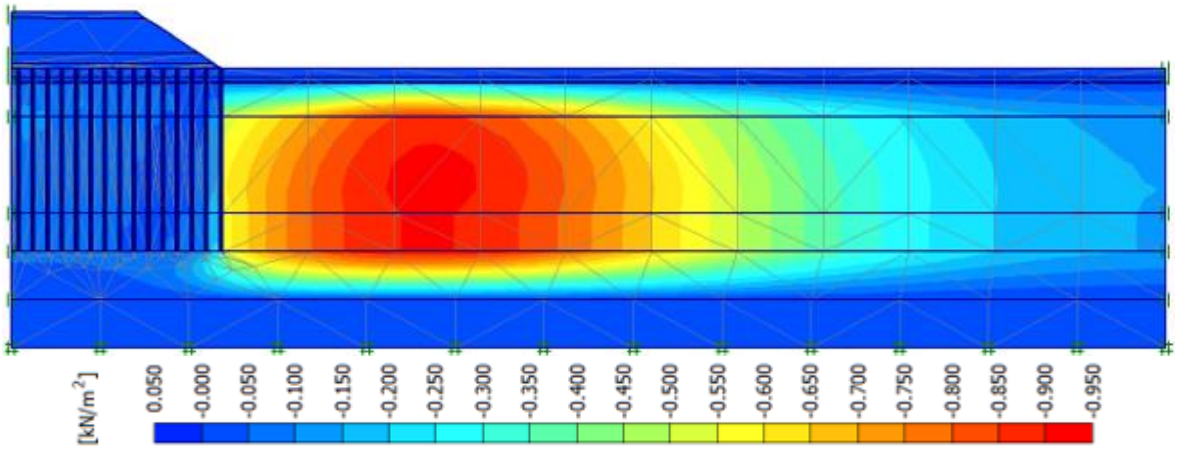

Figure C. 3 EPP of test embankment in eastern China for Method A

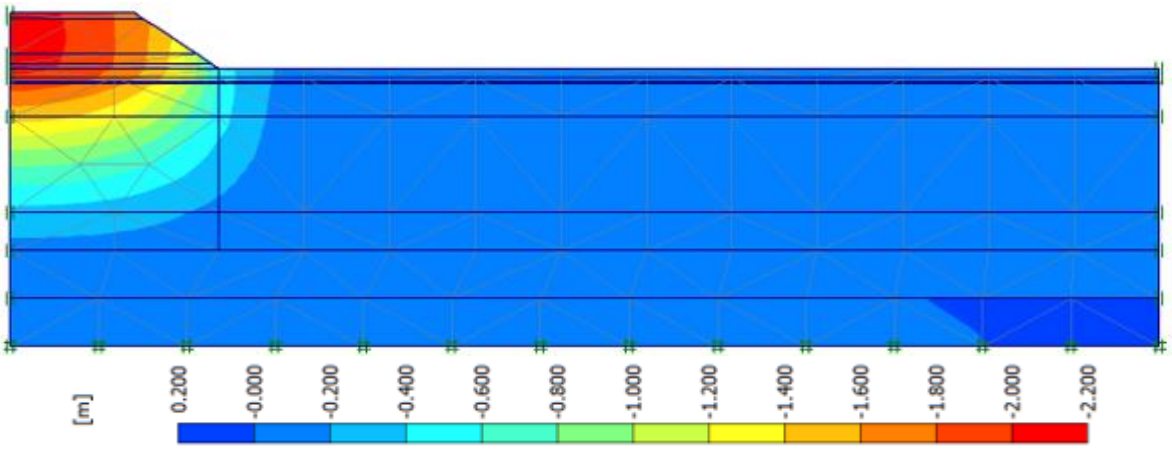

Figure C. 4 Vertical deformation of test embankment in eastern China for Method B

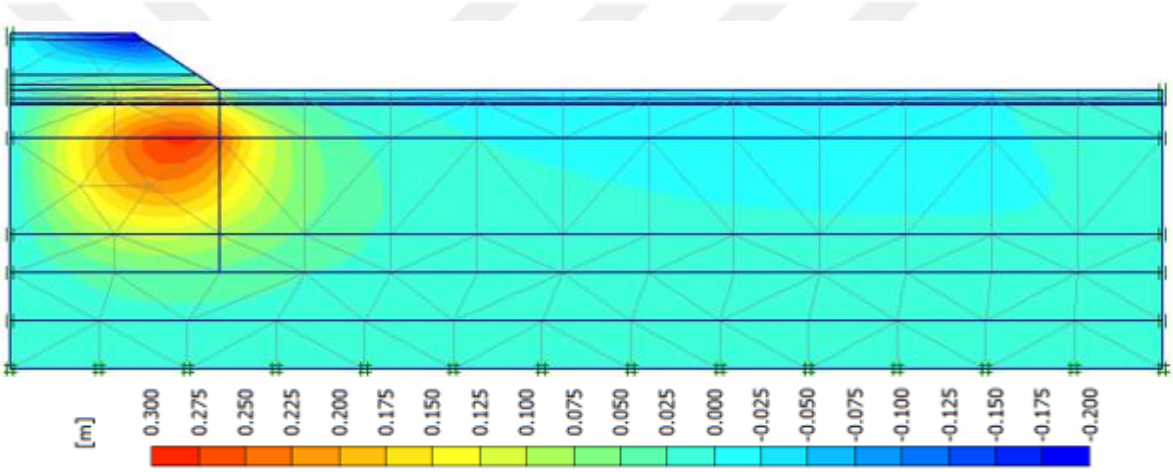

Figure C. 5 Horizontal deformation of test embankment in eastern China for Method B

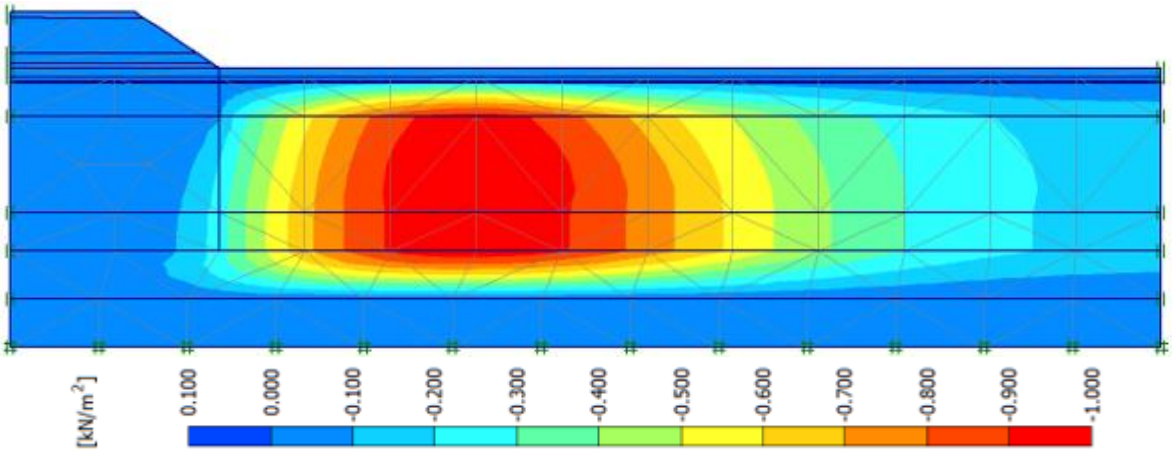

Figure C. 6 EPP of test embankment in eastern China for Method B

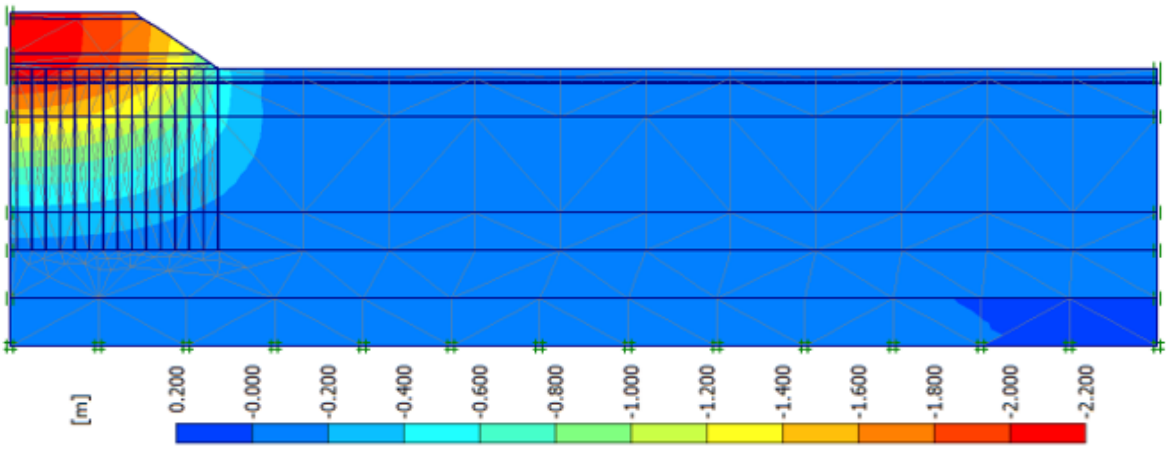

Figure C. 7 Vertical deformation of test embankment in eastern China for Method C

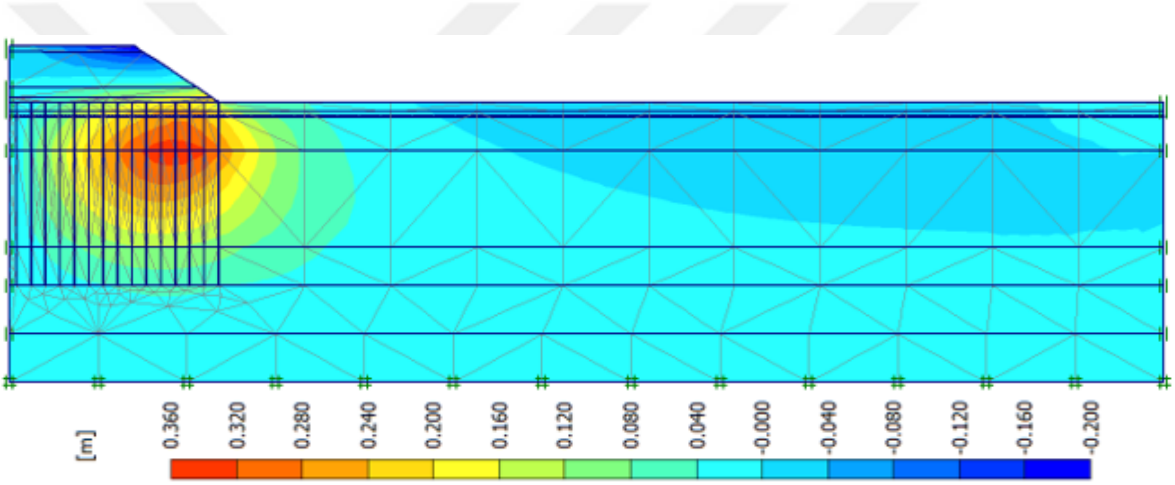

Figure C. 8 Horizontal deformation of test embankment in eastern China for Method C

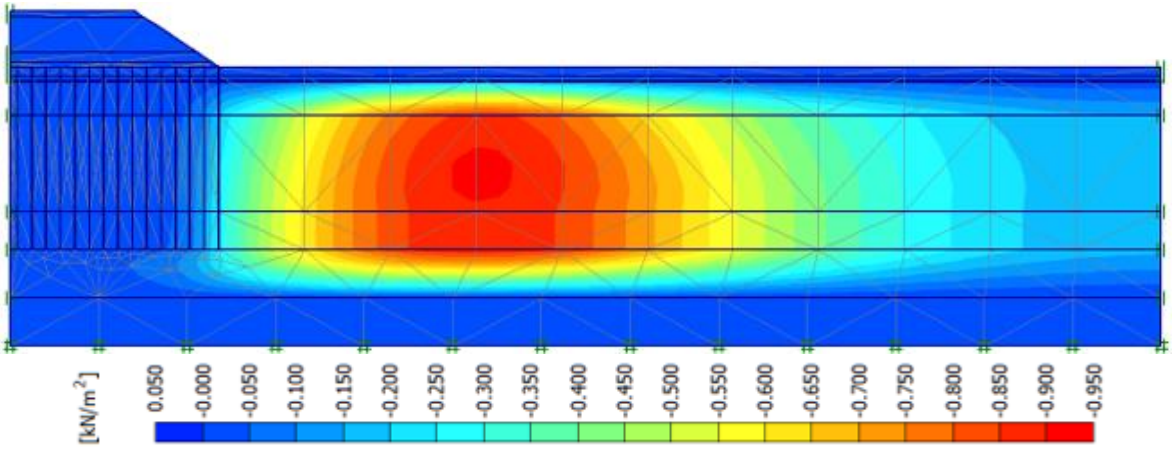

Figure C. 9 EPP of test embankment in eastern China for Method C

APPENDIX D

NUMERICAL OUTPUT FOR SEGMENT 1 0F TEST EMBANKMENT FOR DIFFERENT CONSTITUTIVE MODELS (SSCM, SSM and MCCM)

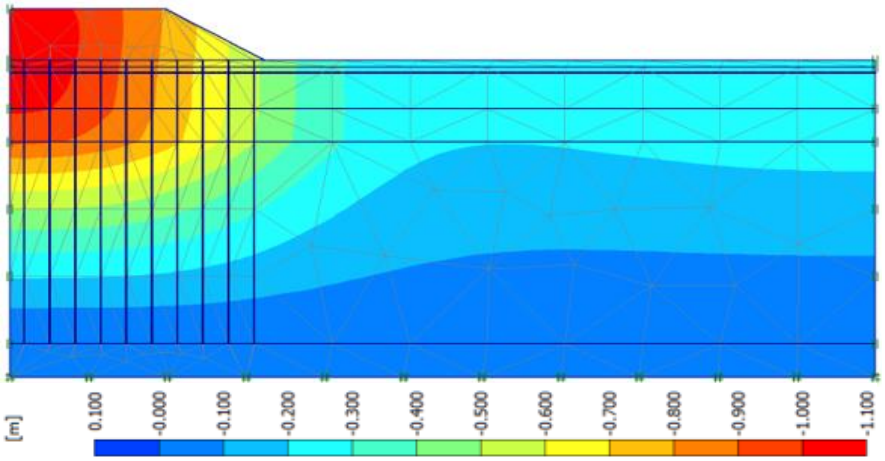

Figure D. 1 Vertical deformation in Dover NH test embankment Segment 1 in SSCM

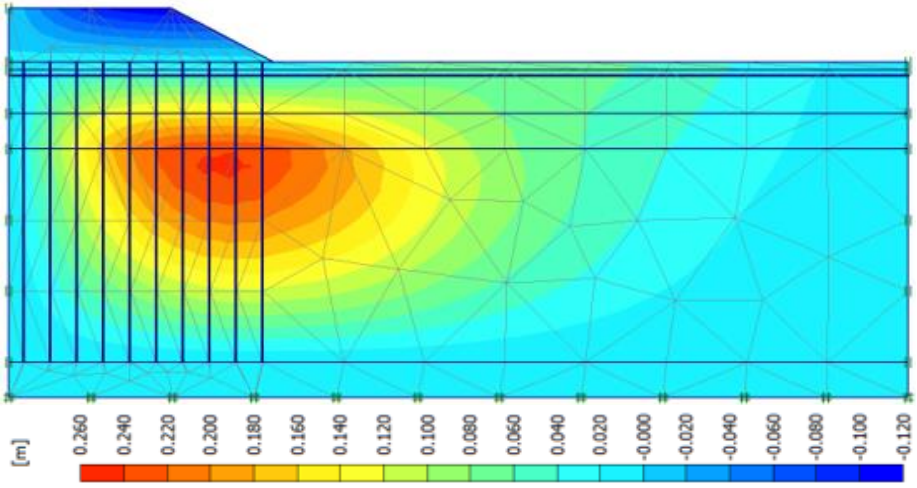

Figure D. 2 Horizontal deformation in Dover NH test embankment Segment 1 in SSCM

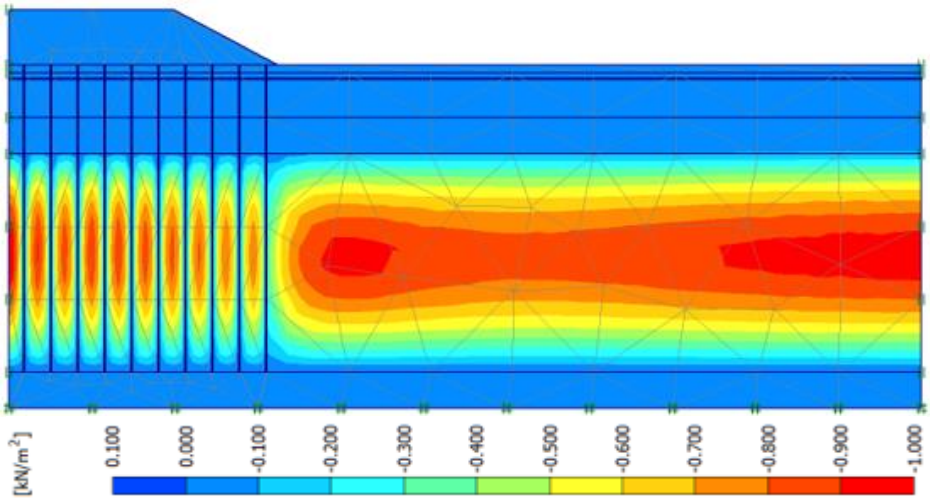

Figure D. 3 Excess pore pressure in Dover NH test embankment Segment 1 in SSCM

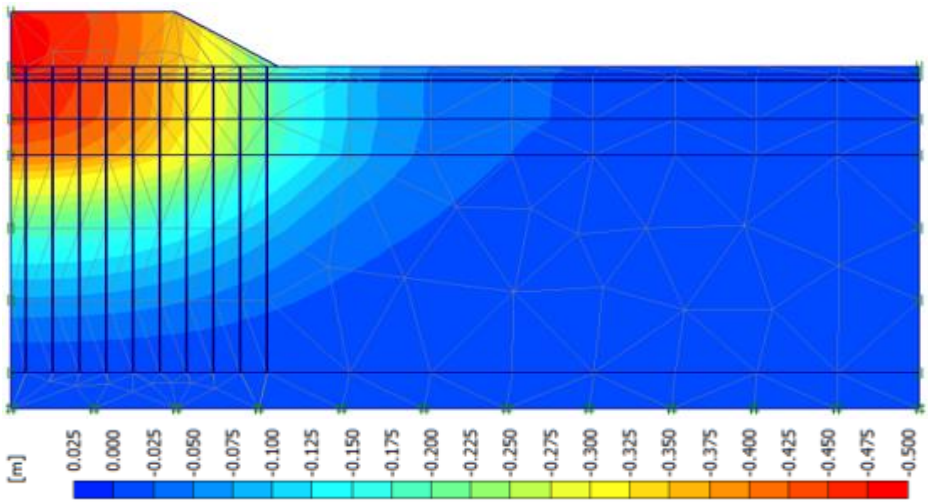

Figure D. 4 Vertical deformation in Dover NH test embankment Segment 1 in SSM

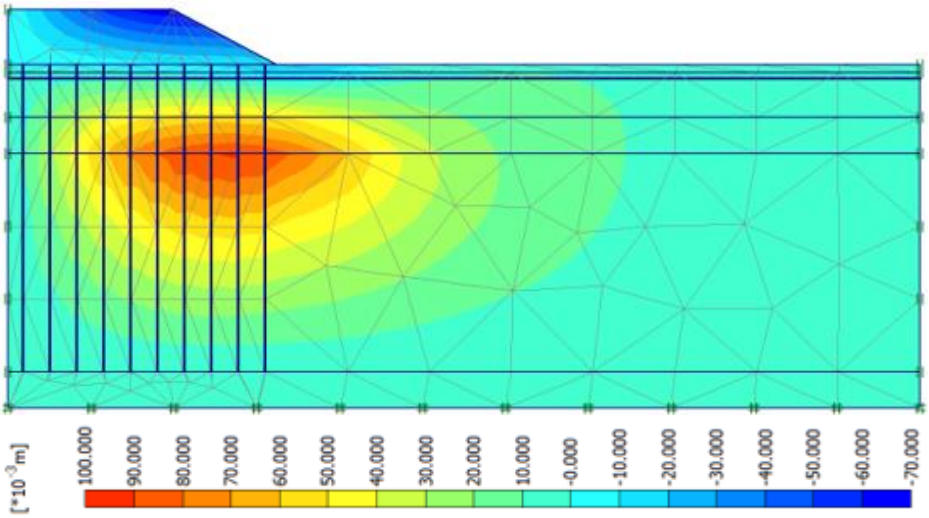

Figure D. 5 Horizontal deformation in Dover NH test embankment Segment 1 in SSM

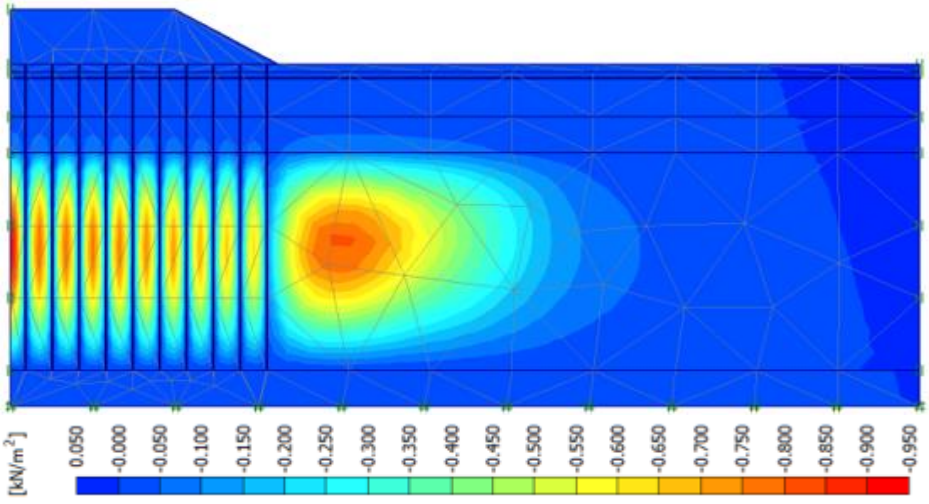

Figure D. 6 Excess pore pressure in Dover NH test embankment Segment 1 in SSM

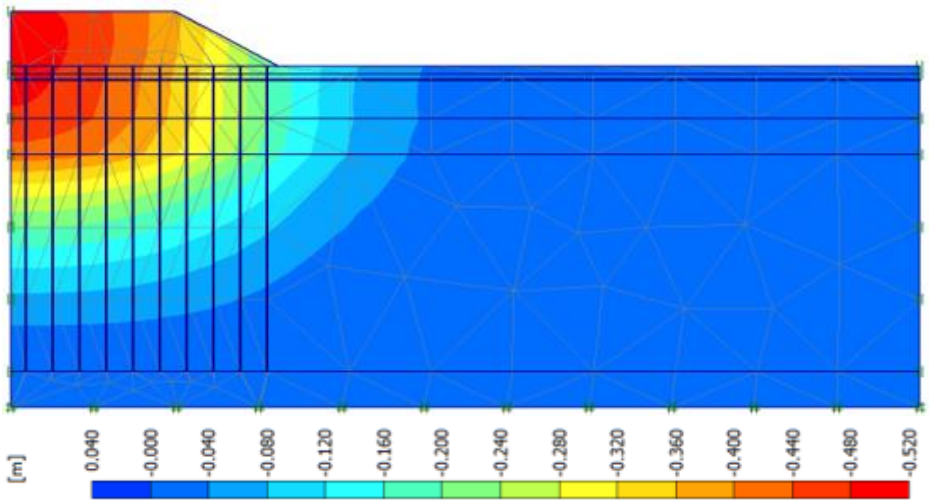

Figure D. 7 Vertical deformation in Dover NH test embankment Segment 1 in MCCM

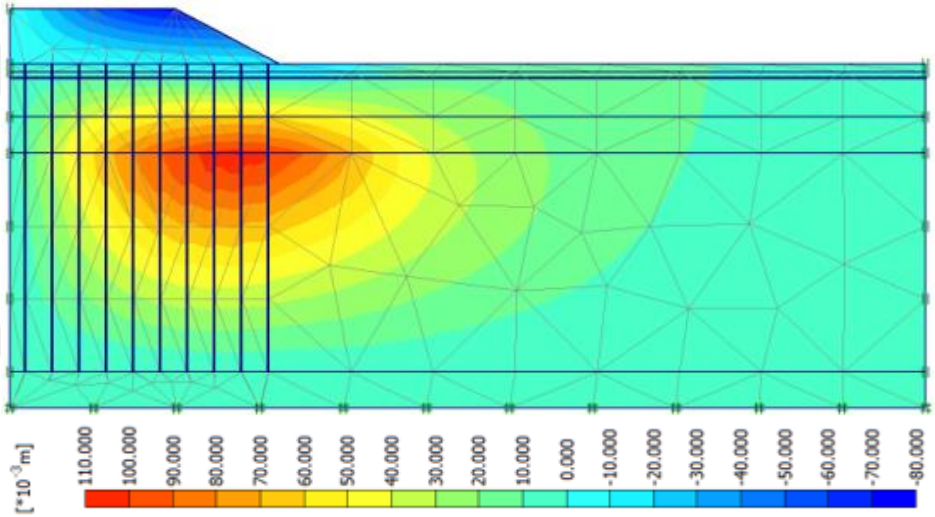

Figure D. 8 Horizontal deformation in Dover NH test embankment Segment 1 in MCCM

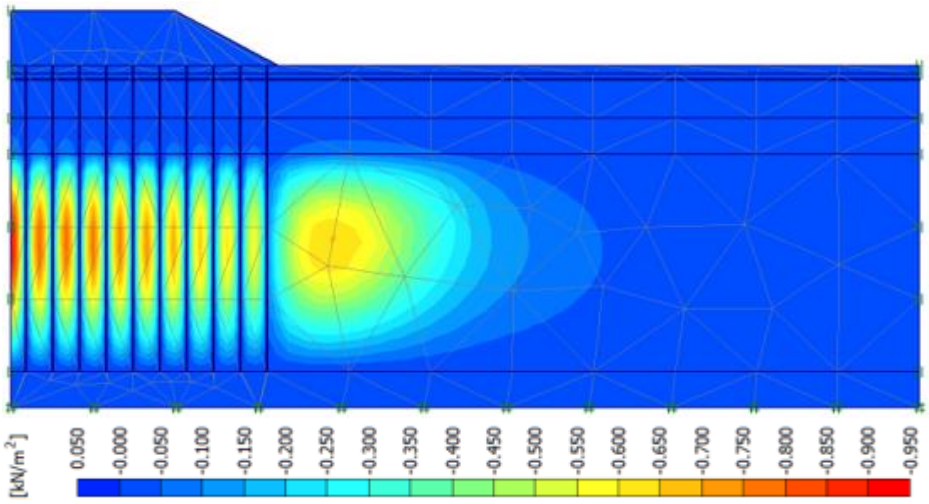

Figure D. 9 Excess pore pressure in Dover NH test embankment Segment 1 in MCCM

APPENDIX E

NUMERICAL OUTPUT FOR SEGMENT 4 0F TEST EMBANKMENT FOR DIFFERENT CONSTITUTIVE MODELS (SSCM, SSM and MCCM)

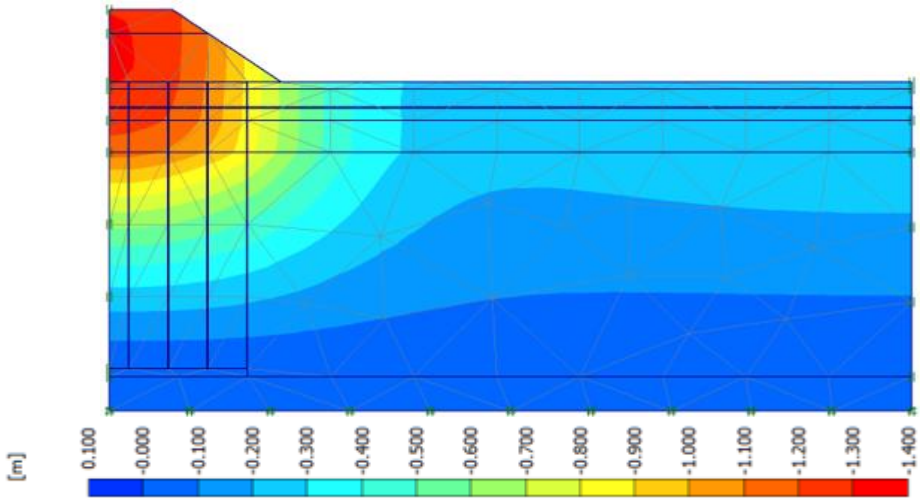

Figure E. 1 Vertical deformation in Dover NH test embankment Segment 4 in SSCM

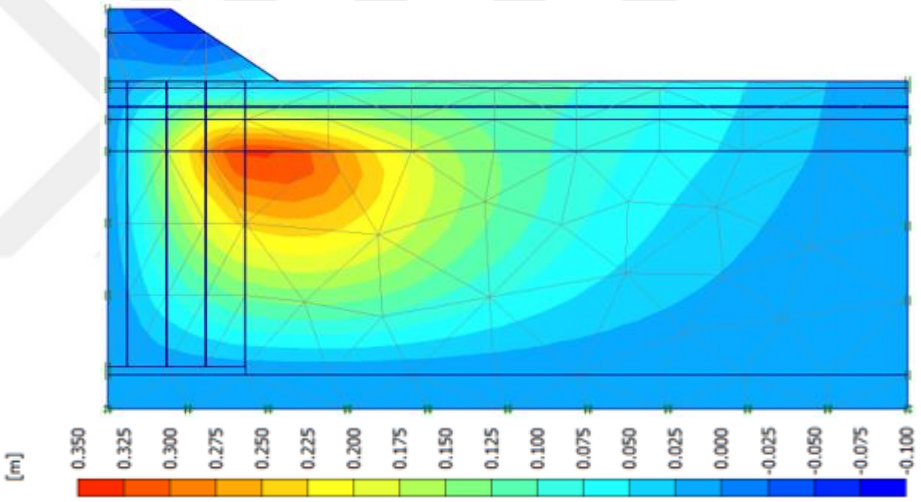

Figure E. 2 Horizontal deformation in Dover NH test embankment Segment 4 in SSCM

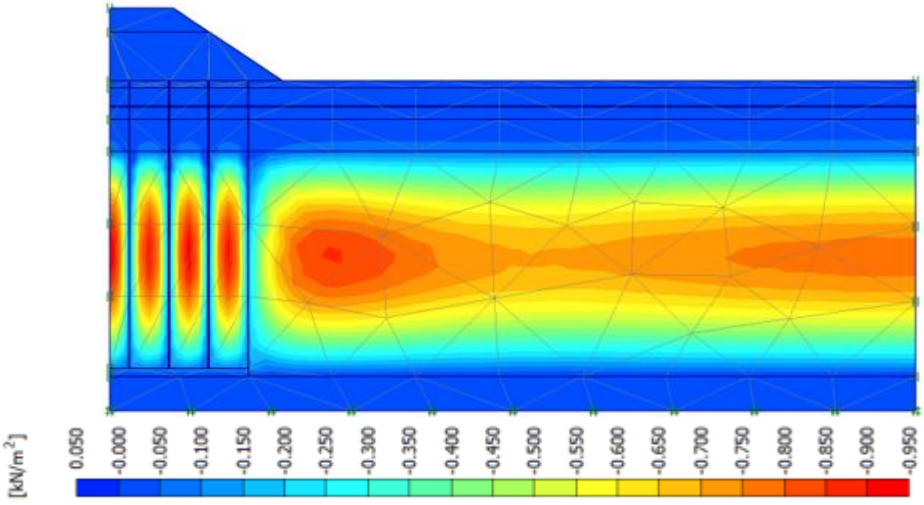

Figure E. 3 Excess pore pressure in Dover NH test embankment Segment 4 in SSCM

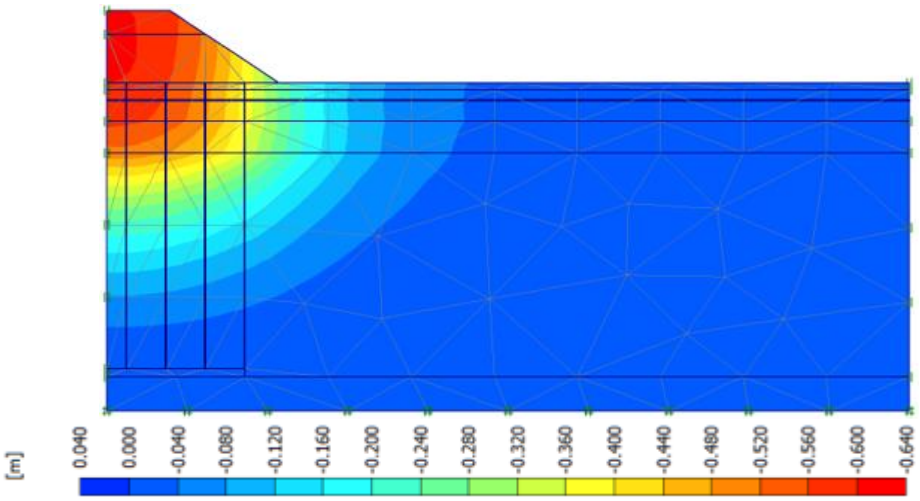

Figure E. 4 Vertical deformation in Dover NH test embankment Segment 4 in SSM

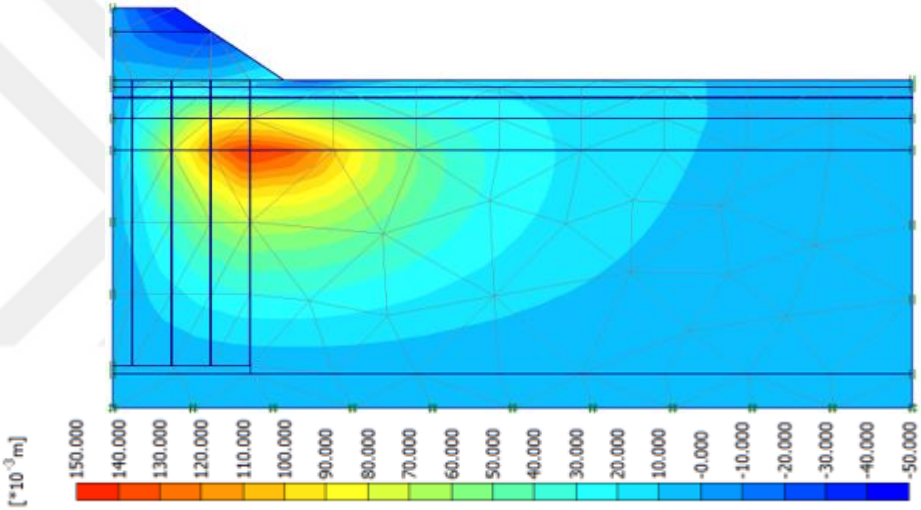

Figure E. 5 Horizontal deformation in Dover NH test embankment Segment 4 in SSM

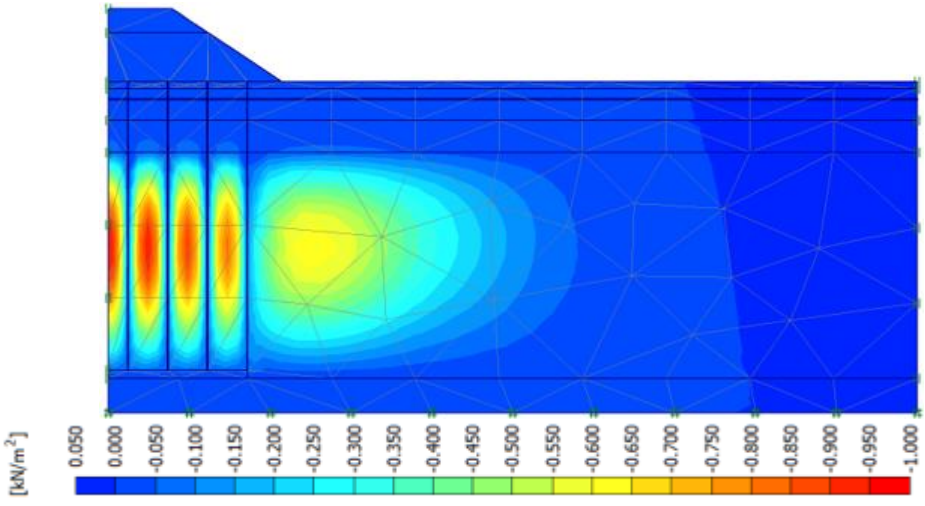

Figure E. 6 Excess pore pressure in Dover NH test embankment Segment 4 in SSM

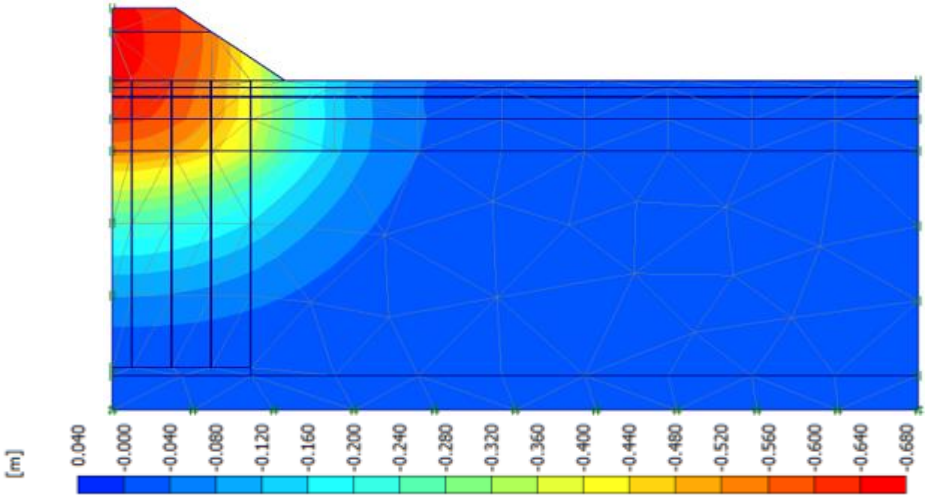

Figure E. 7 Vertical deformation in Dover NH test embankment Segment 4 in MCCM

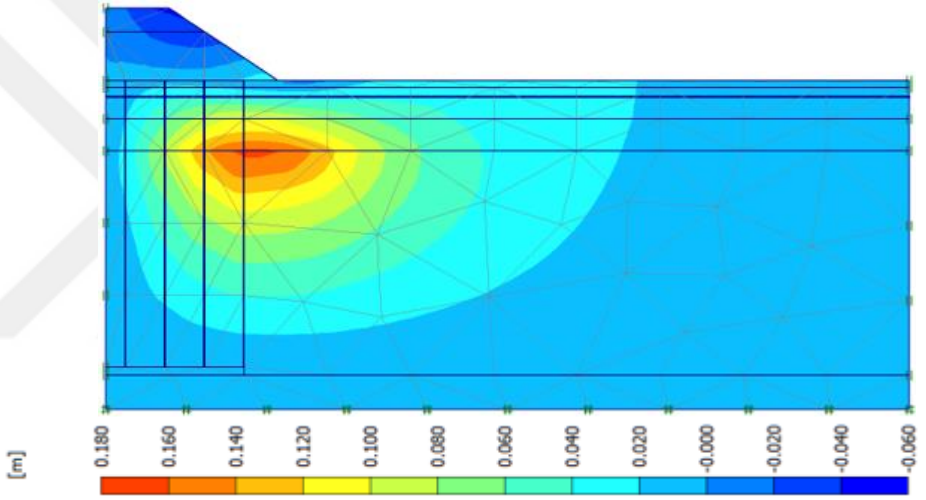

Figure E. 8 Horizontal deformation in Dover NH test embankment Segment 4 in MCCM

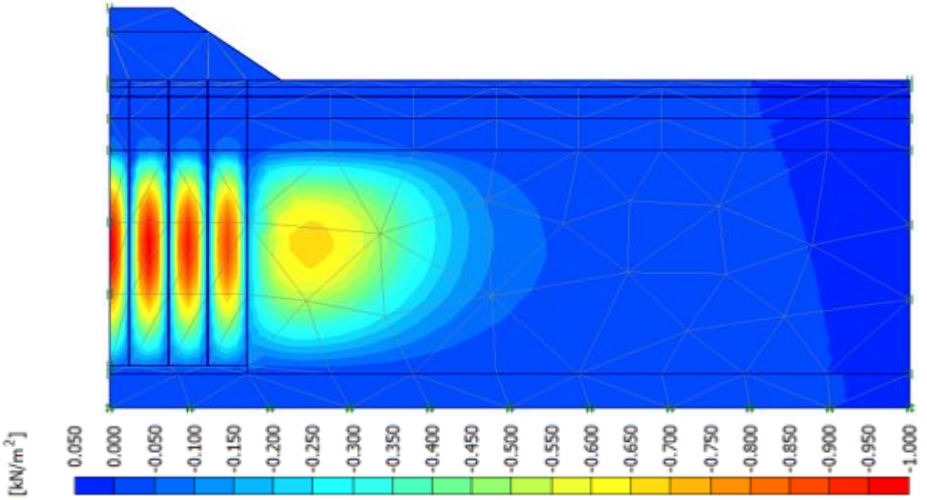

Figure E. 9 Excess pore pressure in Dover NH test embankment Segment 4 in MCCM

APPENDIX F

NUMERICAL OUTPUT FOR SEGMENT 5 0F TEST EMBANKMENT FOR DIFFERENT CONSTITUTIVE MODELS (SSCM, SSM and MCCM)

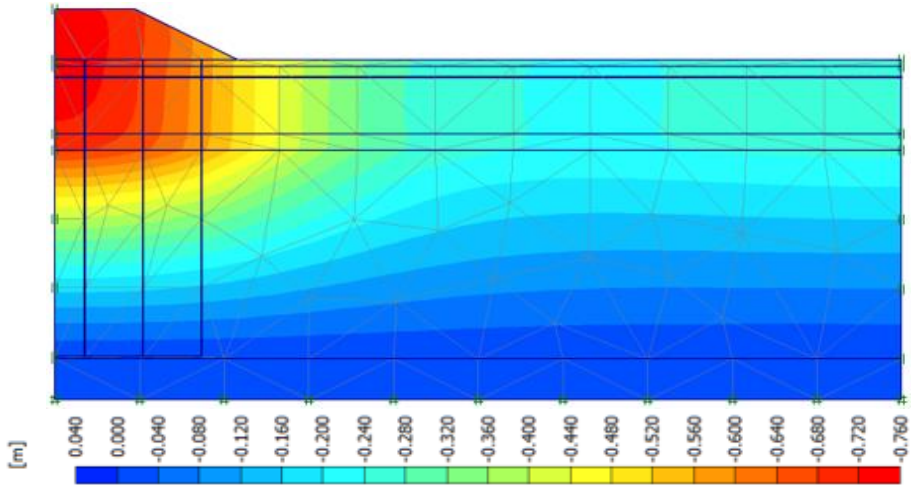

Figure F. 1 Vertical deformation in Dover NH test embankment Segment 5 in SSCM

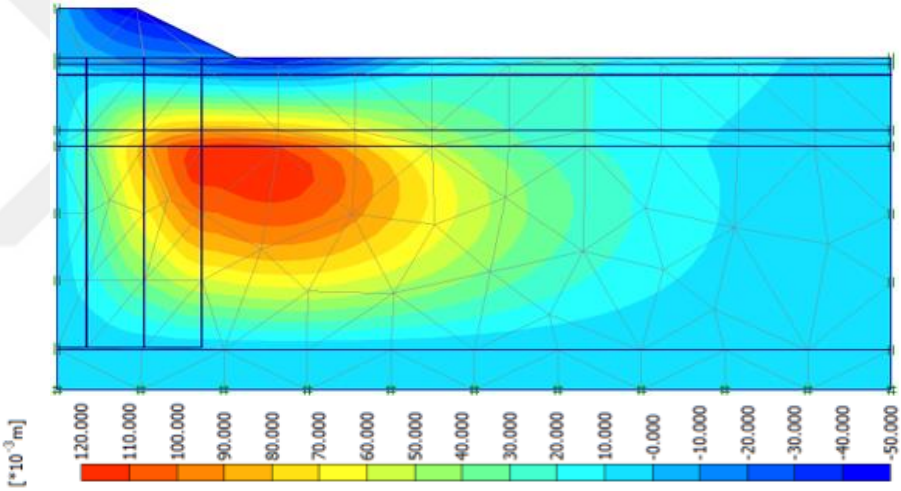

Figure F. 2 Horizontal deformation in Dover NH test embankment Segment 5 in SSCM

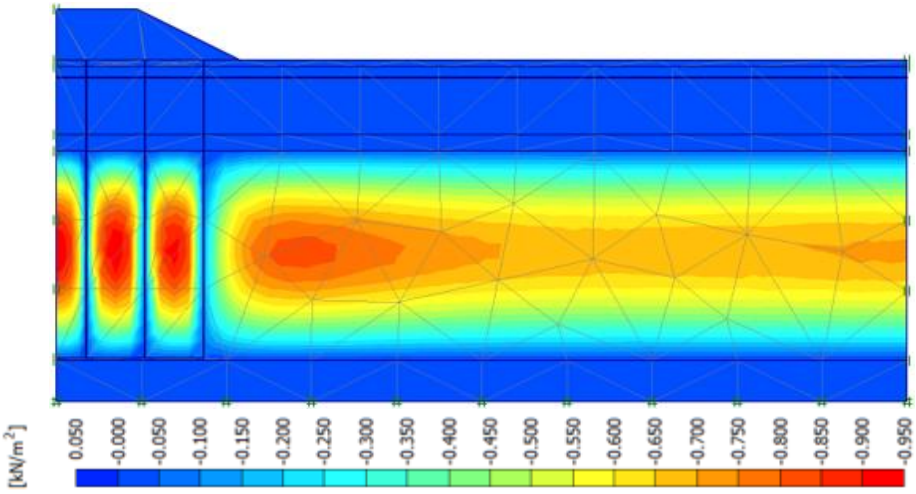

Figure F. 3 Excess pore pressure in Dover NH test embankment Segment 5 in SSCM

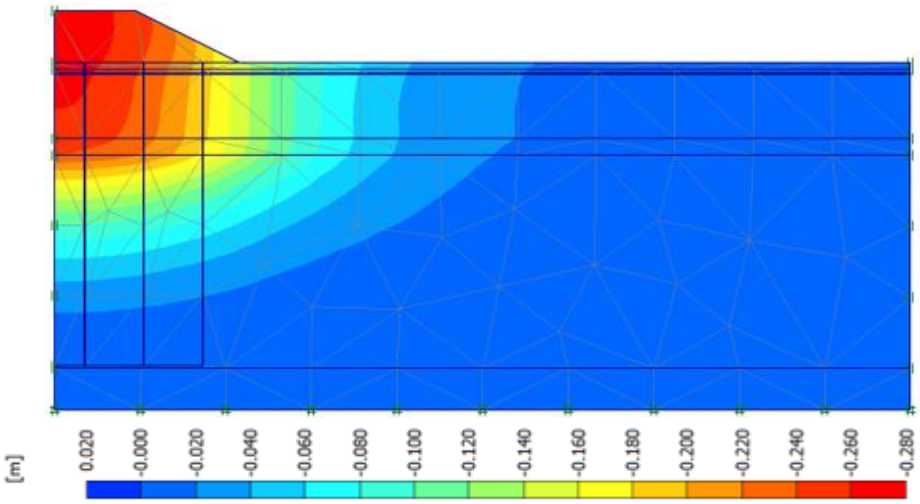

Figure F. 4 Vertical deformation in Dover NH test embankment Segment 5 in SSM

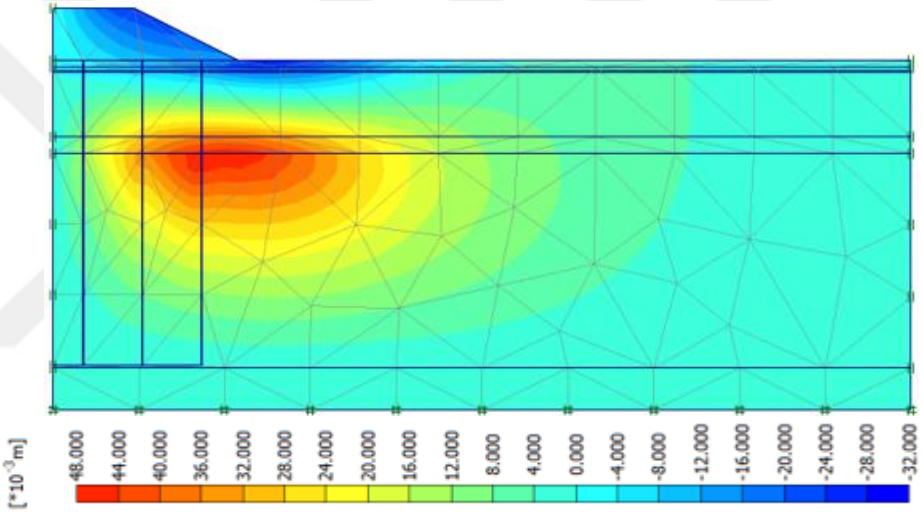

Figure F. 5 Horizontal deformation in Dover NH test embankment Segment 5 in SSM

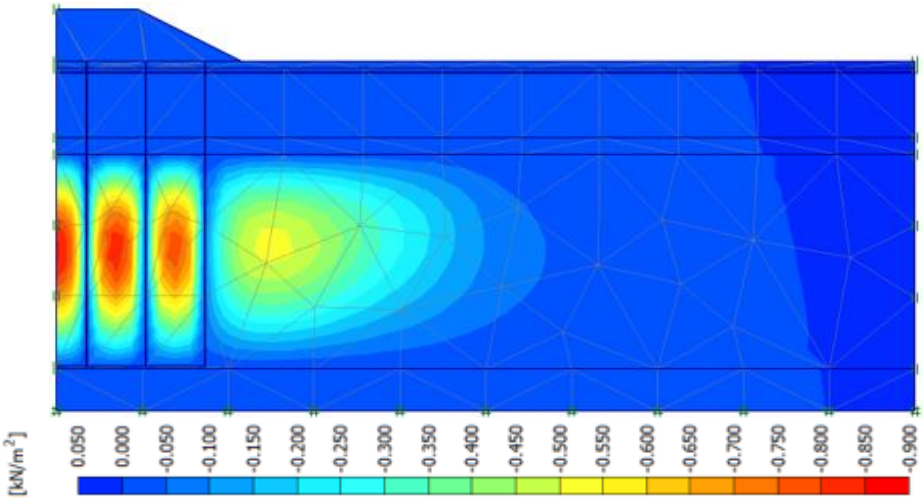

Figure F. 6 Excess pore pressure in Dover NH test embankment Segment 5 in SSM

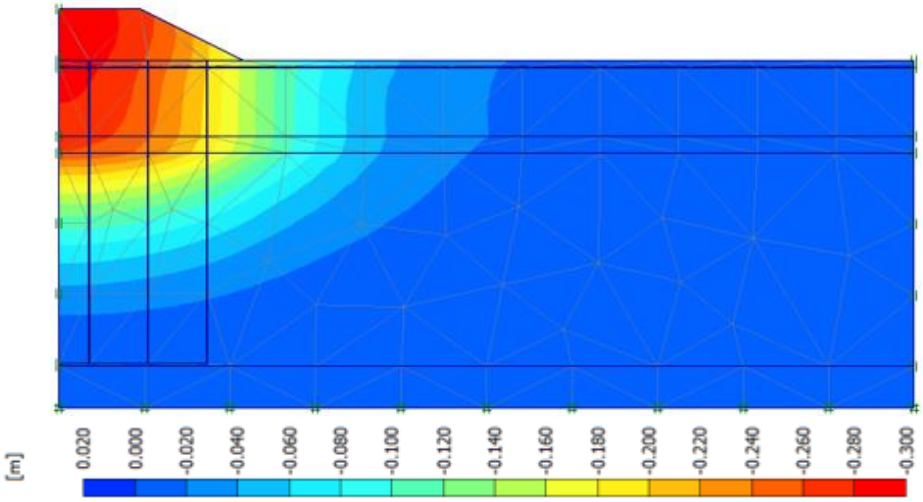

Figure F. 7 Vertical deformation in Dover NH test embankment Segment 5 in MCCM

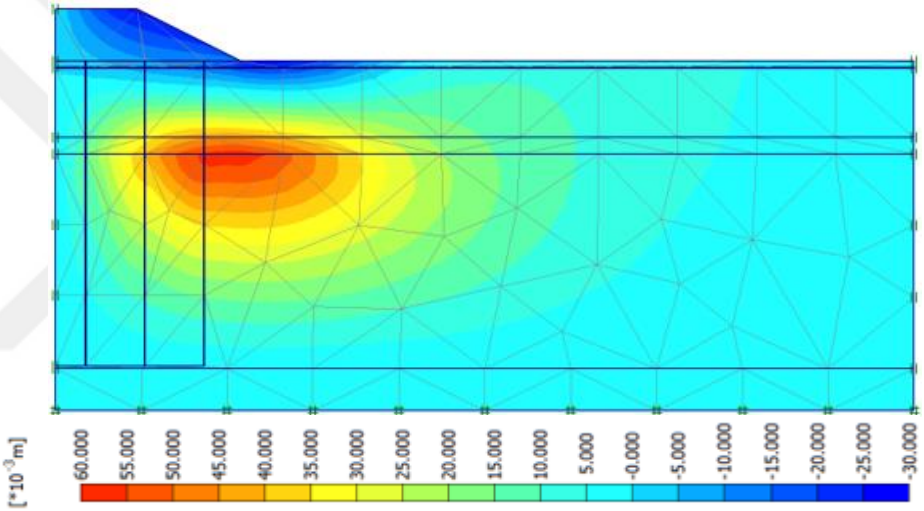

Figure F. 8 Horizontal deformation in Dover NH test embankment Segment 5 in MCCM

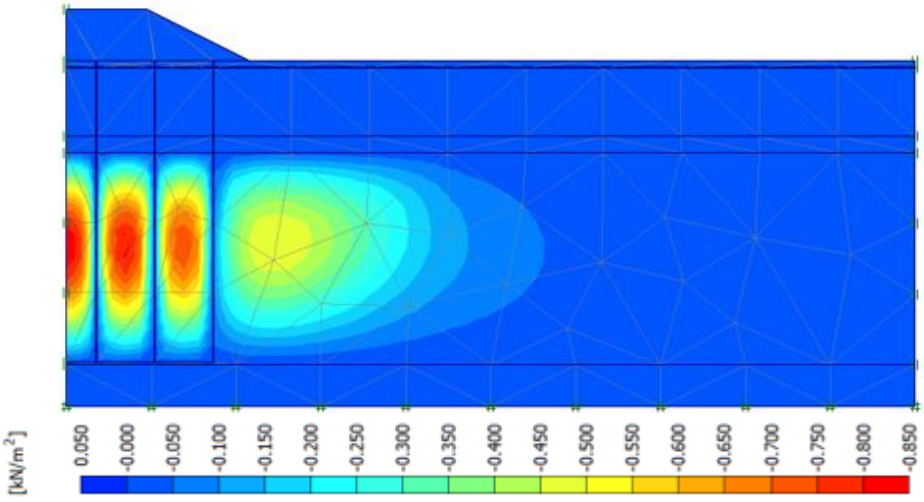

Figure F. 9 Excess pore pressure in Dover NH test embankment Segment 5 in MCCM